TELOMERASE: DISSECTING THE ENDS

By

Basma Masraf Klump

A DISSERTATION

Submitted to
Michigan State University
in partial fulfillment of the requirements
for the degree of

Cell and Molecular Biology–Doctor of Philosophy

2023

ABSTRACT

Telomere syndromes are a group of pathologies associated with severely short telomeres that encompass dyskeratosis congenita, idiopathic pulmonary fibrosis, progeria, and aplastic anemia. Telomere shortening results from the inability of DNA polymerase to replicate the ends of chromosomes. Thereby, with time shortening chromosomes leads to cell senescence and apoptosis. To maintain telomere length, proliferating cells such as stem cells express telomerase ribonucleoprotein (RNP). Over 90% of cancer types are characterized by aberrant telomerase RNP expression. In contrast, inactivating mutations in the telomerase RNP can lead to telomere syndromes. The telomerase RNP consists of the telomerase reverse transcriptase (TERT) protein, the telomerase RNA (TR), Telomerase Cajal Body associated protein 1 (TCAB1), glycine-arginine rich protein 1 (GAR1), dyskerin, NOP10, NHP2 and H2A/H2B dimer. Loss of function mutations in the RNP, importantly TCAB1, are associated with telomere shortening in familial dyskeratosis congenita. TCAB1 maintains the telomere length by facilitating TR localization. Our work sheds light on the role and mechanism of TCAB1 in promoting telomerase RNP assembly by preventing phase-separation of TR with nucleoli, a sub-nuclear compartment, using a variety of approaches. We have shown that telomerase RNP assembly markedly diminished in the absence of TCAB1 through the compact nucleolar sequestration of TR in nucleoli. TR is stabilized by the nucleolar proteins DKC1, GAR1, NOP10 and NHP2. Our current work proposes that the conserved protein complex, known as the H/ACA complex, has a role in counteracting telomerase RNP assembly and trafficking and may play a role in RNA retention in nucleoli. In my dissertation, I will discuss what is known about the telomerase RNP, my contributions to the field, and future work toward unraveling the roles of the factors involved in the telomerase.

To my parents and husband, thank you for your unwavering support and motivation throughout this adventure, and to God, thank you for answering my prayers.

ACKNOWLEDGEMENTS

The work outlined in this dissertation would not have been possible without the support of the community at Michigan State University and our collaborators. I would like to extend my deepest gratitude to my advisor, Dr. Jens Schmidt my laboratory to his guidance and support throughout my work on this dissertation. I would also like to thank my committee for being available to guide and encourage my success inside the laboratory and outside in my extracurricular activities, for providing feedback and for advocating for me. I am grateful for the past members of the laboratory, Dr. Eric Patrick and Kate Adams-Boone and current members Dr. Gloria Perez and Maddison Turley for their contributions and feedback. I would like to extend my gratitude to Dr. Chase Weidmann for his unwavering support and contribution to the RNP-MaP project. I am grateful for Drs. Kefei Yu, Li Han, and Scott Cohen for their contributions to the manuscript (chapter 2). I am grateful to Dr. Matt Bernard for providing me with training in flow cytometry for cell cycle distributions.

I thank current lab members, Drs. Carlo Barnaba, Josh Heyza, Tomas Janovic, David Broadbent, and Madison Turley, Maria Mikhova, and Cody Phillips for their companionship throughout this journey. I would like to thank the Cell and Molecular Biology program and the DO/PhD program, Dr. Brian Schutte, Dr. John Goudreau, Dr. Justin McCromick, Michelle Volker, Bethany Heinlen for their continued support, mentorship and guidance in completing the degree. I am grateful for my friends who I met at the graduate school (Aiko Turmo, Alice Chu, Ana-Maria Raicu, and many others) for exchanging scientific conversations and motivating me to write this dissertation. I am grateful for the Klump family (Nan and Don Klump) and the Al Masraf family specifically, my loving mother, Dr. Thamira Hindo, my endearing father, Sabah Al Masraf, my sisters, Nagham Al Masraf and Dr. Nora Al Masraf, and my brother-in-law, Samir Alaifat for cheering on and empowering me to succeed. Lastly, I am grateful for my husband, Austin Klump, for his devoted support of my career choice, comforting me during difficult times with experiments and exams, and for always reminding me of the light at the end of the tunnel.

TABLE OF CONTENTS

CHAPTER 1: INTRODUCTION

1.1: History of telomeres and telomerase

The research era of telomeres started with Hermann Muller in 1931 describing them as chromosome ends that are not attached to one another. In 1939, Muller named the ends "telomeres" (Muller, 1939). Years later, beginning with Leonard Hayflick, the relevance of telomeres in human cells was re-examined. In addition to his outstanding discoveries of the polio vaccine and *Mycoplasma pneumoniae* (Shay and Wright, 2000), Hayflick established that human diploid cells have a limited proliferative potential (Hayflick, 1965). Relatedly, Watson observed that DNA polymerase could not replicate the ends of chromosomes at telomeres yielding what is known as "the end replication problem" (Watson 1972). A year later, Olovnikov connected the two findings in his "theory of marginotomy" that the inability of DNA polymerase to replicate the chromosomes ends leading to shortening of telomeres may consequently explain "Hayflick's limit" of cellular proliferation (Olovnikov, 1973) (Fig. 1.1).

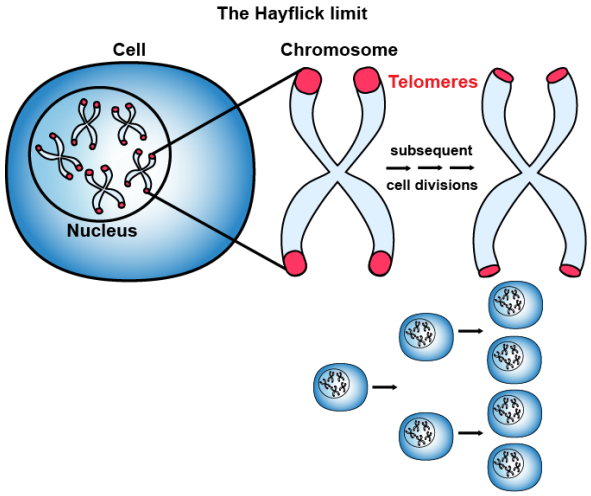

Figure 1.1. The Hayflick limit. The Hayflick limit of cellular proliferation potentially due to telomere shortening after rounds of cellular divisions.

It was not until 1978 when Elizabeth Blackburn delved deeper into telomeres, she found that they are made up of 20-70 TTGGGG consecutive repeats in *Tetrahymena thermophila*. Shortly after Blackburn's discovery, in 1984, Janice *et al.* found telomeres elongating in yeast

cells (Janice et al., 1984). They believed that a non-polymerase enzyme was mediating this activity (Blackburn et al., 2006). Greider and Blackburn developed an activity assay where a single stranded oligonucleotide was combined with dTTP and radioactive dGTP nucleotides and Tetrahymena extract (Greider and Blackburn, 1985). They found that the oligonucleotide was elongated when incubated with the Tetrahymena extract. They called this elongation activity "telomere terminal transferase" which was later renamed "telomerase" (Greider and Blackburn, 1985).

Then, they sought to investigate if the activity was dependent on RNA. They treated Tetrahymena extract and DNA oligonucleotide with RNase to degrade all RNA in the extract and observed a decrease in the extension of the oligonucleotide (Greider and Blackburn, 1987, 1989). This revealed that there is an RNA component necessary for telomere elongation. In 1989, they discovered that the telomerase RNA (TR) contains a region complimentary to the repeated telomere sequence used as a template for telomere elongation, which was a groundbreaking discovery in understanding telomere elongation that earned Greider, Blackburn, and Szostak the Noble Prize in Medicine in 2009 (Greider and Blackburn, 1987, 1989). These findings paved the way for uncovering the telomerase ribonucleoprotein (RNP) and its components in vertebrate cells. The components of telomerase were identified in yeast, human fibroblasts, human cancer cells and mutations were revealed in those components that were linked to premature aging diseases (Harley et al., 1990; Hastie et al., 1990; Blackburn et al., 2006).

1.2: Telomeres and their replication problem

Telomeres are repeat regions of DNA located at the end of the eukaryotic chromosomes. Most telomeres are double stranded and can span 2-20 kb in length. The double stranded ends consist of a G-rich strand organized in repeats that differs slightly among species. In *Plasmodium falciparum*, a malaria causing organism, telomeres consist of CAGGGTTT repeats; In *Tetrahymena thermophila*, the repeats consist of TTGGGG; in vertebrates, telomeric repeats are made up of TTAGGG (Bottius et al., 1998; Blackburn et al.,

2006; Palm et al., 2008). During DNA replication, the removal of RNA primer on the C strand of the chromosome end results in a short single stranded region that DNA polymerase cannot replicate due to lack of primer binding beyond the overhang. The C-strand of chromosome ends become vulnerable to 5' to 3' exonucleolytic digestion similar to the proteins that catalyze the initial double stranded breaks. CtIP (human homolog of Sae2) and MRN initiate the first step of end resection by binding to the 5' C strand which is then resected by Exo1 or Sgs1-bound Dna2 (Clerici et al., 2005; Longhese, 2010). End resection of telomeres results in short single stranded regions known as 3' overhangs which can range from 20-500 nucleotides in length (Kim et al., 1994). Shortening of the telomeres with rounds of cell division disrupts the protection complex that spans telomeres known as shelterin (Palm and De Lange, 2008; Fig. 1.2). Shelterin plays two major roles: telomere protection and telomerase recruitment (more on recruitment on page 20).

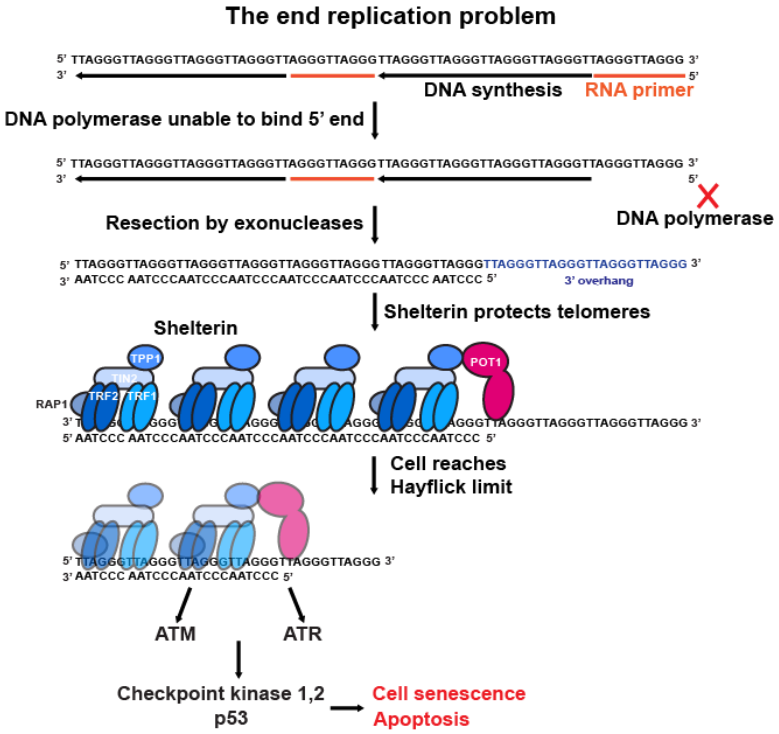

Figure 1.2. The end replication problem. The end replication problem of DNA polymerase and critically short telomeres triggering DNA damage repair pathway leading to cell senescence and apoptosis.

Shelterin is made up of a stable six-protein complex that covers the single- and double-stranded telomeres to protect the strands from misrecognition by DNA damage repair proteins as breaks. TRF1 (Telomere Repeat binding factor 1) and TRF2 (Telomere Repeat binding factor 2) bind to double stranded telomeric regions. TRF2 associates with RAP1 (Repressor/Activator protein 1) which increases TRF2 association with telomeres (Fig. 1.2). TRF1 and TRF2 recruit TIN2 (TRF1-interacting Nuclear protein 2) to stabilize TRF1 and TRF2 on telomeres. TIN2 then recruits TPP1-POT1 to telomeres where POT1 (Protection of Telomeres 1) binds the single-stranded 3' overhang. TPP1 bridges between the dsDNA and ssDNA by binding TIN2 and POT1, respectively, to stabilize the complex onto telomeres (Shay et al., 2013).

In the absence of TRF2, DNA damage proteins are recruited to the double stranded regions of telomeres leading to ATM activation (Denchi et al., 2007). In contrast, absence of POT1 triggers the ATR repair pathway at the single-stranded overhang (Denchi et al., 2007). In either signaling pathway, ATM or ATR phosphorylates H2AX which amplifies the DNA damage response at telomeres. In addition, ATM and ATR may also phosphorylate checkpoint kinase 1 and 2 to signal cell cycle arrest in S- and G2-phase (Denchi et al., 2007). Another pathway that ATM and ATR activate to mediate senescence or apoptosis is p53. Other DNA damage repair pathways are activated in the absence of shelterin factors at telomeres (Denchi et al., 2007).

Non-homologous end joining is an error-prone DNA damage repair pathway involved in the recognition of telomeres as sites of DNA damage in the absence of TRF2. Ku70/80 ring is recruited to single stranded telomeres to process the ends and recruit DNA ligase which joins the telomeres of two chromosomes, creating a fusion. Taken together, TRF2 and POT1 are both indispensable for their role in protecting telomeres DNA damage repair activation (Palm and De Lange, 2008) (Fig. 1.2). The mechanism by which the absence of TRF2 and POT1 sensitizes the DNA damage repair response is unknown.

To protect telomeres from attrition, cells use mechanisms of telomere lengthening. For example, the bacteria Borrelia Borgdorferi *(the bacteria associated with Lyme disease)*, in which

chromosomes are linear, expresses telomere resolvase to maintain its telomeres (Mir et al., 2013). The resolvase acts in a two- step reaction: first it cleaves the chromosomes and creates a hairpin at the end of the cleaved telomeres creating a closed telomere end that rescues the chromosomes from the end replication problem (Mir et al., 2013). Importantly, human cells express telomerase to elongate chromosome ends.

While over 90% of cancer types maintain telomere length by expressing telomerase, 10% of cancer cell types such as glioblastoma multiforme and osteosarcoma use alternative lengthening of telomeres (Sarkar et al., 1995). In telomerase-negative cancer cells, alternative lengthening of telomeres is crucial in telomere protection and lengthening (Cesare et al., 2010). The phenomenon is characterized by telomere loops at the chromosome ends known as displacement (D) and telomeric (T) loops (Cesare et al., 2010). The D- and T-loops are formed by the invasion of the 3’ G-rich overhang, initiated by TRF2, into 5' double stranded telomeric region displacing the G-strand to base-pair with the C-rich strand (De Lange, 2004; Cesare et al., 2010). Following strand invasion and T loop stabilization, the DNA replication machinery elongates the 3’ overhang using the complementary telomeric C-strand to lengthen telomeres (De Lange, 2004). Hence, shelterin protein, TRF2, is essential in promoting T-loop formation, and lack thereof triggers DNA damage repair factors, resulting in resection and chromosomal fusions leading to apoptosis (Lim et al., 2021; Doksani et al., 2013).

Progressive telomere shortening decreases the amount of shelterin at chromosome ends, making telomeres vulnerable to recognition by the DNA damage repair factors as double stranded breaks (Takai et al., 2003). DNA damage repair pathway triggers activation of p53 and p16, known mediators of apoptosis and cell-cycle arrest (Fagagna et al., 2003). Therefore, triggering DNA damage at telomeres limits the proliferative potential, leading to cell senescence and apoptosis.

To combat telomere attrition, proliferating cells and stem cells express the telomerase ribonucleoprotein (RNP). The telomerase RNP recognizes, binds to and elongates the telomeric

3’ overhang, increasing telomere length and thereby extending the replicative capacity. Over 90% of cancer types have increased levels of telomerase RNP to maintain the length of telomere with successive cell divisions (Sarkar et al., 1995). Therefore, telomerase RNP is crucial in elongating telomeres to maintain the proliferative potential of cancer cells. In contrast, a dysfunction in the telomerase RNP is associated with short telomeres in a variety of multi-system diseases collectively known as the telomere syndromes (Armanios and Blackburn, 2012). Biallelic or monoallelic mutations in the components of the telomerase RNP are associated with telomere syndromes. Telomere syndromes are a set of pre-mature aging diseases defined by very short telomeres in human regenerative cells such as epithelial cells, skin, progenitor platelets, white and red blood cells. The following are examples of telomere syndromes:

1.3: Telomere syndromes

1. Dyskeratosis congenita can occur in autosomal recessive or dominant forms. Patients present with a triad of symptoms marked by hyperpigmentation, nail dystrophies and oral leukoplakia with increased risk of malignancies (Fernández et al., 2014). Mutations in TCAB1, DKC1, TERT, TR, NOP10 and NHP2 have been found in a fraction of patients with dyskeratosis congenita (Armanios and Blackburn, 2012; Zhong et al., 2010). 90% of patients exhibit severely short telomeres that are below the 1st percentile in length which increases their risk of bone marrow failure (Zhong et al., 2010; Fernández et al., 2014). Currently, the only treatments available to date for dyskeratosis congenita are hormone therapy and bone marrow transplant (Fernández et al., 2014).
2. Hoyeraal Hreiderson syndrome is an early pediatric syndrome marked by cerebellar hypoplasia, immunodeficiencies, bone marrow failure, and severe gastrointestinal complications (Glousker et al., 2015). HHS patients carry mutations in a variety of components of the telomerase RNP and the shelterin complex (Glousker et al., 2015).
3. Pulmonary fibrosis is an interstitial disease marked by thickening of alveolar and interlobular tissue within the lung, obstructing proper oxygen flow and exchange between

capillaries and alveoli. Pulmonary fibrosis is often associated with emphysema, chronic hypersensitivity, autoimmune diseases like scleroderma and rheumatoid arthritis, occupational exposure to chemical substances, or most commonly an idiopathic entity (Noble et al, 2012). One of the mutations that predispose to idiopathic pulmonary fibrosis is dysfunctions in telomerase RNP pathway as it may be associated with inherited or sporadic mutations in *TERT* and *TR*, leading to dysfunctions in telomere elongation (Armanios, 2012).

4. Aplastic anemia is the lack of development in red blood cells, platelets, and white blood cells and is often lethal due to bone marrow failure. Aplastic anemia has been associated with possible triggers such as parvovirus B19, Epstein-Barr, cytomegalovirus, chemotherapy and radiation and some antibiotics (Mayo Clinic). Mutations in patients with aplastic anemia have been linked to TERT mutations that result in reduced telomerase activity and short telomeres in leukocytes (Yamaguchi et al., 2005).
5. Liver cirrhosis: cirrhosis is associated with shortening in telomeres and reduction of TERT levels in hepatocytes. However, in hepatocellular carcinoma, patients can have TERT promoter mutations turn on TERT expression, leading to telomere elongation, thereby tumorigenesis and ultimately liver failure (Nault et al., 2019).

1.4: Telomerase anti-cancer therapies

In addition to the role of the telomerase RNP in telomere syndromes, it contributes to tumorigenesis. Current and past therapies that underwent clinical trials inhibited a compartment of the telomerase RNP in cancer models. Imetelstat is an oligonucleotide competitive inhibitor that base-pairs with the template region of TR, blocking TR binding to telomeres thereby depleting telomerase activity in cancer (Chiappori et al., 2015).). In clinical trials, imetelstat has been associated with toxic side effects such as anemia and thrombocytopenia (Chiappori et al., 2015). GV1001 is a vaccine that contains a TERT peptide that upon transduction, antigen presenting cells will present the peptide on their cell surface and induce cytotoxic damage in cancer cells

Despite the lack of adverse effects on bone marrow cells, clinical trials failed to show a significant survival advantage with GV1001 even with concurrent administration of chemotherapies (Mizuhoshi and Keneko, 2019; Middleton et al., 2014). Another vaccine, GRNVAC1, consists of TERT mRNA and a lysosomal protein that helps mediate TERT degradation into small peptides by facilitating cytotoxic T cell response against telomerase (Mizuhoshi and Keneko, 2019). Another potential inhibitor is BIBR1532, a small molecule inhibitor targeting TERT at the TR binding domain. An additional inhibitor is T-oligos that block TR binding to telomeres by binding TR at the template region. BIBR1532 and T-oligos are still in preclinical phases (George et al., 2020). Other inhibitors such as G-quadruplex stabilizers block telomerase association with the T loop (George et al., 2020). Therapies with less adverse side effects are still needed for cancer therapies. Defining the role of the telomerase RNP in cancer development and progression will uncover novel therapeutic targets for cancer and potentially premature aging diseases.

1.5: Components of the Telomerase Ribonucleoprotein

The human telomerase RNP is a 12-subunit complex consisting of TR, telomerase reverse transcriptase (TERT), telomerase Cajal body protein 1 (TCAB1), a histone H2A-H2B dimer, along with the H/ACA complex bound to each hairpin loop: dyskerin (DKC1), GAR1, Non-Histone Protein 2 (NHP2) and Nucleolar Protein 10 (NOP10) (Egan and Collins, 2012; Nguyen et al., 2018; Ghanim et al., 2021; Garus et al., 2021) (Fig. 1.3B). The following sections are details related to each component of the telomerase RNP and the roles they play in the complex:

Telomerase Reverse Transcriptase

TERT is a highly conserved gene among different organisms such as yeast, ciliates, Tetrahymena, and vertebrates (Greider and Blackburn, 1989; Harrington et al., 1997; Lingner et al., 1997; Nakamura et al., 1997). The reverse transcriptase motif in Est2p in yeast shares sequence similarity with RT in HIV-I and TERT in eukaryotes. In addition to TLC1 RNA and Est2p, Est1 and Est3 are also involved in the *S. cerevisiae* telomerase RNP (Lee et al., 2008). TERT

encodes the reverse transcriptase that is 127 kDa in size and 1132 amino acid in length in human cells.

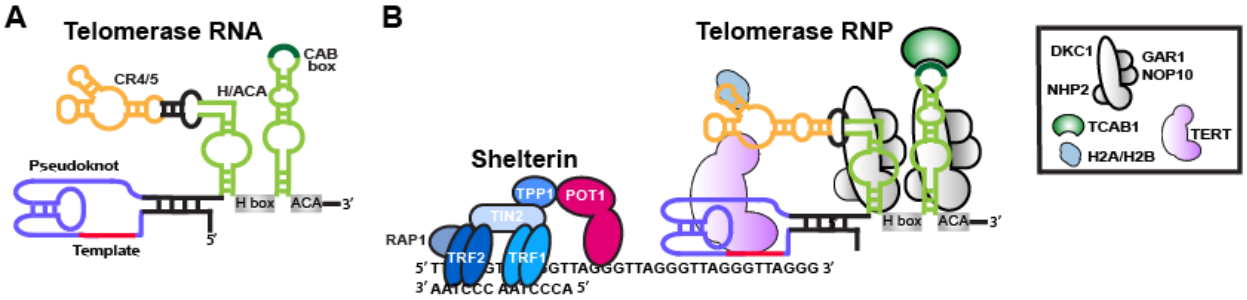

Figure 1.3. Components and motifs of the telomerase RNA, the telomerase ribonucleoprotein, and the shelterin complex. **(A)** Regions of the telomerase RNA: the pseudoknot, template, the Conserved Region (CR) 4/5 where TERT binds, the H/ACA domain where the H/ACA complex associates and the Cajal Body (CAB) box specific to TCAB1 binding. **(B)** The telomerase RNP components at the overhang of telomeres binding to the DNA substrate through the complementary RNA template. The shelterin components bridging the dsDNA and ssDNA regions protecting the chromosome ends.

The domain of TERT that renders it evolutionary conserved is the catalytic domain also known as the reverse transcriptase located in the C-terminal extension, Tetrahymena, and other non-eukaryotic species such as retroviral reverse transcriptase of HIV-I (Harrington et al., 1997; Peng et al., 2001). In addition to the reverse transcriptase domain, vertebrate TERT contains three other domains: a conserved TR binding domain and telomerase essential N-terminal domain (Steczkiewicz et al., 2011; Autexier and Lue, 2006). The pseudoknot domain of TR contacts multiple residues of TERT: the TR binding domain, the reverse transcriptase domain and the C-terminal domain (Nguyen et al., 2018; Ghanim et al., 2021). Residues in the C-terminal extension and the reverse transcriptase domain of TERT bind to the DNA substrate and stabilize the interaction during repeat elongation, contributing to processivity of the enzyme. The processivity is defined as the number of repeats synthesized before telomerase dissociation (Wang et al., 2007). In addition to TERT association with the pseudoknot of TR, the C-terminal extension of TERT also interacts with a residue in the CR4/5 region of TR creating another anchor for the stability of TERT association with TR (Nguyen et al 2018; Ghanim et al., 2021).

Current known *TERT* mutations in patients with autosomal dominant dyskeratosis congenita affect the reverse transcriptase domain, leading to a loss of function of TERT (Armanios et al 2005). On the contrary, TERT promoter mutations result in the production of TERT in a variety of cancer types, making them gain of function mutations (Huang et al., 2013; Borah et al., 2015; Shay et al., 2013). *TERT* promoter sporadic and hereditary mutations have been identified most frequently in human melanoma, glioblastoma, bladder, head and neck, hepatocellular cancers and urothelial cancers (Huang et al., 2013; Heidenreich et al., 2014). The incidence of *TERT* promoter mutations exceeds that of other common mutations such as BRAF and KRAS mutations in melanoma (Huang et al., 2013). *TERT* promoter mutations lead to increased transcriptional activity by 2-3 folds. Since TERT is a catalytic unit in the telomerase RNP, its increase leads to upregulation in telomerase activity (Borah et al., 2015; Huang et al., 2013; Shay et al., 2013). Consequently, upregulation of telomerase elongates telomeres, increasing the proliferative potential of cells (Chiba et al., 2017). In non-cancerous cells, the regulation of the telomerase RNP expression is dependent upon the cell type and developmental stage.

After birth, most human somatic cells silence the expression of TERT. However, cells that have a capacity to proliferate such as stem cells and cancer cells express telomerase. Telomerase expression is a way for cells to regulate their expansion. Another regulatory mechanism in the expression of TERT occurs at the developmental stage via alternative splicing (Penev et al., 2021). Alternative splicing that retains exon 2 is associated with increased TERT levels (in stem cells) while exon 2 skipping is associated with decreased TERT levels (in differentiated somatic cells).

Human fibroblasts do not express TERT to elongate telomeres limiting their potential to proliferate. Eventually fibroblasts undergo senescence or apoptosis resulting from telomere fusions due to lack of TERT or through the activation of the p53 and the pRB/p16 pathways, both of which prevent progression of cells into S phase thereby preventing indefinite growth (Wright et al., 2000). Human adult stem cells such as mesenchymal stem cells, mammary epithelial,

intestinal crypts express relatively lower levels of telomerase compared to other cells with higher proliferative capacity such as germ cells, embryonic stem cells, hematopoietic progenitor cells, and neural precursor cells in the brain (Hiyama et al., 2007). The difference in proliferation capacity is attributed to levels of TERT expression and telomerase activity. While TERT is a critical catalytic unit, it is alone not sufficient for telomere elongation. An additional component that makes up the catalytic unit is the telomerase RNA.

The Telomerase RNA

TR, a 451-nucleotide telomerase RNA, is transcribed by RNA polymerase II (Zaug et al.,, 1996; Mitchell et al., 1999). During maturation, the 3' end of TR undergoes a post-transcriptional modification. The Poly-A polymerase PAPD4/5 adds a poly-A tail to the 3' end of TR which is then recognized and digested by the exonuclease poly-A Ribonuclease (PARN, Moon et al., 2015). PARN is essential for the accumulation of TR and mutations in PARN are associated with telomere syndromes due to disruption in TR maturation (Moon et al., 2015). Dyskerin, a component of the telomerase RNP, is another protective factor for TR as it prevents the recognition of the 3' end of TR by exonucleases (Shukla et al., 2016). Without dyskerin or PARN, TR becomes vulnerable to exonucleases in the nucleus or cytoplasm by EXOSC10 or DCP2/Xrn1 respectively, leading to its decay (Shukla et al., 2016, 2020). In addition to the role of PARN in TR maturation, TR transcript also receives a trimethyguanosine cap at the 5' end which contributes to its accumulation and maturation (Jady et al 2004). The mature TR then assembles with the telomerase proteins either in the nucleus or the cytoplasm (Shukla et al., 2016). However, it is not established when and where TR is assembled with the rest of the telomerase proteins. It may assemble with some factors co-transcriptionally, in CBs, nucleoplasm or the cytoplasm.

TR contains three regions that are essential for the catalytic activity of the telomerase RNP: the CR4/5, pseudoknot and the template domain (Nguyen et al., 2018; Chen et al., 2018; Ghanim et al., 2021) (Fig. 1.3A). The TR template 3'-CAAUCCCAAUC-5' base-pairs with the TTAGGG repeats on the G-rich overhang of telomeres, only four bases at a time due

to obstruction of the first two nucleotides, TT, by the C-terminal extension of TERT. The 3' half of TR folds into two hairpin stem loops known as the H/ACA domain. The H/ACA region contributes to TR stability and trafficking of telomerase (Shukla et al., 2016). The H/ACA lobe consists of a hinge box followed by an ACA motif located between two stem loops (Mitchell et al., 1999). Each hairpin in the H/ACA lobe serves as a binding site for each heterodimer of the H/ACA complex: dyskerin, GAR1, NOP10 and NHP2 (Nguyen et al., 2018).

Most of the functional regions of TR are highly conserved among other species and other RNAs. *Tetrahymena thermophila* TR is 159 nucleotides in length, consisting of a template for reverse transcription, binding regions for TERT (template boundary element, pseudoknot and the stem-terminus element). The pseudoknot, conserved between *Tetrahymena thermophila* and human TR's, is essential for association with TERT (Jiang et al., 2015). The 3' end of the *T. thermophila* RNA is the stabilizing domain functionally homologous to the H/ACA binding complex and a uridine tail (Jiang et al., 2015). Unlike human TR which is transcribed by RNA polymerase II, transcription of ciliate TR is performed via RNA polymerase III (Egan and Collins, 2012). The 3' stem and the polyuridine tail serve as binding sites for p65, a component of the active complex that induces a folding change in TR to promote association with TERT contributing to TR and TERT stability and accumulation (Egan and Collins, 2012). Following the binding of p65-TERT to TR, a complex of factors, required for the activity, interacts with the RNP stabilizing it on the DNA substrate (Egan and Collins, 2012).

The telomerase RNA in yeast Saccharomyces *cerevisiae,* TLC1, is about 1000 bp in length, more than twice the length of the human TR. TLC1 consists of a template that base-pairs to telomeres, template boundary element, a pseudoknot, a stability element, and a stem-terminus element (Egan et al., 2012). The stem-terminus element interacts with Ku to drive localization to the nucleus and telomeres (Egan et al., 2012). In the maturation of TLC1, RNA polymerase II recruits a protein complex that terminates the transcription of the RNA, then a complex known as TRAMP (a yeast homolog of the human PAPD5) adds the poly-A tail which is later removed by

exosome to form a mature TLC1 (Egan et al., 2012). In addition, like TR, TLC1 also gets a trimethylguanosine cap that promotes its steady-state accumulation (Egan et al., 2021). The catalytic unit of *S. cerevisiae* telomerase RNP consists of TLC1 and Est2p which are the homologues of TR and TERT, respectively, and are essential in telomere maintenance in *S. cerevisiae.*

The H/ACA lobe is shared by other non-coding RNAs such as small Cajal body RNA (scaRNA) and small nucleolar RNAs (snoRNA) (Jady et al., 2004; Fu et al., 2003). In scaRNAs and snoRNAs, the H/ACA box is a binding site for factors that guide modifications of RNAs in the splicing pathway and ribosomal RNA pathway (Mitchell et al., 1999). However, the H/ACA domain in TR lacks a complementary target sequence to other RNAs therefore it is unlikely that TR has a guiding function for the modifications of RNAs like in snoRNAs and scaRNAs (Ergan et al., 2012). Importantly, within the H/ACA domain is a 4-nucleotide binding sequence, UGAG, called the Cajal body box (CAB) (Jady et al., 2004). The CAB region is also a highly conserved feature in scaRNAs and TR and is highly specific for TCAB1 binding (Jady et al., 2004). 3' of the CAB box is the biogenesis-promoting box (BIO) which enhances stability and accumulation of TR by interacting non-specifically with an additional telomerase RNP factor, NHP2 (H/ACA RNP subunit 2) (Ergan et al., 2012; Nguyen et al., 2018; Ghanim et al., 2021). A mutation in the fourth nucleotide of the CAB is sufficient to disrupt TCAB1 binding, telomerase localization, assembly and activity (Jady et al., 2004; Klump et al., 2023; Chen et al., 2018)

Familial mutations in TR have been associated with dyskeratosis congenita (Vulliamy et al., 2004). Strikingly, the majority of the associated mutations occur at the pseudoknot domain and notably in the stem loops of the H/ACA domain leading to instability and vulnerability of TR to exonucleases. The types of mutations that occur in TR are base changes and deletion mutations and these include regions in the 5' and 3' regions such as the pseudoknot (G143A, A117C, C116U, C72G, GC107-108AG, del79, del96-97, and del110-113), the template (del52-55 and A48G), the CR4/5 (G257U, C287G, G305A, G309U, G322A, C323U, and G325U) and other

regions such as the H/ACA domain (C408G, G450A, , del377-451, , del316-451) and a region that links the pseudoknot to the H/ACA domain (C204G) (Vulliamy et al., 2004; Chen et al., 2004). Patients with homozygous mutations in TR have shorter telomeres (Zhong et al., 2010). Therefore, in familial dyskeratosis congenita, the affected offspring has a younger onset of symptoms and shorter telomeres than the parent generation. Consequently, relative to age, short telomeres are indicative of severity of clinical manifestations (Armanios, 2022). Another type of mutation that obliterates TR levels in dyskeratosis congenita occurs in *DKC1, a Dyskerin pseudouridine synthase 1*, also known as dyskerin (Mitchell et al., 1999; Garus et al., 2021).

Dyskerin pseudouridine synthase 1

DKC1 is a highly conserved and abundant protein that resides in nucleoli and CBs of the nucleus. *DKC1* is located on the X chromosome and the protein contains 514 amino acids and is about 58 kDa in size (Garus et al., 2021). Dyskerin consists of lysine- and arginine-rich nuclear (NLS) and nucleolar localization signals (NoLS), pseudouridine synthase and archaeosine transglycosylase domain (PUA), and unstructured N- and C-terminal regions (Heiss et al., 1999; Garus et al., 2021). The domains of dyskerin are essential in ribosomal RNA (rRNA) processing and association with the telomerase RNP complex.

The most frequent dyskerin mutations in patients with dyskeratosis congenita include T66A and delL37 which are located in the N-terminal extension (Mitchell et al., 1999; Garus et al., 2021). The N-terminal extension contributes to changes in conformation upon associating with other proteins (Garus et al., 2021). The PUA, catalytic and RNA-binding domains of dyskerin bind small nucleolar RNA (snoRNA). SnoRNAs are coupled with a complex of dyskerin, GAR1, NHP2, and NOP10 known as the H/ACA complex (Kiss et al., 2006). SnoRNAs then guide dyskerin to ribosomal RNA and spliceosomal snRNA for pseudouridylation (Kiss et al., 2006).

Pseudouridylation is an isomerization reaction that converts uridine into 5-ribosyluracil carried out by the aspartate in the active site of the PUA in dyskerin (Sloan et al., 2017). Isomerization is the rotation of the base, uracil, by 180° replacing the uracil-ribose nitrogen bond

with a carbon bond. The resulting glycosidic bond between pseudouridines and the ribose provides stability, folding and maturation to the modified snRNA and rRNA (Sloan et al., 2017). Additionally, ribosomal regions that associate with the modifications on the rRNA are sites for tRNA binding and ribosomal subunit interactions thus rRNA modification is essential in ribosomal function (Sloan et al., 2017). The role of dyskerin in stabilizing TR from exonucleolytic digestion may be its main role in telomerase RNP as it does not serve a role in pseudouridylation of TR or using TR as a guide for pseudouridylation of other RNAs. The role of dyskerin and the H/ACA components is yet to be dissected in TR and snoRNAs. It is not determined whether snoRNAs and scaRNAs are impacted by dyskerin mutations in dyskeratosis congenita and whether those RNAs contribute to symptoms. Dyskeratosis congenita-associated mutations in TERT, TR, dyskerin mutations are often haploinsufficient (mutations in one allele is enough to cause a phenotype); however, other telomerase RNP mutations, such as those in TCAB1, are recessive. (Armanios and Blackburn, 2012).

Telomerase Cajal body protein 1

TCAB1, telomerase Cajal body protein 1 (also known as *WRAP53 or WDR79*), is a critical component in the telomerase RNP that is essential for telomere lengthening and is also known as WD40 repeat-containing antisense to TP53 (WRAP53). The first study on TCAB1 defined its role as a post-transcriptional regulator of *p53* (Mahmoudi et al., 2009). Up until 2009, the only known components of the telomerase RNP were TERT, TR, dyskerin, NOP10, NHP2 and GAR1. In 2009, Venteicher et al. identified another factor in the telomerase RNP; they identified a WD40-repeat containing protein in a purified telomerase RNP purification which they named TCAB1 (Venteicher et al., 2009). The following year, Savage et al. identified a TCAB1 loss-of-function mutation in the telomerase RNP in patients with dyskeratosis congenita exhibiting severely short telomeres (Savage et al., 2010). Given its critical association with telomeres, understanding the role and mechanism of TCAB1 in RNPs is essential in establishing TCAB1 as a potential target for therapeutic agents.

TCAB1, is 75 kDa in size and is 548 amino acids in length of which 285 amino acids yield seven WD40 repeats that make up the β propeller structure flanked by two disordered domains (Tycowski et al 2009; Bergstrand et al 2020). The highly conserved WD40-repeat domain in TCAB1 recognizes the specific 4-nucleotide UGAG sequence called the Cajal Body (CAB) Box in scaRNAs (Richard et al 2004; Tycowski et al 2009). Association of TCAB1 with RNPs requires recognition of the CAB motif and is required for overall function, localization and assembly with RNPs (Jady et al 2004; Venteicher et al 2009; Klump et al 2023). One study has suggested that the disordered N-terminus is not necessary for TCAB1 localization to Cajal bodies however the function of the disordered domains remains unknown (Mahmoudi et al. 2010).

Folding of TCAB1

For proper function within the cell, TCAB1 must be stabilized and folded by chaperones. The three most common chaperone complexes are HSP70, HSP90, and chaperonin (Freund et al., 2014) HSP70, HSP90 and chaperonin are ATP-dependent chaperones that mediate protein remodeling, maturation and trafficking (Genest et al., 2019). Certain chaperone complexes mediate folding of newly synthesized proteins and others mediate refolding of denatured proteins. An important example of chaperonins that mediate folding of nascent proteins is the TCP-1 Ring Complex (TRiC), a cytoplasmic protein that is arranged in a stack of two rings each containing 8 subunits. TRiC contributes to telomere length by mediating the folding of TCAB1 through its interactions with the WD40 domain (Freund et al., 2014). Curiously, TRiC-mediated TCAB1 folding and thereby association with TR are disrupted in dyskeratosis congenita patients with single amino acid mutations in the WD40 domain (Freund et al., 2014). Moreover, telomerase localization to Cajal bodies (CBs), where it typically resides, is also diminished in these patients. (Freund et al., 2014).

Sub-nuclear localization of TCAB1

TCAB1 resides in the CBs, a phase-separated subnuclear organelle in eukaryotic cells. CBs, previously named nucleolar accessory bodies by Santiago Ramon y Cajal, are subnuclear

structures and sites for post-transcriptional modification of snRNA and assembly of the spliceosome, histone gene transcription and mRNA processing, RNA polymerase assembly, and RNP maturation (Mahmoudi et al., 2009). CBs vary in size and number depending on the type of cells (Ogg and Lamond, 2002). They consist of a structural protein called coilin that is required for their maintenance (Stern et al., 2012). RNP complexes that contain non-coding RNAs reside in CBs where they guide RNA modification and RNP formation (Henriksson and Farnebo, 2015).

CBs contain the structural protein coilin that has been long been used as a CB marker (Morris, 2008). Coilin mediates efficiency of RNP complex assembly by enriching RNP components in CBs (Morris, 2008). Contents of CBs dynamically exchange with the nucleoplasm likely because some of the RNPs and factors only transiently localize to CBs; CBs are small and their capacity to hold RNPs is significantly less than that of other cellular compartments (Sleeman et al., 2003; Dundr et al., 2004). In proliferating cells, the number of CBs is greater than in non-dividing cells due to the increased RNA production and as a consequence RNA processing which requires CBs (Lemm et al., 2006).

TCAB1 interacts with non-coding RNAs, other than TR, called small Cajal body RNA (scaRNA) that are responsible for guiding modifications of spliceosomal RNAs and messenger RNAs. ScaRNAs mediate post-transcriptional pseudouridylation and methylation of snRNAs (Henriksson and Farnebo, 2015). ScaRNAs also guide the methyltransferase, fibrillarin, to snRNAs by complementary sequence binding (Darzacq et al., 2002; Jady et al., 2004). Importantly, TCAB1 is another factor in the maturation of the spliceosome complex. TCAB1 recruits scaRNAs to CBs by recognition of CAB box(es) on scaRNAs to guide modifications of snRNAs in the spliceosome (Mahmoudi et al., 2010). Absence of the CAB box prevents scaRNPs from binding TCAB1 and localizing to CBs (Kiss, 2002). The role of TCAB1 in CB formation is controversial; some studies suggest that TCAB1 is essential in forming CBs and others claim that it is not essential in CB formation (Chen et al., 2018; Stern et al., 2012; Chen et al., 2015; Mahmoudi et al., 2010). Nevertheless, TCAB1 is widely enriched in CBs and is implicated in a

variety of cellular functions: telomere elongation, spliceosome function, DNA repair and apoptosis.

The role of TCAB1 in cancer

Mutations in TCAB1 are associated with cancer progression. Prior studies have shown that TCAB1 is upregulated in colorectal cancer while a knockdown of TCAB1 is associated with apoptosis and cell cycle arrest reducing proliferation (Zhu et al., 2018). TCAB1 has also been shown to be upregulated in patients with poorer prognosis in patients with head and neck cancers and esophageal squamous cell carcinoma (Mahmoudi et al., 2011; Rao et al., 2014). Another study showed that patients with breast cancers that express less nuclear TCAB1 have reduced survival compared (Silwal-Pandit et al., 2015). It is possible that increased nuclear TCAB1 promotes telomere lengthening; however, it is unknown why TCAB1 localization may be different in high vs low grade breast cancer. Interestingly, TCAB1 has been proposed as a possible prognostic factor for several types of cancers (Zhang et al., 2012; Gadelha et al., 2022). Patients with telomere syndromes have increased risk of developing cancer, however the etiology and whether TCAB1 plays a role in the increased risk have yet to be dissected.

Other roles of TCAB1 in essential cellular functions

TCAB1 serves a role in the regulation of cell death (or apoptosis). Cells respond to accumulation of DNA damage by inducing apoptosis. P53 initiates the apoptotic response that may be mediated by TCAB1. *TCAB1* is located upstream of *p53* on chromosome 17. One of the alternatively spliced *TCAB1* transcripts shares an exon that is antisense to the first exon of *p53* mRNA (Mahmoudi et al., 2009). The complimentary binding of *TCAB1* to *p53* mRNAs promotes increased p53 mRNA and protein levels hence the other name for TCAB1, WRAP53. However, p53 has no reciprocal regulatory role on TCAB1 (Mahmoudi et al., 2009).

Importantly, TCAB1 plays a role in DNA damage repair. Upon a double stranded DNA break, MDC1 associates with TCAB1 at double stranded DNA breaks and that TCAB1 then recruits downstream repair factors to enable DNA repair (Henriksson et al., 2014). It has also

been noted by the same group that Hoyeraal-Hreidarsson patient mutations have a deficiency in the recruitment of DNA repair factors correlated to a loss of function of TCAB1 (Bergstrand et al., 2020).

TCAB1 is also involved in neuromuscular diseases such as spinal muscular atrophy, a hereditary disease marked by muscle wasting and respiratory failure (Markowitz et al., 2012). The Survival of Motor Neuron (SMN) complex plays an essential role in the assembly of spliceosomal RNPs (Pellizzoni et al., 2002). TCAB1 mediates the recruitment SMN to CBs where spliceosomal RNP assembly is thought to occur. Spinal muscular dystrophy patients with mutations in *SMN1* have reduced interactions with TCAB1 and lack of localization at CBs (Hebert et al., 2001; Mahmoudi et al., 2010). Therefore, SMN recruitment to CBs via TCAB1 is an essential mechanism that if dysfunctional may lead to neuromuscular disorders (Mahmoudi et al., 2010).

TCAB1 in premature aging diseases

In 2010, Savage et al. (2010) found a *TCAB1* mutation in a premature aging disease, dyskeratosis congenita, linked with telomerase RNP loss of function. Patients with dyskeratosis congenita had below the 1st percentile for telomere length (Zhong et al., 2010). Loss of TCAB1 has also been associated with other premature aging diseases such as Hoyeraal-Hreidarsson, a form of progeria, and Revesz syndrome (Armanios, 2012). Patients with these severe premature aging diseases present with developmental delays, immune deficiency, aplastic anemia and a short life span expectancy due to bone marrow failure. Bone marrow failure is associated with loss of proliferation of progenitor red blood cells, immune cells and platelets; lack of proliferation of progenitor cells is due to very short telomeres. The diseases associated with short telomeres are also termed telomere syndromes. Mutations in TCAB1 and other proteins described above (TERT, TR, DKC1, PARN, TINF2, NHP2 and NOP10) are associated with telomere syndromes. In patients with Hoyeraal-Hreidarsson, the WD40 domain of *TCAB1* (L283W and R398W) are mutated in both alleles (Bergstrand et al., 2020; Vulliamy et al., 2008; Walne et al., 2007). The

TCAB1 mutations in dyskeratosis congenita, known to date, are L298W, F164L, H376Y, R398W and G435R and also fall within the WD40 domain (Shao et al., 2018; Zhong et al., 2011).

1.6: Telomerase RNP assembly, recruitment and telomere synthesis and protection

There are three steps that are important for telomere elongation: telomerase assembly, recruitment to telomeres, and telomere synthesis. Telomere elongation requires an active telomerase at chromosome ends. The catalytically active components of telomerase are TR and TERT (Greider, 1990).

Shelterin and telomerase recruitment and regulation:

The major pathway that is associated with the regulation of telomerase recruitment to telomeres is the shelterin complex (Palm and De Lange, 2008). TPP1 enhances telomerase recruitment to telomeres and promotes telomerase processivity (Wang et al., 2007). In contrast, POT1 plays a regulatory role in telomerase; POT1 accumulation on a 3' overhang blocks telomerase from binding onto telomeres, thus negatively regulating telomere elongation (Kelleher et al., 2005). Importantly, deletion of the DNA-binding region of POT1 prevents its accumulation at the overhang, allowing for telomerase binding while POT1-TPP1 mediated telomerase recruitment remains intact independent of POT binding to DNA (Loayza et al., 2003). POT1-TPP1 mediated telomerase recruitment depends on the association of TPP1 with the N-terminus of TERT (Schmidt et al., 2014). The function and structure of shelterin is conserved among other species. In yeast, Est3 is involved in regulation of telomere maintenance and contains an oligo-binding domain structurally similar to that of TPP1 in eukaryotic cells. Like the shelterin protein TPP1, Est3 is also involved in the recruitment of telomerase and telomere protection (Lee et al., 2008). Thus, shelterin plays multiple roles in protecting telomeres and a dual role in telomerase recruitment and regulation.

Telomerase recruitment and the cell cycle

A mammalian cell goes through the cell cycle to replicate its DNA and then divides into daughter cells. Dysfunctions in the cell cycle regulation leads to uncontrolled cell divisions thereby promoting cancer progression (Mercadante et al., 2022). The somatic cell cycle is unequally divided into interphase and mitosis. Interphase consists of three stages: G1, S, and G2. Cells spend most of their time in the G1 undergoing gene expression in preparation for DNA replication. In the S phase, DNA undergoes replication. In the G2 phase, cells grow and express proteins in preparation for mitosis for division. Instead of returning to G1, a cell destined for apoptosis or senescence enters G0. In mitosis, the replicated chromosomes condense and segregate into two daughter cells. There are many known factors that regulate the cell cycle to prevent or promote cell division at the proper place and time. These factors include checkpoint signals such as cyclin and cyclin-dependent kinases, tumor repressors, oncogenic factors, and DNA damage repair proteins.

Importantly, cell cycle regulation is also associated with the telomerase RNP. In cells that proliferate to establish differentiation, TERT expression stays on until cells are differentiated. Once differentiated, cells reversibly turn off telomerase expression to enter senescence (Holt et al., 1996). Like stem cells, some somatic cells such as hepatocytes, epithelial cells of the skin and gastrointestinal tract also proliferate beyond differentiation. Proliferating cells express differential amounts of telomerase depending on the cell type and proliferating capacity. Embryonic stem cells and cancer cells express significantly more telomerase than dividing somatic cells (Hiyama et al., 2007). In dividing cells, telomerase is expressed throughout the cell cycle except if the cell is destined for senescence, the expression of telomerase decreases substantially (Hiyama et al., 2007). A study in 1996 shows that telomerase activity peaks in S phase but is almost abolished in G2/M phase in colon carcinoma cells (Zhu et al., 1996); however, Holt et al., (1997) show that telomerase activity does not differ among cell cycle phases in a prostate carcinoma cell line.

Some steps in the telomerase RNP function are dependent on the cell cycle. It has been previously shown that telomerase recruitment to telomeres is cell-cycle dependent (Jady et al 2006). TR and TERT foci localize at the telomeres during S phase and do not localize throughout the rest of the cycle (Tomlinson et al., 2006; Jady et al., 2006). However, not all steps in the telomerase RNP are associated with the cell cycle. Our recent study establishes that TCAB1-mediated telomerase RNP assembly is not dependent upon the cell cycle (Klump et al., 2023). The mechanism of cell cycle dependent telomerase recruitment to telomeres is still undetermined.

The role of TCAB1 in telomerase RNP recruitment, assembly, and telomere maintenance.

TCAB1 is a critical factor in the telomerase RNP and its absence is detrimental to telomere elongation (Chen et al., 2018). TCAB1 has been shown to be essential in telomerase recruitment to telomeres (Stern et al., 2012). Localization of telomerase to chromosome ends requires an assembled RNP. There are controversies regarding the role of coilin in telomerase recruitment. Some studies suggest that telomerase recruitment to telomeres requires an intact CB containing coilin and TCAB1 (Stern et al., 2012). The work by Stern et al showed that inhibiting coilin or TCAB1 with siRNAs significantly reduces telomerase localization at telomeres. However, they propose that coilin does not directly impact catalysis of telomerase since coilin is not involved in the telomerase complex. Interestingly, overexpression of telomerase overcomes the need for coilin but not for TCAB1; TCAB1 remains essential in mediating telomerase localization (Stern et al., 2012). In contrast, work by Chen et al. (2018) propose that telomere length is unaffected by absence of coilin over time creating a controversy to the role of coilin in telomerase pathways. The same group suggests that TCAB1 is not only required for telomerase recruitment to telomeres but also to CBs (Venteicher et al., 2009).

The same group showed that TCAB1, has also been proposed that it is not essential for telomerase activity (Venteicher et al., 2009). Later, they argue that TCAB1 is indeed involved in the catalytic activity (Chen et al., 2018). Chen et al. (2018) claimed that in the absence of TCAB1, the CR4/5 region of TR does not fold properly thereby disrupting TR interactions with TERT. They

claim that the folding defect is not sufficient to disrupt assembly with TERT but impacts catalytic activity of TERT. However, Nguyen et al. (2018) in the cryo-EM structure of telomerase RNP discover that the CR4/5 region is not in close proximity to TCAB1 on the TR, therefore, it is unlikely for TCAB1 to affect the folding of CR4/5. Importantly, Chen et al. (2018) claim that telomerase assembly is unaffected by the absence of TCAB1 which was refuted by our study using multiple approaches to assess assembly (Klump et al., 2023). However, the caveat to their study is the lack of quantitative analysis and comparison to controls. Observing no qualitative difference does not exclude the possibility of observing a quantitative difference. For example, observing no differences in TR band intensities among samples on a northern blot may be attributed to differences in RNA extraction or loading of the sample into the gel. Therefore, quantitative analysis in the context of assembly analysis must be carried out (Klump et al., 2023). In addition, Chen et al. (2018) used a lysis buffer that contains a much higher salt concentration that has been shown to disrupt nucleoli (Klump et al., 2023) potentially yielding telomerase assembly in vitro (Holt et al 1999).

TR and TERT can assemble and function in vitro (Weinrich et al., 1997; Beattie et al., 1998; Holt et al., 1999). However, physiologically, there are barriers and regulators that associate with the telomerase RNP, impacting telomerase assembly, localization and activity (Holt et al., 1999; Schmidt et al., 2015). The factors that mediate telomerase assembly are not agreed upon. Proteins that are claimed to promote telomerase assembly are p23 and Hsp90; however, the authors addressed telomerase “assembly” by measuring a downstream effect, telomerase activity (Holt et al., 1999). They neglected to directly quantify telomerase assembly (Holt et al., 1999). The observed reduction in telomerase activity upon inhibition of p23 may be due to misfolding of TERT, yielding dysfunctions in its catalytic activity. Further biochemical analysis studies are needed to uncover the specific roles of Hsp90 and p23 in the telomerase complex by analyzing TERT stability, telomerase recruitment, localization and assembly.

Therefore, we sought to properly define the role of TCAB1 in telomerase assembly using a variety of approaches in lysate, fixed, and living cells (Klump et al., 2023). We generated TCAB1 knockout cells in HeLa cells using CRISPR Cas9 and two guide RNAs (sgRNA) to guide the excision of exons 2 and 3, leading to a frameshift in the sequence and loss of TCAB1 protein in the cell. Our first approach in measuring assembly was a biochemical technique. We first immune-purified TERT using an antibody then quantified co-purified TR by normalizing its levels to an internal control. We carried out this process with the endogenous telomerase and found that telomerase assembly is only 20-40% in TCAB1 knockout compared to wild type HeLa cells. We next applied this method with overexpressed telomerase, which is frequently used in prior studies to dissect telomerase activity, structure and localization. We found that overexpressed telomerase does not override the role of TCAB1 in the assembly of the telomerase RNP

Our next approach was in living cells using single molecule imaging, where we found that >90% TERT is localized in the nucleoplasm, is freely diffusing and not assembled with the telomerase RNP. We applied a newly established technique in living cells to measure validate our findings on RNP assembly, leading to the discovery that absence of TCAB1 is associated with absence of TERT on TR, further confirming reduced assembly in absence of TCAB1 (Fig. 1.4; unpublished data; chapter 3) Another new approach that we used is described in chapter 3 of this dissertation. Dissecting the role of TCAB1 in the telomerase RNP will uncover potential therapeutic targets in cancer and premature aging diseases. In the next section, I outline our recent study in the role and mechanism of TCAB1 in promoting the telomerase RNP (Klump et al., 2023).

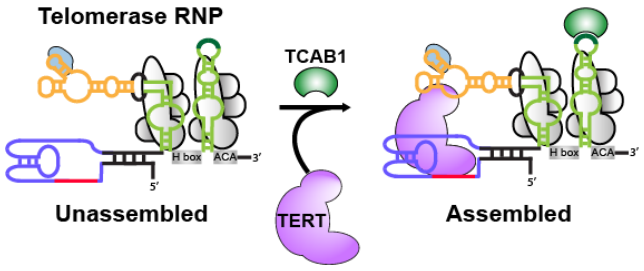

Figure 1.4. The role of TCAB1 in telomerase assembly. The telomerase ribonucleoprotein in

Figure 1.4 (cont'd)

an unassembled state in the absence of TCAB1. When TCAB1 is present, TR assembles with TERT required for RNP catalytic function.

CHAPTER 2: TCAB1 PREVENTS NUCLEOLAR ACCUMULATION OF THE TELOMERASE RNA TO PROMOTE TELOMERASE ASSEMBLY

Basma M. Klump, Gloria I. Perez, Eric M. Patrick, Kate Adams-Boone, Scott B. Cohen, Li Han, Kefei Yu, Jens C. Schmidt.

2.1: Abstract

Localization of a wide variety of RNAs to non-membrane bound cellular compartments such as nucleoli, Cajal bodies, and stress-granules is critical for their stability and function. The molecular mechanisms that underly the recruitment and exclusion of specific RNAs from these phase-separated organelles is incompletely understood. Telomerase is a ribonucleoprotein (RNP) that is composed of the reverse transcriptase protein TERT, the telomerase RNA (TR), and several auxiliary proteins that associate with TR, including TCAB1. Here we show that in the absence of TCAB1, a large fraction of TR is tightly bound to the nucleolus, while TERT is largely excluded from the nucleolus, significantly reducing telomerase assembly. This suggests that nuclear compartmentalization by the non-membrane-bound nucleolus counteracts telomerase assembly and TCAB1 is required to retain the telomerase RNA in the nucleoplasm. Our work provides insight into the mechanism and functional consequences of RNA recruitment to organelles formed by phase separation and proposes a new model explaining the critical role of TCAB1 in telomerase function.

2.2: Introduction

Human cells contain a number of non-membrane-bound organelles that carry out critical cellular functions. For instance, nucleoli and Cajal bodies are phase-separated nuclear organelles that play important roles in the biogenesis and maturation of many cellular RNAs (Hyman et al., 2014; Mitrea and Kriwacki, 2016). Nucleoli and Cajal bodies contain a wide range of small nucleolar and small Cajal body-specific RNAs (snoRNAs and scaRNAs, respectively). A subset of these snoRNAs and scaRNAs are bound by the H/ACA complex, which contains NOP10, NHP2, GAR1, and the pseudouridylase dyskerin, which modifies ribosomal and spliceosomal

RNA precursors and other RNAs (Angrisani et al., 2014). A key difference between snoRNAs and scaRNAs is the presence of the Cajal-body box (CAB-box) motif in scaRNAs that directly associates with the telomerase Cajal body protein 1 (TCAB1, also known as WRAP53) (Jády et al., 2004; Schmidt and Cech, 2015; Venteicher et al., 2009). TCAB1 is required for the recruitment of scaRNAs to Cajal bodies and scaRNAs localize to the nucleolus when the CAB-box is mutated (Jády et al., 2004; Tycowski et al., 2009; Venteicher et al., 2009). Therefore, TCAB1 controls which phase-separated nuclear organelle scaRNAs associate with. Importantly, the molecular mechanism by which TCAB1 drives exclusion of scaRNAs from the nucleolus and facilitates their recruitment to Cajal bodies is unknown. In addition, it is unclear whether mislocalization of scaRNAs to the nucleolus has functional consequences.

The telomerase RNA (TR) is a scaRNA and, like other scaRNAs, its association with nucleoli and Cajal bodies is controlled by TCAB1 (Schmidt and Cech, 2015). Telomere maintenance by telomerase is essential for continuous proliferation of stem cell populations in the human body, and most cancers require telomerase activity for their survival (Stewart and Weinberg, 2006). To compensate for the incomplete replication of chromosome ends, telomerase appends TTAGGG repeats to the telomeric single-stranded overhang (Schmidt and Cech, 2015). Telomerase-mediated telomere maintenance requires three critical steps: telomerase assembly, telomerase recruitment to telomeres, and telomeric repeat synthesis (Schmidt and Cech, 2015). Mutations in several genes have been identified that cause deficiencies in one of these critical steps and lead to a variety of diseases known as telomere syndromes, which are characterized by premature depletion of stem cell populations (Armanios and Blackburn, 2012). In addition, telomerase is inappropriately activated in >90% of cancers (Stewart and Weinberg, 2006). While telomerase recruitment to telomeres (Nandakumar and Cech, 2013) and telomerase catalysis (Wu et al., 2017) have been studied extensively, much less is known about telomerase assembly. Importantly, telomerase assembly could be targeted to reduce telomerase activity in cancer cells,

or to increase telomerase function in patients affected by genetically-defined telomerase deficiency syndromes (Nagpal et al., 2020; Shukla et al., 2020).

Telomerase is a complex ribonucleoprotein (RNP). The core components of telomerase are the telomerase reverse transcriptase (TERT) protein, TR, the H/ACA complex, and TCAB1 (Schmidt and Cech, 2015). The primary function of the H/ACA complex is to stabilize TR, by directly binding to its 3'-end, preventing the exonucleolytic degradation of TR (Stuart et al., 2015; Tummala et al., 2015). The 3'-end formation of TR is tightly regulated by the competing activities of the poly-(A) polymerase PAPD5 and the nuclease PARN (Shukla et al., 2016; Tseng et al., 2015). Loss of TCAB1 function leads to telomere attrition in a variety of cell lines (Chen et al., 2018; Venteicher et al., 2009; Vogan et al., 2016; Zhong et al., 2011). In addition, multiple mutations in TCAB1 have been identified that cause misfolding of TCAB1 and lead to dyskeratosis congenita, a telomere syndrome (Freund et al., 2014; Zhong et al., 2011). While these observations highlight that TCAB1 is necessary for telomere synthesis, the underlying molecular mechanism is unclear. Initially, it was proposed that TCAB1 is required for telomerase recruitment to telomeres (Stern et al., 2012; Venteicher et al., 2009). A more recent study suggested that TCAB1 is required for the correct folding of TR, and that its absence results in a reduction in telomerase activity (Chen et al., 2018). All previous studies claim that TCAB1 does not mediate telomerase assembly, a critical step in telomere maintenance.

Here, we analyze telomerase assembly in intact cells and, by purification of the telomerase RNP, demonstrate that contrary to previous findings, TCAB1 promotes telomerase assembly *in vivo.* In the absence of TCAB1, a large fraction of TR is tightly associated with the nucleolus while TERT is largely excluded from the nucleolus. This spatial separation of TERT and TR, in the absence of TCAB1, is incompatible with proper telomerase assembly. Furthermore, we show that the limited amount of telomerase that can assemble in the absence of TCAB1 is fully active, suggesting that TCAB1 is not necessary for the enzymatic function of telomerase. Finally, analysis of the sub-cellular dynamics of TCAB1 revealed that it rarely enters the nucleolus, suggesting that

TCAB1 associates with TR in the nucleoplasm and prevents its entry into the nucleolus rather than extracting TR molecules from the nucleolus. Collectively, our results support a model in which TCAB1 facilitates telomerase assembly by promoting nucleoplasmic accumulation of TR to increase encounters with TERT, which is also localized in the nucleoplasm. Furthermore, our observations suggest that the nucleolar phase separation constitutes a barrier for telomerase RNP assembly and that incompletely assembled telomerase RNPs are associated with the nucleolus and do not readily enter the nucleoplasm. Thus, it raises the possibility that cellular compartmentalization by phase-separated organelles, such as the nucleolus, can directly regulate RNP function in human cells.

2.3: Results

2.3.1: Loss of TCAB1 leads to nucleolar accumulation of TR

To assess whether TR is sequestered in the nucleolus, in the absence of TCAB1, we knocked out TCAB1 in HeLa cells and in HeLa cells expressing 3xFLAG-HaloTag-TERT (Halo-TERT) using Cas9 with two guide RNAs to delete exons 2 and 3 from the TCAB1 gene, which removes the coding sequence for residues 144-214 of TCAB1 and results in a frame shift (Fig. A1A). TCAB1 knock-out was validated by Southern blot, PCR, western blot, and immunofluorescence imaging (IF, Fig. 2.1A-C, Fig. A1B-C). To assure that no truncated form of TCAB1 was expressed in TCAB1 knock-out cells, we analyzed TCAB1 expression using two antibodies, targeting the N-terminus and C-terminus of TCAB1, respectively (Fig. A1D). Both HeLa and Halo-TERT TCAB1 knock-out cell lines continuously grew at approximately 60% of the rate of their parental cell lines (Fig. 2.1D).

Telomeres in cells lacking TCAB1 were stable over time at a shorter length than telomeres in control cells, as previously described (Fig. A1E) (Vogan et al., 2016). Fluorescence *in situ* hybridization (FISH) demonstrated that TR accumulated in the nucleolus in cells that lack TCAB1, as indicated by co-localization of TR and nucleolar dyskerin signals (Fig. 2.1C). To confirm the dyskerin signal marks nucleoli, we transiently expressed HaloTag-dyskerin and GFP-NPM1, a

well-established marker of the granular component (GC) of the nucleolus, in control and TCAB1 knock-out cells. Dyskerin was enriched in nucleolar regions with low NPM1 intensity in the presence and absence of TCAB1 (Fig. A1F), consistent with previously observed localization of dyskerin to the dense fibrillar component (DFC) of the nucleolus (Yao et al., 2019). Importantly, expression of GFP-TCAB1 in TCAB1 knock-out cells rescued TR localization to Cajal bodies (Fig. 2.1E), confirming that the mislocalization of TR to nucleoli is caused by absence of TCAB1. These observations demonstrate that TCAB1 is required to prevent TR accumulation in nucleoli.

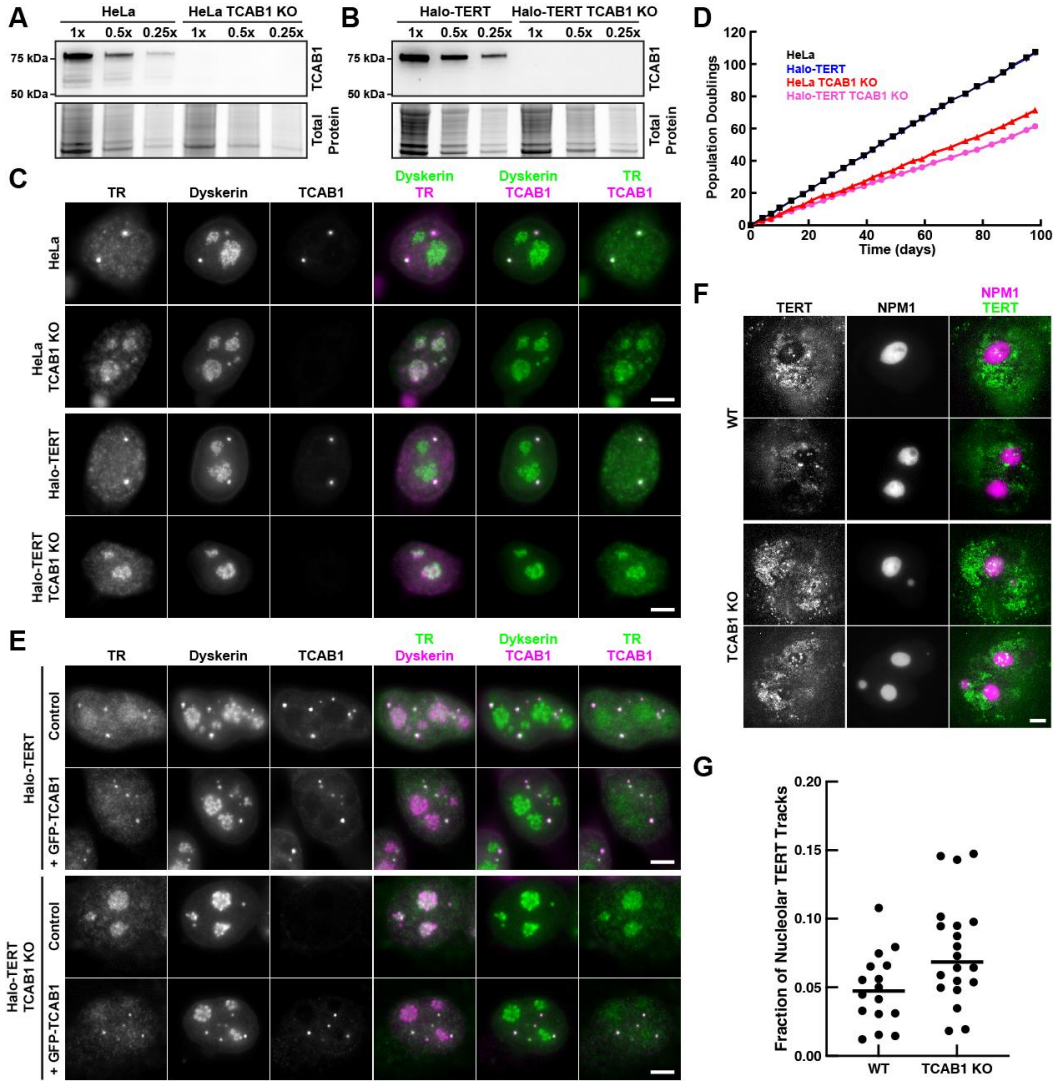

Figure 2.1. TR is localized to nucleoli in TCAB1 knock-out cells. (A-B) Western blot demonstrates the absence of TCAB1 protein in TCAB1 knock-out cell lines generated from

Figure 2.1 (cont'd)

(A) HeLa and **(B)** Halo-TERT parental cell lines (probed with Proteintech TCAB1 antibody). **(C)** Immuno-fluorescence with anti-dyskerin and anti-TCAB1 antibodies coupled to fluorescence in-situ hybridization with probes against TR, demonstrating the absence of TCAB1 and TR localization to nucleoli in TCAB1 knock-out cells (scale bar = 5 μm). **(D)** Growth rate of parental and TCAB1 knock-out cell lines. **(E)** Immuno-fluorescence with anti-dyskerin and anti-TCAB1 antibodies coupled to fluorescence in-situ hybridization with probes against TR, demonstrating that expression of GFP-TCAB1 in TCAB1 knock-out cells rescues TR localization to Cajal bodies (scale bar = 5 μm). **(F)** Maximum intensity projection (1000 frames at 10 ms per frame) of HaloTag-TERT (JFX650) in control and TCAB1 knock-out cells expressing GFP-NPM1 to mark nucleoli (scale bar = 5 μm). **(G)** Quantification of the fraction of TERT trajectories that overlap with the nucleolus in control and TCAB1 knock-out cells.

2.3.2: TERT is not enriched in nucleoli in the absence of TCAB1

Our previous observations demonstrated that TERT does not enter nucleoli in wild type human cancer cells (Schmidt et al., 2016). To test whether TERT, like TR, is enriched in nucleoli in the absence of TCAB1, we performed single-molecule imaging of 3xFLAG-HaloTag-TERT in living HeLa and TCAB1 knock-out cell lines transiently expressing GFP-NPM1 as a nucleolar marker. 3xFLAG-HaloTag-TERT was largely excluded from the nucleolus in the presence and absence of TCAB1 with a small number of TERT molecules localizing to nucleoli marker by NPM1 (Fig. 2.1F, Movies S1-2). Single-particle tracking revealed that 4.9% and 7.7% of TERT trajectories overlapped with the nucleolus in control and TCAB1 knock-out cells, respectively (Fig. 2.1G). To exclude the possibility that nucleolar exclusion is a consequence of the 3xFLAG-HaloTag on the N-terminus of TERT used in our experiments, we transiently expressed the 3xFLAG-HaloTag fused to a nuclear localization sequence (NLS) in HeLa cells. Single-molecule imaging demonstrated that the nuclear 3xFLAG-HaloTag signals overlapped with nucleoli (Fig. A1G-H, Movie S3). Similar to the 3xFLAG-HaloTag alone, 3xFLAG-HaloTag-dyskerin also localized to nucleoli (Fig. A1F). These results demonstrate that 3xFLAG-HaloTag-TERT is largely excluded from the nucleolus in the presence and absence of TCAB1 and that this exclusion is not caused by the 3xFLAG-HaloTag but instead is an intrinsic property of TERT. In contrast, TR accumulates in the nucleolus in the absence of TCAB1 which demonstrates that the vast majority

of TERT does not co-localize with TR in cells lacking TCAB1 suggesting that TERT may not be assembled with TR.

2.3.3: TCAB1 promotes telomerase RNP assembly

Previous studies by other laboratories have concluded that telomerase assembly is unaffected by the absence of TCAB1 and whether TCAB1 is required for telomerase activity is controversial (Chen et al., 2018; Venteicher et al., 2009; Vogan et al., 2016). Importantly, telomerase assembly was only qualitatively assessed in these studies. To quantitatively analyze the role of TCAB1 in telomerase assembly, we immuno-purified endogenous telomerase using a well-established anti-TERT antibody (Cohen et al., 2007). The amount of TERT purified from TCAB1 knock-out cells was reduced to 80% and 50% for the two independent TCAB1 knock-out clones compared to control cells (Fig. 2.2A), which likely indicates a lower expression level of TERT in cells lacking TCAB1. Surprisingly, TR levels were increased ~2-fold ($p < 0.02$) in cells lacking TCAB1 compared to parental controls in both TCAB1 knock-out clones (Fig. 2.2B). To quantify telomerase assembly, we measured TERT levels by western blot and determined the amount of TR co-purified using Northern blot (Fig. 2.2A,B). The amount of TR associated with TERT relative to total cellular TR was reduced to <20% in TCAB1 knock-out cells compared to parental controls (Fig. 2.2B-C). In addition, the ratio of TR relative to TERT, which is a direct measure of telomerase assembly, was reduced to 20-40% in cells lacking TCAB1 relative to controls (Fig. 2.2A-B,D). This excludes the possibility that the lower amount of TR co-purified with TERT from TCAB1 knock-out cells is a consequence of the reduction of total TERT immuno-precipitated from these cells (Fig. 2.2A,D). These observations strongly suggest that telomerase assembly is defective in cells lacking TCAB1.

To verify that the reduction in telomerase assembly observed in TCAB1 knock-out cells is a consequence of the inability of TR to interact with TCAB1, rather than an indirect effect in these slowly growing cells, we overexpressed TERT and a previously described CAB-box mutant (G414C) of TR that disrupts the TCAB1 interaction site in parental HeLa cells (Egan and Collins,

2010; Jády et al., 2004). Similar to wildtype TR in TCAB1 knock-out cells, TR^{G414C} was enriched in nucleoli (Fig. A2A), consistent with previous findings (Jády et al., 2004). Compared to wildtype TR, telomerase assembly was significantly reduced to about 54% in parental HeLa cells expressing TR^{G414C} (Fig. 2.2E-I). The increased amount of telomerase purified after overexpression allowed us to assess telomerase assembly by measuring the amount of dyskerin and GAR1 associated with TERT via TR, which showed a similar reduction in telomerase assembly by ~50% in cells expressing TR^{G414C} compared to wildtype TR (Fig. 2.2F,I). We also confirmed that TCAB1 did not associate with TERT purified from cells expressing TR^{G414C} (Fig. 2.2F,I).

To assure that reduction of telomerase assembly observed in the absence of TCAB1 was not a result of altered TR and TERT expression in the TCAB1 knock-out cells (Fig. 2.2A,B), we overexpressed TERT and TR in parental and TCAB1 knock-out cells and immuno-purified TERT (Fig. A2B-L). Consistent with a reduction in telomerase assembly, both TR and dyskerin associated with TERT purified from TCAB1 knock-out cells was significantly reduced to ~20-30% compared to parental controls (Fig. A2B-L).

Finally, to assure that the reduction in telomerase assembly observed in TCAB1 knock-out cells is not a consequence of an altered cell cycle distribution of cells that lacked TCAB1, we purified telomerase from cells sychronized in various stages of the cell cycle. Due to the slow growth of the TCAB1 knock-out cells, a double thymidine block was not feasible. We therefore synchronized cells using thymidine for 24 hours, released and harvested cells immediately (early S phase), 4 hours (mid S phase), and 8 hours (G2/M phase) after release. Cell-cycle synchronization was confirmed by DNA content analysis using propidium iodide staining and flow cytometry (Fig. A2M). Telomerase assembly was reduced in TCAB1 knock-out cells in all cell cycle stages analyzed (Fig. A2N-P). This demonstrates that the reduction of telomerase assembly observed in cells lacking TCAB1 is not a consequence of an aberant cell-cycle distribution of TCAB1 knock-out cells. Altogether, these results demonstrate that telomerase assembly is

significantly reduced in the absence of TCAB1 and when the TR-TCAB1 interaction is disrupted by expressing a TR with a mutated CAB-box.

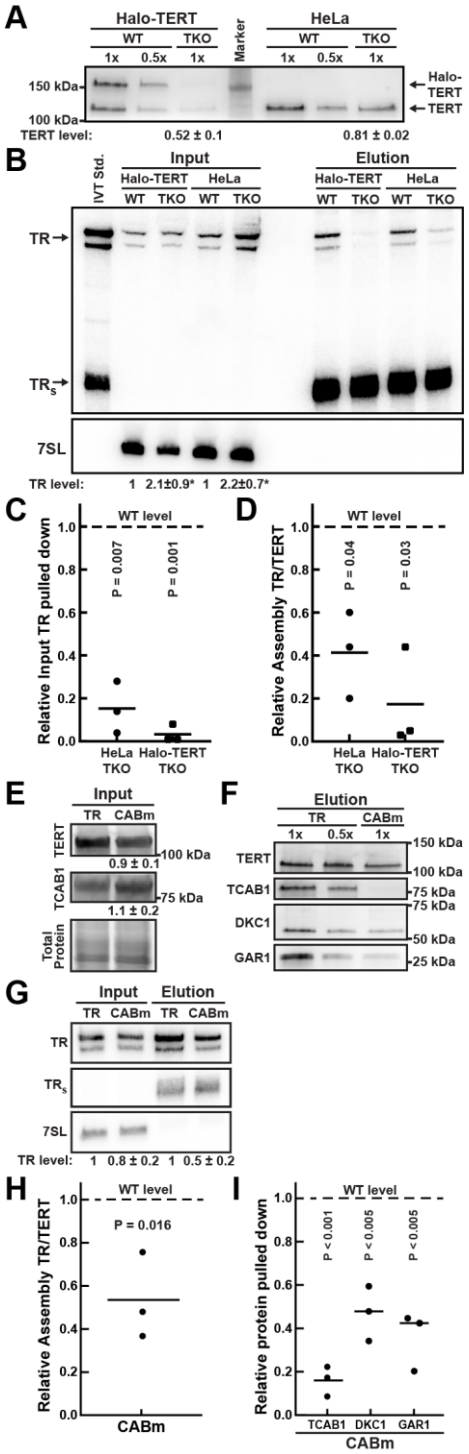

Figure 2.2. Telomerase Assembly is reduced in the absence of TCAB1. (A) Western blots analyzing endogenous TERT immuno-purification (using a sheep anti-TERT antibody) probed with a rabbit anti-TERT antibody (Abcam). TERT level normalized to WT (n = 6, SEM).

Figure 2.2 (cont'd)

(B) Northern blot of RNA extracted from input and purified endogenous TERT samples probed with radiolabeled DNA oligonucleotides complementary to TR. Standards are *in vitro* transcribed full-length TR and truncated TR_S. TR_S was added to samples prior to RNA extraction as loading and recovery control. Input samples were also probed for 7SL RNA as loading control. Input TR levels relative to WT control normalized to 7SL RNA (n = 3, SD). **(C-D)** Quantification of the amount of **(C)** TR purified relative to input RNA levels, and **(D)** the ratio of TR relative to endogenous TERT in telomerase purified from TCAB1 knock-out cells compared to controls (n = 3, mean, T-Test). The dashed lines indicate the level in telomerase purified from wild-type TCAB1 cells which was normalized to 1.0. **(E-I)** TERT immuno-purification from HeLa cells overexpressing TERT and TR (WT) or TR^{G414C} (CABm). **(E)** Western blots to analyze TERT and TCAB1 levels in lysates of cells overexpressing TERT and TR or TR^{G414C} (CABm). TERT and TCAB1 levels were normalized to total protein levels. **(F)** Western blots of immuno-purified TERT probed with a rabbit anti-TERT antibody (Abcam) and an anti-TCAB1, DKC1, and GAR1 antibodies. **(G)** Northern blot of RNA extracted from input and purified TERT (Elution) samples from cells overexpressing TERT and TR or TR^{G414C} (CABm), probed with radiolabeled DNA oligonucleotides complementary to TR. Standards are *in vitro* transcribed full-length TR and truncated TR_S. TR_S was added to elution samples prior to RNA extraction as loading and recovery control. Input samples were also probed for 7SL RNA as loading control. **(H-I)** Quantification of the amount of **(H)** TR relative to TERT (n = 3), **(I)** the ratio of TCAB1, DKC1 and GAR1 (n = 3) co-purified with TERT from cells expressing TR^{G414C} (CABm) relative to WT controls (mean, T-Test). The dashed lines indicate the level in telomerase purified from WT TR which was normalized to 1.0.

2.3.4: TCAB1 is not required for telomerase catalytic activity

To assess whether TCAB1 plays a role in telomerase catalysis, we first analyzed the enzymatic activity of endogenous telomerase purified from TCAB1 knock-out cells using the direct telomerase extension assays (Fig. 2.3A,B). Consistent with previous results (Chen et al., 2018), telomerase activity was strongly reduced in the absence of TCAB1 (Fig. 2.3C). To address whether this reduction in telomerase activity was a consequence of the defect in telomerase assembly observed in TCAB1 knock-out cells, we determined the specific activity of telomerase by dividing the measured activity by the amount of TR present in the respective telomerase sample. Due to the very small amount of TR detected in endogenous telomerase samples (Fig. 2.2B-C), the specific activity of endogenous telomerase was highly variable in TCAB1 knock-out cells but did not appear to be reduced compared to telomerase purified from control cells (Fig. S3A).

To overcome this limitation, we determined the specific activity of telomerase purified from cells overexpressing TERT and TR. Similar to endogenous telomerase, activity of overexpressed telomerase purified from HeLa and Halo-TERT cells lacking TCAB1 was significantly reduced to 24% and 34% compared to controls, respectively (Fig. 2.3D-F, Fig. A3B). The specific activity of overexpressed telomerase purified from HeLa and Halo-TERT cells lacking TCAB1 was slightly reduced (84% and 77% relative to control, respectively), but this reduction was not statistically significant (Fig. 2.3G). Together these observations demonstrate that, net cellular telomerase activity is reduced in the absence of TCAB1, while specific enzymatic activity is not. The reduction in cellular telomerase activity corresponds closely to the reduction of telomerase assembly observed in TCAB1 knock-out cells, suggesting that the smaller number of telomerase RNPs that form in the absence of TCAB1 are fully active.

2.3.5: TCAB1 mediates telomerase assembly in living cells

The experiments presented thus far demonstrate that telomerase assembly is reduced in the absence of TCAB1 but were carried out in fixed cells or cell lysates. To analyze telomerase assembly in intact cells, we carried out live cell single-molecule imaging of 3xFLAG-HaloTag-TERT (Movie S4-5). We have previously demonstrated that there are three distinct TERT populations in the nuclei of human cancer cells (Schmidt et al., 2016): a static population (assembled telomerase RNPs bound to telomeres, Cajal bodies or other cellular structures), a slowly diffusion population, and a rapidly diffusing population (Fig. 2.4A). The slowly diffusing population likely includes assembled telomerase RNPs, while the rapidly diffusing particles represents TERT molecules, which are not assembled with TR (Fig. 2.4A-B).

To determine the diffusion properties of TERT, when telomerase assembly cannot occur, we knocked out TR. TR knock-out was confirmed by PCR and Sanger sequencing, FISH, and qPCR (Fig. A4A-C). To define the diffusion rate of free TERT molecules, we determined the diffusion coefficient of rapidly diffusing 3xFLAG-HaloTag-TERT molecules in TR knock-out cells using the Spot-On tool, which calculates the diffusion coefficient and the fraction of particles in

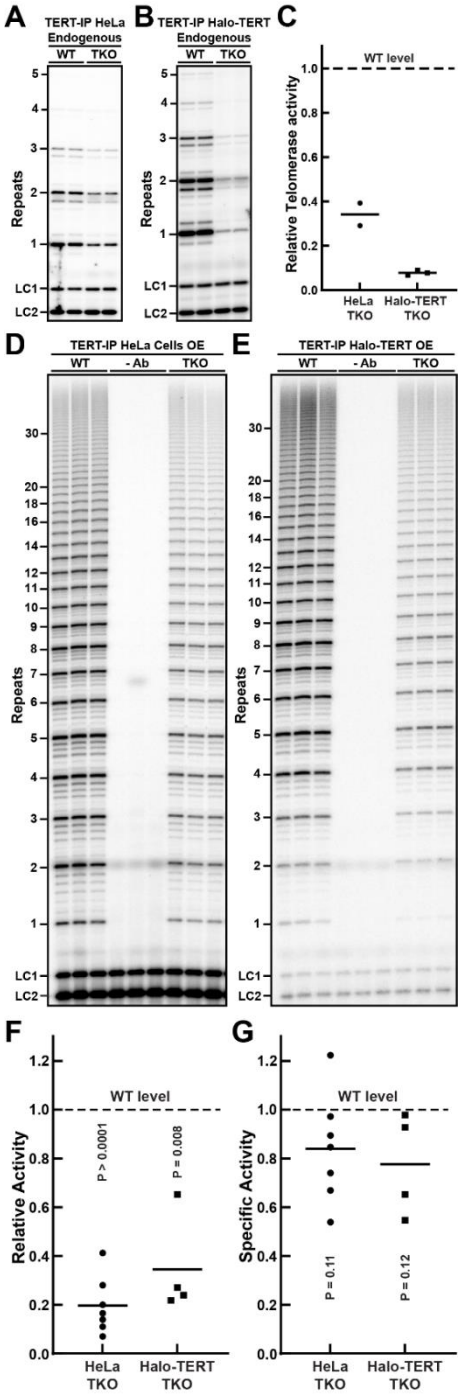

Figure 2.3. The specific activity of telomerase is unchanged in the absence of TCAB1. (A-B) Direct telomerase extension assay of endogenous telomerase immuno-purified from parental (WT) and TCAB1 knock-out (TKO) **(A)** HeLa and **(B)** Halo-TERT cell lines. Assays were carried out in the presence of 300 mM KCl and limiting amounts of dGTP. LC1 and LC2, radiolabeled DNA oligonucleotide loading controls. **(C)** Quantification of endogenous telomerase activity in samples from TCAB1 knock-out cells relative to parental controls (n = 3, mean). **(D-E)** Direct telomerase extension assay of telomerase immuno-purified from parental (WT) and TCAB1

Figure 2.3 (cont'd)

knock-out (TKO) overexpressing TERT and TR. **(D)** HeLa and **(E)** Halo-TERT cell lines. Assays were carried out in the presence of 150 mM KCl and 10 µM dATP, dTTP, and dGTP. LC1 and LC2, radiolabeled DNA oligonucleotide loading controls. In -Ab samples the TERT antibody was omitted during the immuno-purification. **(F)** Quantification of telomerase activity in samples from TCAB1 knock-out cells relative to parental controls (n = 4-7, mean). **(G)** Specific activity of overexpressed telomerase purified from TCAB1 knock-out cells relative to parental controls (n = 4-7, mean, T-Test). Specific activity was calculated by dividing the relative activity (see Fig. 2.3F) by the relative amount of TR present in immuno-purified TERT samples (Fig. A2). The dashed lines indicate the activity level in telomerase purified from wild-type TCAB1 control cells which was normalized to 1.0.

each TERT population by fitting the step-size distribution of TERT particles (Fig. 2.4A-B, Fig. A4D). Similarly, we defined the rate of diffusion of assembled telomerase RNPs by measuring the diffusion coefficient of slowly moving 3xFLAG-HaloTag-TERT molecules in control cells (Fig. 2.4A-B, Fig. A4D). These measurements, in TR knock-out and control cells, are the most accurate estimations possible for the diffusion coefficient of free TERT (D_{fast} = 1.9 ± 0.2 µm^2/s) and TERT that is part of a telomerase RNP (D_{slow} = 0.35 ± 0.2 µm^2/s), respectively.

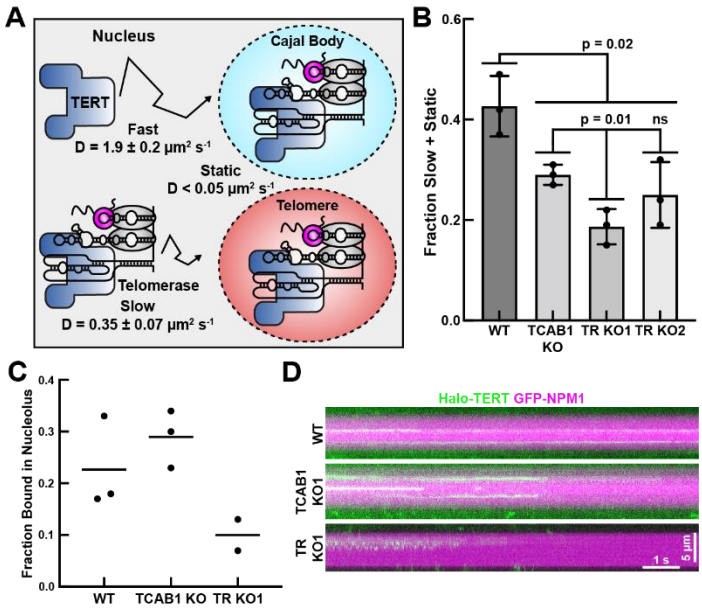

Figure 2.4. Telomerase assembly is reduced in live TCAB1 knock-out cells. (A) Diagram of distinct populations of TERT particles detected in control cells. Fast and slow diffusion coefficients were determined using Spot-On in control and TR knock-out cells, respectively (3 independent experiments, >15 cells per experiment per cell line, mean ± standard deviation). **(B)** Fraction of slow plus static TERT particles in control, TCAB1 knock-out, and TR knock-out

Figure 2.4 (cont'd)

cells expressing 3xFLAG-HaloTag TERT (3 independent experiments, >15 cells per experiment per cell line, mean ± standard deviation, t-test). **(C)** Quantification of the fraction of TERT particles statically bound to the nucleolus in control (WT), TCAB1 knock-out, and TR knock-out cells (2-3 independent experiments, >18 cells per experiment per cell line). **(D)** Kymographs of HaloTag-TERT particles that co-localized with nucleoli marked by GFP-NPM1 in control (WT), TCAB1 knock-out, and TR knock-out cells (also see Movies S6).

Using the diffusion coefficients, we fit the step-size distributions of TERT trajectories in control, TR knock-out, and TCAB1 knock-out cells to determine the fraction of TERT molecules in the fast, slow, and static TERT populations. Our key assumption is that rapidly diffusing TERT particles represent free TERT, while the much larger telomerase RNP is part of the slowly moving and static TERT populations. Consistent with this assumption, the fraction of TERT particles in the slowly diffusing and static populations was significantly reduced in TR knock-out cells (19 ± 4 %, 25 ± 7 %) compared to control cells (43 ± 6 %) (Fig. 2.4B). It is important to note that, even in TR knock-out cells, 19-25% of TERT particles are slowly diffusing or static (Fig. 2.4B). Because TR is absent in these cells, the slowly diffusing and static TERT molecules must be the result of interactions of TERT with cellular components other than Cajal bodies or telomeres. Importantly, we also observed a significant reduction in the fraction of slowly diffusing and static TERT particles in TCAB1 knock-out cells (29 ± 2 %) compared to control cells (43 ± 6 %) (Fig. 2.4B), consistent with a defect in telomerase assembly when TCAB1 is absent. The fraction of slowly diffusing and static TERT particles in TCAB1 knock-out cells (29 ± 2 %) was higher than in TR knock-out cells (19 ± 4 %, 25 ± 7 %), suggesting that telomerase assembly is strongly reduced but not completely lost in the absence of TCAB1, which is consistent with our telomerase assembly analysis using purified telomerase (Fig. 2.2). In addition, in the absence of TCAB1, the reduction of telomerase assembly was only detected for TERT particles that localized to the nucleoplasm (i.e. the non-nucleolar region of the nucleus) but not the nucleolus (Fig. 2.4C-D, Fig. A4E).

Because stable binding of telomerase to the telomere requires base-pairing of TR with the single-stranded telomeric overhang (Schmidt et al., 2018), we analyzed the interaction of TERT with telomeres. To assess TERT association with telomeres, we plotted the step size of TERT trajectories vs. the distance from the closest telomere for each step of these trajectories (Fig. A5A). In control cells, we observed an enrichment of TERT particles in close proximity to telomeres that do not move (i.e. have small step sizes), consistent with TERT interactions with the chromosome end (Fig. A5A, red boxes). In contrast, TERT trajectories in TCAB1 and TR knock-out cells lacked this enrichment, indicating that interactions between TERT and telomeres are reduced (Fig. A5A). Next, we filtered out TERT trajectories that came into proximity with telomeres marked by mEOS3.2-TRF2, as previously described (Schmidt et al., 2016). Diffusion analysis of these TERT trajectories using SpotOn revealed that the fraction of static TERT particles at telomeres was reduced from 12% in control cells to 4-5% in TCAB1 and TR knock-out cells (Fig. A5B). These observations indicate that, in the absence of either TCAB1 or TR, stable interactions of telomerase with telomeres occur at a lower frequency, because they require TR to stably bind to the chromosome end (Schmidt et al., 2018). Together these single-molecule imaging experiments demonstrate that in living cells, telomerase assembly is significantly reduced in the absence of TCAB1.

2.3.6: TERT is not retained in the nucleolus in the absence of TR

The experiments presented thus far have demonstrated that telomerase assembly is reduced in cell lysates and in living cells when TCAB1 is absent, but do not address the sub-cellular localization of telomerase assembly. It was previously suggested that telomerase is assembled in the nucleolus and active telomerase is enriched in the nucleolus in the absence of TCAB1 (Lee et al., 2013). Alternatively, TERT could associate with TR outside of the nucleolus and a small fraction of the telomerase RNP could localize to the nucleolus after assembly. Importantly, telomerase assembly within the nucleolus would require TERT to localize to the nucleolus independently of TR. To address whether TERT can enter the nucleolus in the absence

of TR, we analyzed TERT trafficking at the single-molecule level in TR knock-out cells synchronized in S-phase of the cell cycle. Nucleoli were marked by transient expression of GFP-NPM1 and TERT trajectories were split up into tracks that overlapped with the location of the nucleolus (Fig. A4E, colored tracks), and nucleoplasmic trajectories that did not overlap with the nucleolus (Fig. A4E, black tracks). As described above (Fig. 2.1F, Movies 1-2), a small fraction of TERT particles was detected within the nucleolus in control and TCAB1 knock-out cells (Fig. A4E, colored tracks). Analysis of the diffusion properties of TERT particles co-localized with GFP-NPM1 revealed that the fraction of static TERT molecules was slightly increased in TCAB1 knock-out cells (29%) compared to controls (23%, Fig. 2.4C-D, A4E-F, Movie S6). In contrast, static TERT molecules that co-localized with the nucleolus were less frequently detected in TR knock-out cells (10%, Fig. 2.4C-D, A4E-F, Movie S6).

Interestingly, we did observe very rare TERT molecules in TR knock-out cells that were mobile but constrained within a sub region of the nucleolus which, based on our other observations, likely corresponds to TERT within the DFC that is not bound to TR (Fig. 2.4D, Movie S6). In total, these results demonstrate that, though rare, TERT can enter the nucleolus independently of TR but does not transition into a stably bound state that likely requires association with TR.

2.3.7: TCAB1 is excluded from the nucleolus

Our experiments demonstrate that the loss of TCAB1 leads to an accumulation of TR in the nucleolus (Fig. 2.1). TCAB1 could lead to the depletion of TR from the nucleolus by binding to TR that has dissociated from the nucleolus and preventing it from re-entering. Alternatively, TCAB1 could bind to TR within the nucleolus and accelerate the export of TR from the nucleolus, which requires TCAB1 entry into the nucleolus. To analyze the sub-nuclear localization of TCAB1, we introduced a 3XFLAG-HaloTag at the endogenous *TCAB1* locus and generated single-cell clones that exclusively expressed 3XFLAG-HaloTag-TCAB1 (Fig. 2.5A). HaloTag-TCAB1 strongly

accumulated at Cajal bodies (marked by BFP-coilin) and was excluded from the nucleolus (Fig. 2.5B, Movie S7).

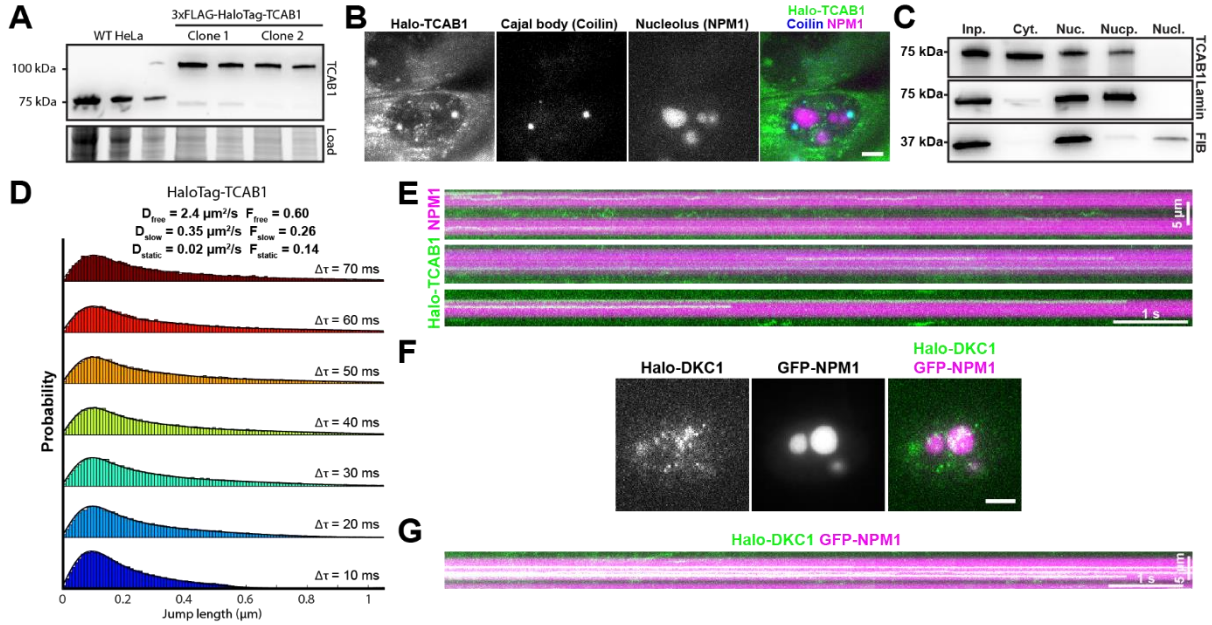

Figure 2.5. TCAB1 is excluded from the nucleolus. (A) Western blot probed with an antibody against TCAB1 demonstrating the exclusive expression of HaloTag-TCAB1 in genome edited Hela cells. **(B)** Maximum intensity projection of a single-molecule imaging movie of HaloTag-TCAB1 labeled with JFX650 in cells transiently expressing BFP-coilin and GFP-NPM1 to mark Cajal bodies and nucleoli, respectively (scale bar = 5 µm) **(C)** Western blots of samples of cellular fractionation experiments (left to right: Input, Cytoplasm, Nucleus, Nucleoplasm, Nucleolus) from HeLa cells. Blots were probed with antibodies against TCAB1, fibrillarin (nucleolar marker), and lamin B1 (nucleoplasmic marker). **(D)** Probability density functions of the step-sizes derived from nuclear HaloTag-TCAB1 trajectories and the corresponding 3-state model fit using the SpotOn tool (pooled data from 2 biological replicates of two independent HaloTag-TCAB1 clones, >10 cells total per replicate). **(E)** Kymograph of nucleolar HaloTag-TCAB1 particles over time. **(F)** Live-cell fluorescence images of single 3xFLAG-HaloTag-dyskerin particles, nucleoli marked by GFP-NPM1 (scale bar = 5 µm). **(G)** Kymograph of nucleolar 3xFLAG-HaloTag-dyskerin particles over time.

Surprisingly, a large fraction of HaloTag-TCAB1 localized to the cytoplasm, suggesting that its import into the nucleus is restricted (Fig. 2.5B). To assure that the cytoplasmic localization of HaloTag-TCAB1 was not an artifact of fusing TCAB1 to the HaloTag, we carried out cell fractionation experiments, which demonstrated that untagged TCAB1 was also detected in the cytoplasm and the nucleus but was not located in the nucleolus (Fig. 2.5C), consistent with our

imaging experiments. Single-particle tracking of HaloTag-TCAB1 within the nucleus revealed that the diffusion dynamics of TCAB1 were similar to those of TERT (Fig. 2.4B, Fig. 2.5D). Like TERT, the step size distribution of HaloTag-TCAB1 particles fit well to a three-state model (Fig. 2.5D). The freely diffusing state of TCAB1 had a higher diffusion coefficient than TERT (D_{fast} = 2.4 μm^2/s vs. 1.9 μm^2/s). Strikingly, the diffusion coefficient of the slow-diffusing state for TCAB1 and TERT were identical (D_{slow} = 0.35 μm^2/s), consistent with TCAB1 and TERT being part of assembled RNPs. On rare occasions, we observed HaloTag-TCAB1 molecules that associated with the nucleolus (Fig. 2.5E, Movie S7-8). In contrast, HaloTag-dyskerin was readily detected stably bound to the nucleolus (Fig. 2.5F-G). In total, these results demonstrate that TCAB1 is largely excluded from the nucleolus and that TCAB1 molecules diffuse through the nucleoplasm at a rate similar to assembled telomerase RNPs.

2.3.8: The majority of TR is tightly associated with the nucleolus in absence of TCAB1

Single-molecule imaging of TERT revealed that <10% of TERT molecules localize to the nucleolus in control and TCAB1 knock-out cells (Fig. 2.1G). To determine the fraction of TR that associates with the nucleolus in the absence of TCAB1, we carried out cellular fractionations to isolate nucleoli. Nucleoli were purified by rupturing isolated nuclei via sonication, followed by centrifugation through a high-density sucrose cushion (Lam and Lamond, 2006). Isolated nucleoli were enriched with the nucleolar protein fibrillarin and U3 snoRNA while being depleted of lamin B1 and the 7SK RNA (Fig. 2.6A,B), which serve as nucleoplasmic markers, demonstrating that we successfully purified nucleoli using this approach.

To determine the amount of TR found in the nucleolus and the nucleoplasm, we quantified the level of TR relative to that of the U3 or the 7SK RNA, respectively. In control cells, the majority of TR was found in the nucleoplasmic fraction, and a small amount of TR was detected in nucleoli (Fig. 2.6B), consistent with previous work that analyzed TR localization by live cell imaging (Laprade et al., 2020). In contrast, in TCAB1 knock-out cells, TR was depleted from the nucleoplasm and enriched in the nucleolus (Fig. 2.6B,C). To assess the impact of high salt

concentrations, used by others to extract telomerase from human cells (Chen et al., 2018), on nucleolar integrity, we supplemented ruptured nuclei with potassium chloride, prior to isolating nucleoli. After exposure to a high salt concentration, fibrillarin and TR were found in the nucleoplasmic fraction instead of the nucleolar pellet (Fig. A6), demonstrating that nucleoli are disrupted, and TR is released when exposed to non-physiological salt concentrations. These observations confirm that >50% of TR is sequestered in the nucleolus in the absence of TCAB1 and strongly suggest that the majority of TR is tightly associated with the nucleolus under these circumstances.

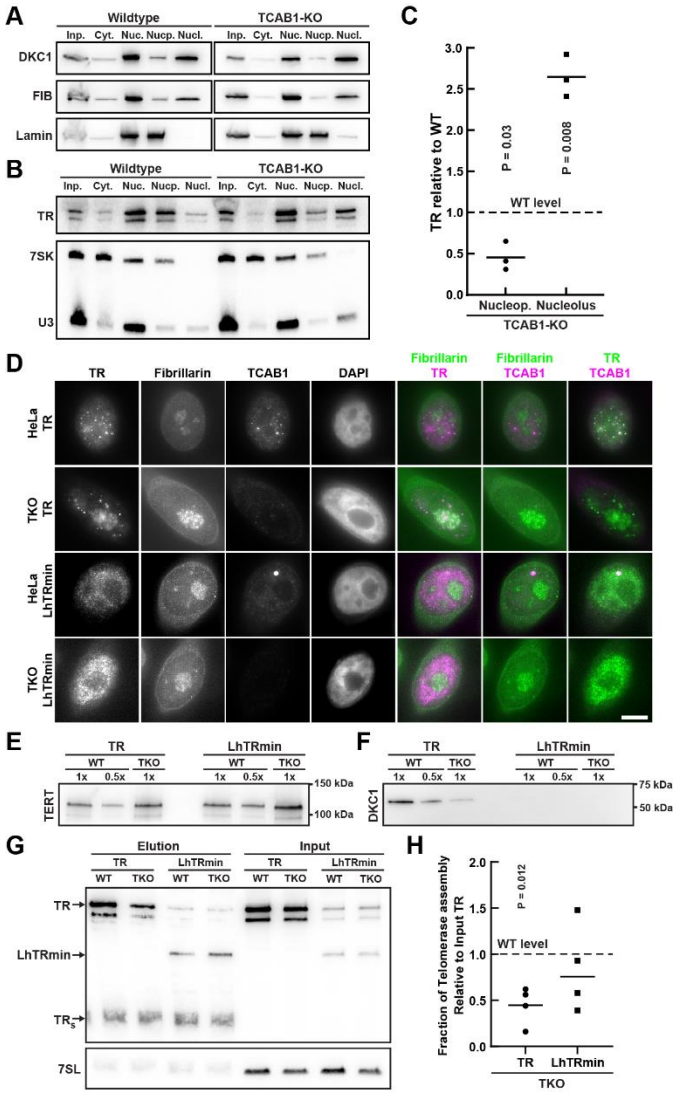

Figure 2.6. Localization of TR to the nucleoplasm rescues telomerase assembly in the absence of TCAB1. (A) Western blots of samples of cellular fractionation experiments (left to

Figure 2.6 (cont'd)

right: Input, Cytoplasm, Nucleus, Nucleoplasm, Nucleolus) from control and TCAB1 knock-out cells. Blots were probed with antibodies against dyskerin, fibrillarin (nucleolar marker), and lamin B1 (nucleoplasmic marker). **(B)** Northern blots of samples of cellular fractionation experiments (left to right: Input, Cytoplasm, Nucleus, Nucleoplasm, Nucleolus) from control and TCAB1 knock-out cells. Blots were first probed with radiolabeled DNA oligonucleotides complementary to TR, followed by probes complementary to the 7SK RNA (nucleoplasmic marker) and the U3 snoRNA (nucleolar marker). **(C)** Quantification of the nucleoplasmic and nucleolar abundance of TR in TCAB1 knock-out cells relative to control cells. Nucleoplasmic TR signal was normalized to the 7SK RNA signal and nucleolar TR signal was normalized to the U3 RNA signal (n = 3, mean, T-Test). **(D)** IF-FISH of control and TCAB1 knock-out cells over-expressing TERT and full-length TR or LhTRmin probed with antibodies for fibrillarin and TCAB1 and anti TR-FISH probes (scale bar = 5 μm). **(E-F)** Western blots or TERT immuno-purified from control and TCAB1 knock-out cells overexpressing TERT and full-length TR or LhTRmin probed with antibodies for **(E)** TERT and **(F)** dyskerin. **(G)** Northern blot of RNA extracted from input and TERT samples purified from control and TCAB1 knock-out cells overexpressing TERT and full-length TR or LhTRmin. Standards are *in vitro* transcribed full-length TR and truncated TR_S. Input samples were also probed for 7SL RNA as loading control. **(H)** Quantification of TR or LhTRmin associated with TERT relative to input RNA of TERT samples purified from TCAB1 knock-out cells compared to control cells.

2.3.9: Localization of the telomerase RNA to the nucleoplasm rescues telomerase assembly in the absence of TCAB1

Our data demonstrate that stable association of TERT with the nucleolus requires its interaction with TR (Fig. 2.4, Fig. A4). Importantly, we cannot distinguish whether static TERT molecules within the nucleolus represent telomerase RNPs that have assembled in the nucleolus or the nucleoplasm. To address whether the telomerase RNP can assemble in the nucleoplasm, we expressed a truncated version of TR (LhTRmin) that lacks the H/ACA domain (Vogan et al., 2016) which binds to dyskerin and TCAB1. Therefore, LhTRmin does not localize to the nucleolus or Cajal bodies (Fig. 2.6D) (Vogan et al., 2016). In addition, because LhTRmin lacks the H/ACA region of TR it does not accumulate to the same level as wildtype TR (Fig. 2.6D) (Vogan et al., 2016). Consistent with our results shown above, assembly of TERT with full-length TR and dyskerin was significantly reduced in the absence of TCAB1 (Fig. 2.6E-H). In contrast, TERT association with LhTRmin was not significantly different in TCAB1 knock-out cells compared to control cells expressing LhTRmin (Fig. 2.6E-H). Importantly, no dyskerin was associated with

TERT purified from cells expressing LhTRmin (Fig. 2.6F). These results demonstrate that forcing TR localization to the nucleoplasm suppresses the telomerase assembly defect observed in TCAB1 knock-out cells and indicate that the telomerase RNP can form outside of the nucleolus. Importantly, these observations suggest that the sequestration of TR in the nucleolus causes the reduction in telomerase assembly observed in the absence of TCAB1.

2.3.10: Analysis of nucleolar telomerase RNA and snoRNP dynamics

The results presented thus far have demonstrated that TR accumulates in nucleoli in the absence of TCAB1 by cell fractionation and in fixed cells, but we have not addressed the dynamic localization of TR in living cells. Since TR is targeted to nucleoli by dyskerin and other H/ACA RNP components, we first used dyskerin as a surrogate for TR and H/ACA snoRNPs in general. We transiently expressed HaloTagged dyskerin in parental HeLa and TCAB1 knock-out cells and analyzed dyskerin binding to the nucleolus using fluorescence recovery after photobleaching (FRAP). We identified cells with two clearly visible nucleoli, completely photo-bleached the dyskerin signal in one of the nucleoli and quantified the recovery of the fluorescence signal (Fig. A7A, Movies S9-10). The dyskerin signal recovered rapidly ($t_{1/2}$ = 28 s) but only ~65% of the signal was recovered after > 4 minutes (Fig. A7B-D, Movies 9-10). This indicates that there are at least two distinct populations of dyskerin molecules in the nucleolus, a rapidly exchanging population and a static population that does not dissociate from the nucleolus over the time course of this experiment (Fig. A7D). The presence of a mobile dyskerin population was confirmed by analysis of the unbleached nucleolus, which lost fluorescence signal with similar kinetics (Fig. A7A,E-F). Importantly, no significant difference in dyskerin dynamics were observed in TCAB1 knock-out cells compared to parental controls (Fig. A7A-F), which indicates that TCAB1 is not required to extract dyskerin-containing scaRNPs from nucleoli.

To directly analyze the dynamics of TR binding to the nucleolus in the absence of TCAB1, we introduced three MS2 stem loops at the 5’ end of the endogenous TR gene (Fig. 2.7A, Fig. A7G-H), as previously described (Laprade et al 2020). This approach allowed us to visualize TR

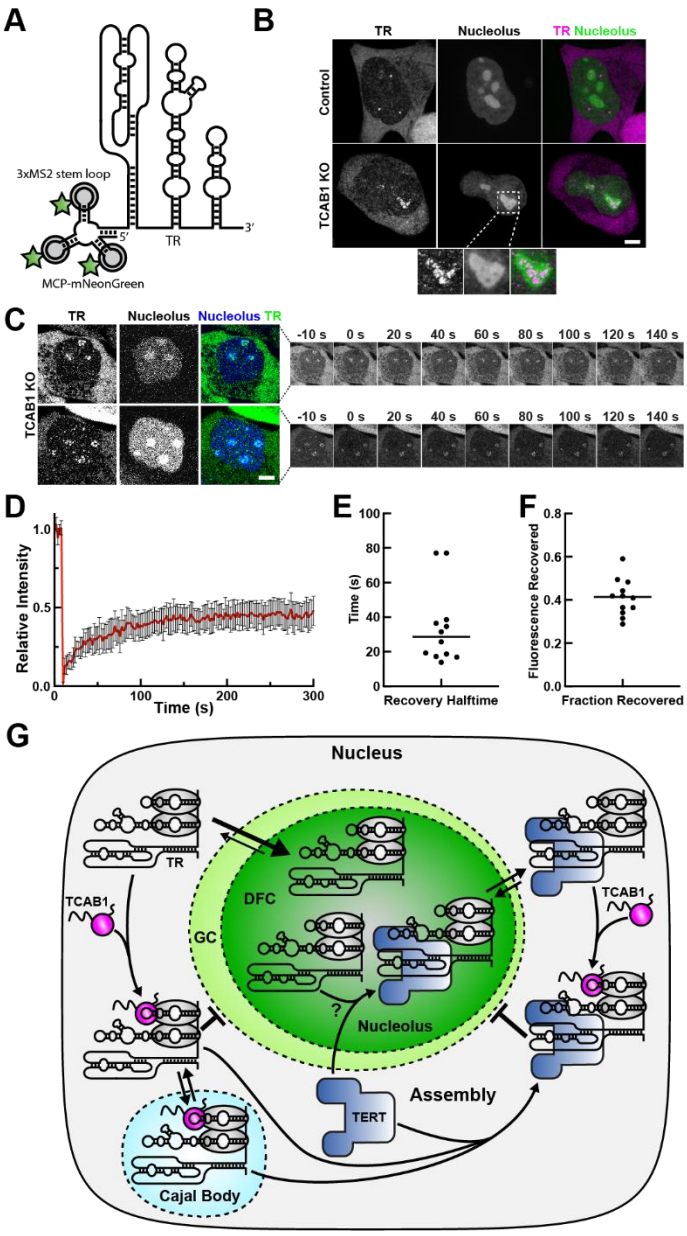

Figure 2.7. Analysis the nucleolar binding dynamics of dyskerin and TR. (A) Model of 3xMS2-TR bound to MCP-mNeonGreen. **(B)** Live cell microscopy images of control and TCAB1 knock-out cells expressing 3xMS2-TR, MCP-mNeonGreen, and BFP-NLS to mark the nucleolus. Zoomed images demonstrate the enrichment of TR in the DFC indicated by low BFP-NLS signal within the nucleolus. **(C)** FRAP of 3xMS2-TR within the DFC of the nucleolus marked by BFP-NLS. **(D)** FRAP curves and single exponential fits of the data (red). **(E)** Quantification of the recovery halftime from single-exponential fits of the recovery curves show in (D). **(F)** Quantification of the fraction of fluorescence recovered from single-exponential fits of the FRAP curves show in (D). **(G)** Model for TCAB1-mediated retention of TR in the nucleoplasm. In the absence of TCAB1, TR is sequestered in the dense fibrillar component (DFC) of the nucleolus. TCAB1, which does not enter nucleoli, promotes telomerase assembly

Figure 2.7 (cont'd)

by increasing the amount of TR that can encounter TERT to assemble into telomerase in the nucleoplasm and potentially Cajal bodies.

in living cells using the MS2 coat protein (MCP) fused to the mNeonGreen fluorescent protein, stably expressed by lentiviral transduction (Fig. 2.7A). Similar to endogenous TR (Fig. 2.1), 3xMS2-TR localized to nucleoplasmic foci in control cells (likely Cajal bodies) and to nucleoli in absence of TCAB1 (Fig. 2.7B, Fig. A7I). Like dyskerin (Fig. A1F), MS2-TR was specifically enriched in nucleolar regions with reduced granular component marker (BFP-NLS, Fig. A1F) intensity in the absence of TCAB1 (Fig. 2.7B, zoomed panels), which corresponds to the dense fibrillar component (DFC) of the nucleolus. To measure the dynamics of TR association with the nucleolus in TCAB1 knock-out cells, we carried out FRAP experiments of MCP-mNeonGreen bound MS2-TR clearly localized within DFC of the nucleolus (Fig. 2.7C, Movie S1-12). After bleaching nucleolar MS2-TR enriched in the DFC in TCAB1 knock-out cells, ~40% of the fluorescence recovered with a halftime of recovery of ~30 seconds (Fig. 2.7D-F). Importantly, no MS2-TR accumulation in nucleoli was observed in control cells, precluding its analysis by FRAP (Movie S13). This demonstrates that, in the absence of TCAB1, the majority of TR is tightly associated with the nucleolus and the remaining TR molecules exchange with the nucleoplasm with kinetics comparable to dyskerin. In total, these results strongly suggest that the reduction of telomerase assembly, observed in the absence of TCAB1, is a consequence of the sequestration of TR in the nucleolus, where it infrequently encounters TERT which is largely localized to the nucleoplasm.

2.4: Discussion

The experiments described in this study demonstrate that TCAB1 promotes telomerase assembly. In the absence of TCAB1, the telomerase RNA is targeted to the nucleolus via its association with dyskerin and other components of the H/ACA complex. In contrast to TR, TERT rarely enters the nucleolus, preventing its association with TR in cells that lack TCAB1. In addition,

we demonstrate that TCAB1 does not enter nucleoli excluding the possibility that TCAB1 extracts TR containing RNPs from nucleoli. These observations suggest that nuclear compartmentalization, which is a consequence of nucleolar phase separation, counteracts telomerase assembly. Our analysis of the dynamic association of dyskerin bound snoRNPs and TR with nucleoli revealed that a significant fraction of TR containing RNPs and snoRNPs in general are tightly associated with the nucleolus. Finally, we demonstrate that while telomerase assembly is limited, the specific activity of telomerase is unchanged in the absence of TCAB1, which excludes a role of TCAB1 in telomerase catalytic function. Altogether our work supports an entirely new hypothesis for the role of TCAB1 in telomerase function in human cells and provides insight into the role phase-separated organelles play in RNA dynamics and RNP assembly and function.

2.4.1: TCAB1 promotes telomerase assembly

The importance of TCAB1 for telomere synthesis is undisputed (Chen et al., 2018; Venteicher et al., 2009). Knock-out or depletion of TCAB1 results in telomere shortening (Chen et al., 2018; Venteicher et al., 2009; Vogan et al., 2016). All previous work also concluded that TR is enriched in the nucleolus in the absence of TCAB1 (Chen et al., 2018; Stern et al., 2012; Vogan et al., 2016; Zhong et al., 2011). However, prior studies conclude that TCAB1 is not required for telomerase assembly but instead plays a role in telomerase trafficking to Cajal bodies and telomeres or is required for telomerase catalysis (Chen et al., 2018; Stern et al., 2012; Venteicher et al., 2009; Vogan et al., 2016; Zhong et al., 2011). The work presented here demonstrates that, in the absence of TCAB1, telomerase assembly is significantly reduced. This finding is supported by two completely distinct and complementary approaches. First, we purified TERT from cell lysates and demonstrated that the fraction of TR associated with TERT is reduced to 20-40% in the absence of TCAB1 compared to control cells. Importantly, TR levels are increased 2-fold in the TCAB1 knock-out cells, potentially because TR enrichment in the nucleolus shields it from exonucleolytic degradation. Consistent with a reduction in telomerase assembly,

only 5-15% of the cellular TR is associated with TERT in the absence of TCAB1 compared to controls.

Secondly, we used the single-molecule diffusion dynamics of TERT as a read-out of telomerase assembly. When telomerase assembly is impossible (in TR knock out cells), the vast majority (~75-80%) of TERT molecules rapidly diffuse through the nucleus. In contrast, in the presence of TR, only ~55% of TERT molecules rapidly diffuse through the nucleus, because the association of TERT with TR leads to the formation of a large RNP that moves through the nucleus at a slower rate. In the absence of TCAB1, the fraction of rapidly moving TERT molecules is significantly increased to ~70%, consistent with a reduction in telomerase assembly. Assuming a maximal change of 25% in the fraction of rapidly diffusing TERT molecules (from 55% in wild type to 80% in TR knock-out cells), the 15% increase, observed in the absence of TCAB1 compared to wild type, corresponds to a 60% reduction (15/25) in telomerase assembly, which is consistent with our results obtained by purifying telomerase from cell lysates.

In addition, we demonstrate that the TERT less frequently forms stable interactions with telomeres in the absence of TCAB1, consistent with fewer TERT molecules being bound to TR. The reduction in telomerase assembly in cells lacking TCAB1 leads to a lower number of telomerase RNPs per cell and in turn, telomere shortening. Importantly, telomerase assembly is reduced but not completely abolished when TCAB1 is absent, which is sufficient to support continuous cell proliferation with a short telomere length set point.

2.4.2: TCAB1 is not required for telomerase catalysis

Previous work by others has reported conflicting results regarding the role of TCAB1 in telomerase catalysis, ranging from full enzymatic activity in initial reports to substantial activity defects in the most recent study (Chen et al., 2018; Venteicher et al., 2009; Vogan et al., 2016). Importantly, both our work and the only other study that analyzed the role of TCAB1 in telomerase activity using the “gold-standard” direct telomerase extension assay concluded that telomerase activity is significantly reduced in the absence of TCAB1. While both studies concur on the degree

to which telomerase activity is reduced in the absence of TCAB1, the proposed underlying molecular mechanisms differ. Chen *et al*. propose that TCAB1 is required for proper folding of the CR4/CR5 region of the telomerase RNA, which directly associates with TERT, without affecting telomerase assembly (Chen et al., 2018).

Recent structural analysis of the telomerase RNP from human cells revealed that TCAB1 is located far away from the CR4/CR5 region of TR (Ghanim et al., 2021). Although it is possible that telomerase can adopt additional conformations, based on the currently available structural information, it is difficult to rationalize a molecular mechanism by which TCAB1 could specifically promote CR4/CR5 folding. In addition, due to the misfolding of TR, telomerase was proposed to adopt a low activity state in the absence of TCAB1. Experimentally such a low activity state would manifest itself as a reduction in the specific activity of telomerase (telomerase activity per assembled telomerase RNP).

Our experiments strongly suggest that, while telomerase assembly is reduced in the absence of TCAB1, the limited amount of telomerase that can assemble is close to fully active (i.e. does not have reduced specific activity). One possible explanation for the discrepancies between the work by Chen *et al*. and our study is the methodology used to generate cell lysates. Our results demonstrate that the high salt concentration used by Chen *et al.* to generate nucleolar extracts dissolves nucleoli and releases TR (Fig. A6). Consistent with this observation, salt concentrations > 250 mM have been shown to disrupt the phase separation phenomena underlying the formation of the nucleolus (Feric et al., 2016). Solubilization of the nucleolus and release of TR would override the localization of TR and TERT to distinct sub-cellular compartments and could allow telomerase to assemble in the nuclear extract. Importantly, our single-molecule imaging of TERT dynamics is consistent with a reduction of telomerase assembly in intact cells. Altogether, our enzymatic analysis, and the positioning of TCAB1 within the telomerase RNP do not support a role of TCAB1 in TR folding and telomerase catalysis but are fully consistent with TCAB1 promoting telomerase assembly.

2.4.3: Location and molecular mechanism of telomerase assembly

The sub-cellular location and order in which telomerase RNP components associate with TR in human cells have largely been unknown. It has been suggested that telomerase assembly occurs in the DFC of the nucleolus (Lee et al., 2013) . While this study clearly demonstrates that catalytically active telomerase can localize to the DFC of the nucleolus (Lee et al., 2013), it fails to show that telomerase is assembled in the nucleolus. Results by others have demonstrated that eliminating Cajal bodies does not impact telomerase activity or telomere maintenance, suggesting that Cajal bodies are not necessary for telomerase assembly (Chen et al., 2018, 2015; Vogan et al., 2016). Our single-molecule live cell imaging of TERT demonstrates that TERT is almost exclusively localized to the nucleoplasm.

Since Cajal bodies are dispensable for telomerase assembly, and TERT is largely excluded from the nucleolus, we believe telomerase assembly occurs in the nucleoplasm. The available data does not rule out that telomerase can also assemble in Cajal bodies, but it is certainly not obligatory. Our model is further supported by our observation that expression of LhTRmin, which lacks the binding sites for dyskerin and TCAB1 and therefore accumulates in the nucleoplasm and is excluded from nucleoli in human cancer cells (Vogan et al., 2016), rescues the telomerase assembly defect observed in the absence of TCAB1. However, it is important to point out that we do observe a very small number of TERT molecules that localize to nucleoli in control and TCAB1 knockout cells. These static nucleolar TERT molecules require the presence of TR and therefore likely represent TERT associated with TR. Unfortunately, we are unable to determine whether this assembly of TERT and TR occurred in the nucleolus or prior to import of an assembled telomerase RNP into the nucleolus.

TCAB1 could counteract TR accumulation in the nucleolus by two possible mechanisms: TCAB1 could prevent the entry of TR into the nucleolus, increasing the nucleoplasmic concentration of TR and the likelihood of assembly with TERT. Alternatively, TCAB1 could extract telomerase assembled in the nucleolus by accelerating the export of telomerase from the DFC.

Because TCAB1 rarely enters nucleoli, we believe that it is unlikely that it contributes to the export of scaRNPs from the nucleolus. In addition, if the presence of TCAB1 accelerated the dynamic exchange of dyskerin-bound scaRNPs between the nucleolus and the nucleoplasm, we would expect dyskerin to bind more tightly to the nucleolus in the absence of TCAB1. Instead, our FRAP experiments demonstrate that the association of dyskerin with the nucleolus is unchanged in the absence of TCAB1.

Altogether, our observations support our model that TCAB1 promotes telomerase assembly by counteracting TR accumulation in the nucleolus to facilitate its assembly with TERT in the nucleoplasm (Fig. 2.7G). Our analysis of the dynamics of nucleolar TR suggests that the majority of TR is tightly associated with the DFC when it is not bound by TCAB1. Since TCAB1 rarely enters the nucleolus, we believe the primary role of TCAB1 is to prevent the entry of TR into the nucleolus. In the absence of TCAB1 the equilibrium of TR localization is shifted towards the nucleolus, because re-entry is not inhibited by TCAB1 and the dissociation of TR from the DFC is very slow. The resulting nucleolar accumulation of TR effectively reduces the amount of TR available to assemble with TERT. Importantly, a very small number of TERT molecules bound to TR can be imported and trapped in the nucleolus, which would further decrease the amount of telomerase available to elongate telomeres.

2.4.4: Regulation of RNP assembly by nucleolar phase-separation

In addition to the mechanistic insight into the role of TCAB1 in telomerase function, our results also demonstrate that nucleolar phase separation can effectively regulate telomerase RNP assembly in the nucleus of human cells (Fig. 2.7G). How RNA molecules are specifically recruited into, excluded from, or expelled from non-membrane bound organelles is a key unanswered question. One model suggests that gradual replacement of non-specific, multivalent interactions of pre-ribosomal RNAs with nucleolar proteins such as NPM1 and fibrillarin, with specific, high-affinity interactions with ribosomal proteins leads to the ejection of mature ribosomal subunits from the nucleolus (Riback et al., 2020). In this model a key driving force for the retention of RNA

in the nucleolus is regions of RNA, not yet bound by ribosomal proteins, are available to interact with nucleolar proteins (Riback et al., 2020). By analogy, this model would explain why TR bound by the H/ACA complex but not associated with TERT would be sequestered in the nucleolus.

Our experiments demonstrate that 60% of nucleolar TR is tightly associated with the nucleolus while the remaining 40% can exchange with the nucleoplasm, which closely corresponds to fraction of telomerase assembly observed in TCAB1 knock-out cells. We believe that TR bound to TERT can exchange with the nucleoplasm, but TR not associated with TERT remains trapped in the nucleolus. In addition to the interactions formed by the H/ACA complex with nucleolar proteins and RNA, the regions of TR that are bound by TERT in the context of telomerase (i.e. the pseudoknot, template, and CR4/CR5) would be available to form non-specific, multivalent interactions with nucleolar proteins to strengthen the association of TR with the nucleolus and prevent its release when it is not associated with TERT (Fig. 2.7G).

TR is unique among the scaRNAs, because it contains the additional domains that associate with TERT. Most other box H/ACA scaRNAs are substantially shorter (<150 nucleotides) than TR (451 nucleotides), and do not contain large regions that are not bound by proteins and could form non-specific interactions with nucleolar proteins. It is, therefore, possible that in cells lacking TCAB1, TR is strongly retained in the nucleolus while other scaRNAs are less tightly bound, because they lack additional interaction sites with nucleolar proteins. Consistent with this hypothesis, we observe multiple populations of dyskerin with distinct binding dynamics in nucleoli. The weakly bound population could include dyskerin bound to scaRNAs that are not retained in the nucleolus because their RNA targets, which would provide an additional interaction site, are not present in nucleoli. In contrast, dyskerin bound to snoRNAs would strongly associate with the nucleolus, because they also bind to their target RNAs. This provides a potential explanation for the phenotypes observed in patients with TCAB1 mutations that suffer from dyskeratosis congenita. The patients have a clear deficiency in telomerase function (Zhong et al.,

2011), but no defects in splicing have been reported, which would be the consequence of complete loss of scaRNA function and their critical role in spliceosome maturation.

The mechanism by which TCAB1 binding leads to the exclusion of TR and other scaRNA from the nucleolus remains a key unanswered question. TCAB1 interacts with a very short sequence motif in TR, which is far removed from the TR regions that associate with TERT (Ghanim et al., 2021). It is, therefore, unlikely that TCAB1 binding leads to exclusion of TR from the nucleolus by reducing the number of non-specific, multivalent interactions TR can form with nucleolar proteins. As outlined above, we believe that TCAB1 prevents localization of scaRNAs to the nucleolus, rather than extracting scaRNAs that are already localized to the DFC. One potential explanation is that TCAB1 counteracts scaRNA recruitment to the nucleolus by inhibiting the nucleolar localization signals within dyskerin (Heiss et al., 1999). Dissecting the molecular mechanism by which TCAB1 leads to exclusion of TR from the nucleolus in future studies will undoubtably shed light on the fundamental principles RNP recruitment to non-membrane bound organelles and its physiological role in cell biology.

2.5: Acknowledgements

We would like to thank members of the Schmidt lab and J. Nandakumar for discussions and critical reading of the manuscript and Luke Lavis (HHMI Janelia Research Campus) for providing HaloTag dyes. This work was supported by grants from the NIH (R00 GM120386, R01GM141354) to J.C.S.. J.C.S. was a Damon Runyon Dale F. Frey Scientist supported (in part) by the Damon Runyon Cancer Research Foundation (DFS-24-17). S.B.C. acknowledges sustained support from the Ernest & Piroska Major Foundation. We acknowledge the Flow Cytometry core (Research Technology Support Facility, Michigan State University) and the Confocal Laser Scanning Microscopy core (Center for Advanced Microscopy, Michigan State University) for supporting our cell sorting and microscopy experiments.

2.6: Author contributions

B.M.K. carried out IF-FISH experiments, cellular fractionations, telomere length by Southern blot, cell cycle flow cytometry and analysis, single molecule imaging, FRAP analysis, telomerase purifications, analyzed telomerase assembly, generated mCherry- and 3xFLAG-HaloTag-dyskerin plasmids and CABm plasmids, determined their sub-cellular localization, and edited the manuscript. G.I.P. maintained cell lines, established TCAB1 and TR knock-out cell lines and carried out IF-FISH experiments. K.A.-B. assisted in establishing the TR knock-out cell line and carried out characterization of the TR knock-out cells. S.B.C. purified and characterized the anti-TERT sheep antibody. L.H. and K.Y. characterized TCAB1 knock-out clones using Southern blots. E.M.P. generated the cell lines expressing 3xMS2-TR. J.C.S. carried out all other experiments, designed the research, analyzed data, and wrote the original draft and edited the manuscript.

2.7: Materials and Methods

2.7.1: Cell Lines and Tissue Culture

All cell lines were based on HeLa-EM2-11ht (Weidenfeld et al., 2009) and were cultured in Dulbecco's Modified Eagle Medium including L-glutamine (Gibco) supplemented with 10% fetal bovine serum, 100 units/ml penicillin and 100 µg/ml streptomycin at 37°C with 5% CO_2. Live cell imaging was carried out using CO_2 independent media supplemented with 2 mM GlutaMAX (Life Technologies), 10% fetal bovine serum, 100 units/ml penicillin and 100 µg/ml streptomycin at 37°C with 5% CO_2. For single-molecule imaging of HaloTag-TERT cell were cultured in homemade imaging dishes made by gluing 22x22 mm Nexterion coverslips (170 ± 5 µm, Schott) onto the bottom of plastic 3.5 x 1.0 cm cell culture dishes with a hole in the middle using an epoxy adhesive. Prior to chamber assembly the coverslips were washed with 1 M KOH and 100% for 30 min each in a sonicating water bath. To enrich for cells in S-phase for live cell imaging experiments, cultures were treated with complete media including 2 mM thymidine for a minimum

of 16 hours. Cells were released 2 hours prior to imaging by replacing the thymidine containing media with fresh media without thymidine. Puromycin selection was carried out at a concentration of 1 µg/ml.

2.7.2: Plasmid Construction and Genome Editing

All plasmids were generated by Gibson assembly (NEB) using standard protocols or by inverse PCR. All plasmids will be made available on Addgene. All Cas9 and sgRNA expression plasmids were based on pX330 (Cong et al., 2013). The homologous recombination donor for the TR knock-out was generated by assembling the genomic sequences immediately upstream and downstream (~500 bp each, gBlocks IDT) of the TR sequence flanking a puromycin resistance cassette into HpaI linearized pFastBac. The homologous recombination donor for the insertion of the 3xMS2-tag at the endogenous locus was generated by cloning a left homology arm (418 bp upstream of the *TERC* gene, gBlock IDT) followed by 3xMS2-TR and 100 bp of the genomic sequence downstream of TR, followed by an SV40-promoter driven puromycin resistance marker, and finally a right homology arm (473 bp, 101-573 bp downstream of the *TERC* gene, gBlock IDT) into pFastBac. The sgRNA were designed to cut at the junction of the 3xMS2-TR insert junctions and the PAM sites were mutated to not be present in the homologous recombination donor plasmid, to assure the recombined allele was not cut by Cas9. The lentiviral plasmids for expression of MCP-NeonGreen was generated by replacing the sfGFP sequence in the pHAGE-UBC-MCP-sfGFP plasmid (a kind gift from Agnel Sfeir) with the coding sequence for mNeonGreen. The lentivirus and cell lines expressing MCP-mNeonGreen were generated as previously described (Querido et al., 2020). The homologous recombination donor for the insertion of the 3xFLAG-HaloTag into the *TCAB1* gene was generated by cloning the 3xFLAG-HaloTag sequence including a SV40-promoter driven puromycin resistance marker flanked by LoxP-sites in between two homology arms (500 bp up and downstream from the start codon, gBlocks IDT). The 3xFLAG-HaloTag-NLS plasmids was generated by adding a 3xFLAG-tag to a previously described HaloTag-NLS plasmid (a kind gift from X. Darzacq and A. Hansen) (Hansen

et al., 2018). The 3xFLAG-HaloTag-dyskerin plasmid was generated by replacing TERT in our previously described 3xFLAG-HaloTag-TERT expression plasmid with the dyskerin coding sequence (Schmidt et al., 2016).

The mCherry-dyskerin plasmid was generated by replacing TERT in our previously described mCherry-TERT expression plasmid with the dyskerin coding sequence (Schmidt et al., 2014). Unless otherwise stated, transfections were carried out with Lipofectamine 2000 (Invitrogen) using the manufacturer's instructions. For FRAP analysis of dyskerin $1x10^6$ HeLa cells were transfected with 1 µg of 3xFLAG-HaloTag-dyskerin plasmid using the Lonza 4D-Nucleofector with the SE Cell Line 4D-Nucleofector X kit (Cat. V4XC-1012) and program CN-114. For single-molecule imaging of dyskerin 1 µg of a GFP-NPM1 plasmid was included in addition to the 1 µg of 3xFLAG-HaloTag-dyskerin plasmid. GFP-NPM1 WT was a gift from Xin Wang (Addgene plasmid #17578; http://n2t.net/addgene:17578; RRID:Addgene_17578) (Wang et al., 2005). For single-molecule imaging of 3xFLAG-HaloTag-NLS, 1 µg of a GFP-Nucleolin plasmid was included in addition to the 1 µg of 3xFLAG-HaloTag-NLS plasmid. The GFP-Nucleolin plasmid was a gift from Michael Kastan (Addgene plasmid #28176; http://n2t.net/addgene:28176; RRID: Addgene_28176) (Takagi et al., 2005). For FRAP analysis of nucleolar 3xMS2-TR 1 µg of mTagBFP-Nucleus-7 was transfected into HeLa cells expressing 3xMS2-TR and MCP-mNeonGreen. mTagBFP-Nucleus-7 was a gift from Michael Davidson (Addgene plasmid # 55265 ; http://n2t.net/addgene:55265 ; RRID:Addgene_55265).

TCAB1 was knocked-out using two separate sgRNA and Cas9 encoding plasmids that were transfected alongside a GFP-expressing plasmid. 24 hours after transfection single-cell clones were sorted using the GFP signal. TCAB1 knock-out clones were screened by PCR and confirmed by western blot, Southern Blotting of the *TCAB1* locus and immunofluorescence imaging. TR was knocked out by transfecting two sgRNA plasmids and a homologous recombination donor plasmid. 48 hours after transfection puromycin selection was initiated and 1 week after the initiation of selection single-cell clones were generated by dilution into 96-well

plates. TR knock-out was confirmed using PCR and Sanger sequencing, fluorescence *in situ* hybridization, and RT-qPCR. TR^{G414C} plasmid was generated by inverse PCR using the vector of the WT TR plasmid.

2.7.3: Immunofluorescence and Fluorescence *In Situ* Hybridization Imaging

Fixed cell immunofluorescence imaging and fluorescence *in situ* hybridization was carried out as previously described (Schmidt et al., 2014). Briefly, cells grown on coverslips were fixed in PBS supplemented with 4% formaldehyde. When using the HaloTag for fluorescence detection cells were incubated with 100 nM of JF646 HaloTag-ligand for 30 min prior to fixation. Unincorporated ligand was removed by 3 washes with complete media followed by placing the cells back in the incubator for 10 min to let additional dye leak out of the cells. mEOS3.2-TRF2 was detected using the intrinsic fluorescence of green form of mEOS3.2. After removing the fixation solution using 2 PBS washes, coverslips were transferred into aluminum foil covered humidity chambers with a parafilm layer and rinsed with 1 ml of PBS with 0.2% Triton X-100. Cells were than incubated in blocking buffer (PBS, 0.2% Triton X-100, 3% BSA) for 30 minutes, followed by incubation with primary antibodies diluted in blocking buffer for 1 hour. All primary antibodies were used at a concentration of 1 µg/ml. After three washes with PBS + 0.2% Triton X-100, coverslips were incubated with secondary antibodies diluted in PBS + 0.2% Triton X-100 for 1 hour.

All secondary antibodies were used at a concentration of 4 µg/ml. Cells were washed three times PBS + 0.2% Triton X-100 prior to a second fixation with PBS + 4% formaldehyde. In cases where nuclear staining was used, the first of the three washing steps also included 0.1 µg/ml HOECHST. After the second fixation steps, coverslips were dehydrated in three steps with ethanol (70%, 95%, 100%), re-hydrated in 2xSSC + 50% formamide, blocked for 1 hour in hybridization buffer (100 mg/ml dextran sulfate, 0.125 mg/ml *E. coli* tRNA, 1 mg/ml nuclease free BSA, 0.5 mg/ml salmon sperm DNA, 1 mM vanadyl ribonucleoside complexes, 50% formamide, 2xSSC) at 37°C, before incubating the coverslips in hybridization buffer supplemented with three

TR probes (30 ng per coverslip, /5Cy5/GCTGACATTTTTTGTTTGCTCTAGAATGAACGGTGGAAGGCGGCAGGCCGAGGCTT, /5Cy5/CTCCGTTCCTCTTCCTGCGGCCTGAAAGGCCTGAACCTCGCCCTCGCCCCCGAGAG , /5Cy5/ATGTGTGAGCCGAGTCCTGGGTGCACGTCCCACAGCTCAGGGAATCGCGCCGCGC GC) overnight at 37°C. Probe sequences were previously described (Tomlinson et al., 2006). After hybridization coverslips were washed twice for 30 minutes in 2xSSC + 50% formamide and then mounted on slides using ProLong Antifade Diamond mounting media (Life Technologies). Microscopy was carried out using a DeltaVision Elite microscope using a 60x PlanApo objective (1.42 NA) and a pco.edge sCMOS camera. We acquired 20 Z-sections spaced by 0.2 µm, followed by image deconvolution and maximum intensity projection of the sections using the DeltaVision Softworx software.

2.7.4: Single-Molecule Live Cell Imaging

Live cell single-molecule imaging was carried out on an Olympus IX83 inverted microscope equipped with a 4-line cellTIRF illuminator (405 nm, 488 nm, 561 nm, 640 nm lasers), an Excelitas X-Cite TURBO LED light source, a Olympus UAPO 100x TIRF objective (1.49 NA), a CAIRN TwinCam beamsplitter, 2 Andor iXon 897 Ultra EMCCD cameras or 2 Hamamatsu Orca BT Fusion cameras, a cellFRAP with a 100 mW 405 nm laser, and a blacked-out environmental control enclosure. The microscope was operated using the Olympus cellSense software. 3xFLAG-HaloTag-TERT was labeled for 2 min in complete media supplemented with 100 nM JF646-HaloTag ligand (Grimm et al., 2015). After removing the HaloTag-ligand with three washes in complete media, cells were placed back in the incubator for 10 min to allow unincorporated dye to leak out of the cells. Cells were then transferred into CO_2 independent media and put on the microscope which was heated to 37°C.

Single-molecule imaging was carried out at 50 or 100 frames per second using highly inclined laminated optical sheet illumination (Tokunaga et al., 2008). Movies were typically 20

seconds in length (2000 frames) and were followed by a transmitted light acquisition to visualize overall cell morphology.For single-molecule imaging of 3xFLAG-HaloTag-Dyskerin, cells were labeled with 100 pM of JFX650-HaloTag Ligand (Grimm et al., 2020) for 1 min. Imaging was carried out at 100 frames per second and images of GFP-NPM1 were taken before and after single-molecule movies of dyskerin to assure the position of the nucleolus had not shifted.

2.7.5: RT-qPCR

RNA samples for RT-qPCR analysis were generated by using RNeasy Mini kits (Qiagen) using ~2 million cells as starting material. Reverse transcription was carried out using random hexamer primers and SuperScript III reverse transcriptase (Invitrogen) according to the manufacturer's instructions. qPCR was carried out using the Maxima SYBR Green qPCR master mix (Thermo Scientific) using primers for GAPDH and TR according to the manufacturer's instructions. All qPCR reactions were carried out in triplicates and three independent biological replicates were analyzed.

2.7.6: Southern Blotting

Southern blotting was carried out using standard protocols (Southern, 2006). Briefly, genomic DNA generated by phenol-chloroform extraction after cell lysis using TE supplemented with 0.5% SDS and 0.1 mg/ml Proteinase K, was digested with BamHI (generating a 1394 bp fragment spanning exons 1-3 of the *TCAB1* locus) and separated on a 0.8% agarose gel. The DNA was then transferred on a Hybond-N+ nylon membrane using capillary transfer. The *TCAB1* locus was detected using radioactive probes (alpha-^{32}P-dCTP) generated by randomly primed DNA synthesis using an 800 bp PCR product overlapping with the 1394 bp restriction fragment as a template and Klenow polymerase (NEB). Telomeric restriction fragment analysis was carried out as previously described (Nandakumar et al., 2012).

2.7.7: Western Blotting

Mini-PROTEAN TGX stain-free gels (Bio-Rad) were used for SDS-PAGE. Total protein was detected using a ChemiDoc MP (Bio-Rad) after a 45 second UV activation. Western transfer

was carried out using the Trans-Blot Turbo transfer system (Bio-Rad) according to the manufacturer's instructions using the mixed molecular weight transfer setting. Immuno-blotting was carried out using standard protocols. The C-terminal TCAB1 antibody (Proteintech, 14761-1-AP) was used at a 1:2000 dilution, the N-terminal TCAB1 antibody (Novus Biologicals, NB100-68252) was used at a 1:1000 dilution, the TERT antibody (Abcam, ab32020) was used at a 1:4000 dilution, the dyskerin antibody (Santa Cruz Biotech, sc-373956) was used at a 1:200 dilution, the GAR1 antibody was used at a 1:2000 dilution (Proteintech, 11711-1-AP), the fibrillarin antibody was used at a 1:2000 dilution (Novus Biologicals, NB300-269), and the lamin B1 antibody was used a 1:2000 dilution. Secondary antibodies were used at a 1:5000 dilution.

2.7.8: Northern Blotting

RNA was extracted from cell lysates, cellular fractions, and purified telomerase samples using the RNeasy Mini kit (Qiagen) and eluted in 30 ul of RNase free water. Purified telomerase samples were supplemented with 10 ng of a loading and recovery control prior to RNA extraction (*in vitro* transcribed TR 34-328). 15 ul of eluted RNA was mixed with 15 ul of 2x formamide loading buffer (0.1XTBE, 25 mM EDTA, 0.1% bromophenol blue, 0.1% xylene cyanol, 93% formamide) and heated to 60 °C for 5 min. Samples were separated on a 6% TBE, 7M Urea, polyacrylamide gel (Life Technologies), and transferred to a Hybond N+ membrane (Cytiva) using a wet-blotting apparatus in 1x TBE for 2 hours at 0.5 A of constant current in the cold room. After transfer, membranes were UV-crosslinked, and pre-hybridized in Church buffer for 2 hours at 50 °C. Three DNA oligos complementary to TR (GACTCGCTCCGTTCCTCTTC, GCTCTAGAATGAACGGTGGAA, CCTGAAAGGCCTGAACCTC, CGCCTACGCCCTTCTCAGT, ATGTGTGAGCCGAGTCCTG), 7SL (GCGGACACCCGATCGGCATAGC), U3 (GCCGGCTTCACGCTCAGGAGAAAACGCTACCTCTCTTCCTCGTGG), and 7SK (GTGTCTGGAGTCTTGGAAGC) were radioactively labeled using T4 PNK (NEB) and ~10x10^6 cpm of each probe were added to the membrane. Hybridization was carried out at 50 °C overnight.

Membranes were washed three times with 2xSSC, 0.1% SDS prior to exposure to a storage phosphorescence screen (Cytiva) which was then imaged on an Amersham Typhoon IP phosphoimager (Cytiva).

2.7.9: Telomerase Expression and Purification

Cell lines were transfected in 15-cm tissue culture plates at ~90% confluency (~25-30x10^6 cells) using 7.5 µg of TERT plasmid, 30 µg of TR plasmid and 75 µl of Lipofectamine 2000 in 1875 ul of Opti-MEM (Cristofari and Lingner, 2006). The same amounts were used in transfecting TR^{G414C}, LhTRmin (Vogan et al., 2016) or pBS U3-hTR-500 (Addgene plasmid # 28170 ; http://n2t.net/addgene:28170 ; RRID:Addgene_28170) (Fu and Collins, 2003) plasmids, which were generously gifted by Kathleen Collins . Transfected cells were split to three 15 cm dishes 24 hours after transfection. 48 hours after transfection cells were counted, harvested, and snap frozen in liquid nitrogen. Cells were lysed in 1 ml of CHAPS lysis buffer supplemented with 5 µl of RiboLock RNase inhibitor (10 mM TRIS pH 7.5, 1 mM $MgCl_2$, 1 mM EGTA pH 8.0, 0.5% CHAPS, 10% glycerol) per 100x10^6 cells and rotated at 4 °C for 30 min. Lysates were cleared in a table-top centrifuge at 21,000xg for 15 min at 4 °C. Identical cell equivalents were used for all samples. 45 µg of anti-TERT antibody was added per ml of cleared lysate and samples were rotated for 1 hour at 4 °C. Lysates were then added to 100 µl of protein G agarose and rotated for 1 hour at 4 °C. The resin was spun down at 1000xg and washed four times with 1 ml of Buffer W (20 mM HEPES pH 7.9, 300 mM KCl, 2 mM $MgCl_2$, 1 mM EDTA, 1 mM DTT, 1 mM PMSF, 0.1% Triton X-100, 10% glycerol). TERT was eluted in 100 µl of Buffer W supplemented with 5 µl of 1 mM TERT peptide by rotating for 30 min at room temperature.

2.7.10: Telomerase Activity Assays

Telomerase assays were carried out in 20 µl of reaction buffer (50 mM TRIS pH 8.0, 150 mM KCl, 1 mM MgCl2, 2 mM DTT, 100 nM TTAGGGTTAGGGTTAGG oligo, 10 µM dATP, 10 µM dGTP, 10 µM dTTP, 0.165 µM dGTP [α-32P] 3000 Ci/mmol) including 2 µl of purified telomerase

for 1 hour at 30 °C. Telomerase was incubated with the substrate oligo for 15 min at room temperature, prior to initiating the reaction by addition of dNTPs. Reactions were stopped by adding 100 µl of 3.6 M of ammonium acetate supplemented with 20 µg of glycogen and 32P 5'-end labeled loading control oligos (TTAGGGTTAGGGTTAGGG, TTAGGGTTAGGGTTAG). Reaction products were precipitated using 500 µl of ice-cold ethanol and stored at -20 °C over-night. Reaction products were spun down in a table-top centrifuge at max speed for 30 min at 4 °C, washed with 500 µl of 70% ethanol, and spun down again speed for 30 min at 4 °C. The 70% ethanol was decanted, and the reaction products were dried in an Eppendorf vacuum concentrator at 45 °C. Reaction products were resuspended in 20 µl of loading buffer (0.05XTBE, 25 mM EDTA, 0.05% bromophenol blue, 0.05% xylene cyanol, 46.5% formamide) and incubated at 95 °C for 5 min. 10 µl of each sample was separated on a 12% polyacrylamide, 7 M urea sequencing gel pre-run for 45 min at 90W. Gels were dried and exposed to a storage phosphorescence screen (Cytiva) and imaged on an Amersham Typhoon IP phosphoimager (Cytiva).

2.7.11: Nucleolar Isolation

Cellular fractionation was carried out using a previously described method (Lam and Lamond, 2006). All procedures were carried out on ice and centrifugations at 4 °C. Approximately $1x10^6$ million cells were harvested by trypsinization, washed with PBS, followed by incubation in a hypotonic buffer (10 mM HEPES pH 7.9, 10 mM KCl, 1.5 mM $MgCl_2$, 0.5 mM DTT) to swell the cells. A small fraction of the swollen cells was collected as input sample. Swollen cells were then ruptured using pre-cooled dounce homogenizer and the tight pestle (VWR Cat. 62400-595). The ruptured cells were centrifuged at 218xg for 5 min to pellet nuclei. Nuclei where then resuspended in buffer S1 (0.25 M sucrose, 10 mM $MgCl_2$), layered on top of buffer S2 (0.35 M sucrose, 0.5 mM $MgCl_2$) in a 15 ml conical tube, and centrifuged at 1430xg in a swinging bucket rotor for 5 min to further purify nuclei. Nuclei were resuspended in buffer S2 and sonicated on ice for 10 seconds

at 30% power (Fisherbrand Model 505, 500W). The sonicated nuclei were then layered on top of buffer S3 (0.88 M sucrose, 0.5 mM $MgCl_2$) and centrifuged at 3000xg in a swinging bucket rotor for 5 min to further purify nucleoli. The nucleolar pellet was suspended in buffer S2 and centrifuged a final time at 1430xg to yield a highly purified nucleolar pellet, which was resuspended in buffer S2. Equal fractions of input, cytoplasm, nuclei, nucleoplasm, and nucleoli samples were collected and analyzed by western and northern blots. To test the impact of salt concentration on the integrity of nucleoli, nuclei ruptured by sonication were mixed 1:1 with buffer S2 containing 40 mM HEPES pH7.9 with and without 715 mM KCl, prior layering the solution on top of buffer S3.

2.7.12: Cell Synchronization and Flow Cytometry

Cell lines in 15-cm tissue culture plates at a 70% confluency were blocked with 2 mM thymidine then released from thymidine after 24 hours and harvested at four time points post release: 0, 4, 8 hours. Along with each synchronization, asynchronous population was also harvested. Cells were harvested using PBS supplemented with 5 mM EDTA then fixed with ethanol, stained with propidium iodide for DNA content, and finally filtered to generate a single cell suspension. Stained samples were run through BD Accuri C6 cytometer and cell-cycle distributions were analyzed on OriginLab.

2.7.13: Single-Particle Tracking

Single-particle tracking was carried out in MATLAB 2019a using a batch parallel-processing version of SLIMfast modified to allow the input of TIFF files (kindly provided by Xavier Darzacq and Anders Hansen) (Hansen et al., 2018), an implementation of the Multiple-Target-Tracing algorithm (Sergé et al., 2008), with the following settings: Exposure Time = 10 ms, NA = 1.49, Pixel Size = 0.16 µm, Emission Wavelength = 664 nm, D_{max} = 5 $\mu m^2/s$, Number of gaps allowed = 2, Localization Error = 10^{-5}, Deflation Loops = 0. Diffusion coefficients and the fraction of molecules in each distinct particle population were determined using the MATLAB version of the Spot-On tool (kindly provided by Xavier Darzacq and Anders Hansen) (Hansen et al., 2018) with the following settings: TimeGap = 10 ms or 20 ms, dZ = 0.700 µm, GapsAllowed = 2,

TimePoints = 8, JumpsToConsider = 4, BinWidth = 0.01 µm, PDF-fitting, D_Free1_3State = [1 25], D_Free2_3State = [0.1 1], D_Bound_3State = [0.0001 0.1]. For all experiments we carried out 3 independent biological replicates with at least 15 cells for each cell line. The statistical significance of differences in particle fractions and diffusion coefficients were assessed using a two-tailed T-Test.

For the analysis of dyskerin trajectories a mask of the nucleolus was generated manually using the threshold function in FIJI. Dyskerin trajectories whose coordinates overlapped with the nucleolar mask for a single frame were designated as nucleolar trajectories. The remaining trajectories were designated nuclear trajectories. All data sets were analyzed using Spot-On as described above.

2.7.14: Fluorescence recovery after photobleaching

Fluorescence recovery experiments (FRAP) of Halo-DKC1 were carried out using the same Olympus microscope used for single-molecule imaging. Cells were stained for 10 min with 100 nM JFX650-HaloTag ligand in complete media. After removing the HaloTag-ligand with three washes in complete media, cells were placed back in the incubator for 10 min to allow unincorporated dye to leak out of the cells. Cells were then transferred into CO_2 independent media and put on the microscope which was heated to 37°C. We identified cells with two clearly visible nucleoli and bleached one of them by placing three diffraction limited bleach spots within the nucleolar 3xFLAG-HaloTag-dyskerin signal. Each spot was bleached for 100 ms at 50% laser power, which lead to complete loss of the fluorescence within the nucleolus. Cells were imaged prior to and after bleaching at 1 frame per second using the Excelitas X-cite TURBO LED light source and the 100x objective. Photobleaching due to LED exposure was negligible. To quantify FRAP we first drift corrected the movie using NanoJ (Laine et al., 2019), we then placed a region of interest (ROI) within the nucleolus and quantified mean intensity within the ROI over time. Background signal was determined in an area of the field of view that was not covered by a cell and subtracted from the nucleolar ROI. In addition, the mean fluorescence after the bleaching

pulse was divided by the fraction of total cellular fluorescence remaining after the bleaching pulse. Because the laser pulse bleaches a significant amount of total cellular fluorescence (typically 20-40%), this normalization is critical to determine the maximal amount of fluorescence recovery possible. For example, if 30% of total cellular fluorescence is lost due to the bleaching pulse, the maximal fraction of pre-bleach fluorescence than can theoretically be recovered is 70%. The recovery data was then fit using a single exponential function ($1-A*e^{-kt}+C$), where k corresponds to the rate constant and C to the fraction of the initial signal that is not recovered (i.e. the static fraction).

For the FRAP analysis of nucleolar 3xMS2-TR bound by MCP-mNeonGreen cells were imaged on a Nikon A1R confocal microscope in the MSU Confocal Laser Scanning Microscopy core. 3xMS2 TR clearly localized to the DFC of the nucleolus marked by mTagBFP-Nucleus-7 was bleached using the 488 nm laser line and recovery of the MCP-mNeonGreen was imaged every 2 seconds using the 488 nm laser line. Data analysis was carried out as described above.

2.7.15: Quantification of RT-qPCR data

RT-qPCR experiments were carried out in triplicate and the TR Ct value was normalized to the GAPDG Ct value. The mean ΔCt (Ct of TR – Ct of GAPDH) value from three independent experiments and the corresponding standard deviation were plotted.

2.7.16: Quantification of Western Blots, Northern Blots, and Telomerase Activity Assays

Gel images from western Blots, northern Blots, and telomerase activity assays were analyzed using ImageQuant TL 8.2. To quantify TR levels in Northern blots the TR band intensity was normalized to the loading and recovery control signal added to the RNA sample prior to RNA purification. To quantify telomerase activity, the whole lane intensity starting at repeat 1 was determined and divided by the sum of the loading control signals. Telomerase processivity was calculated by dividing product intensity > 7 repeats by the total signal in the respective lane. The statistical significance of the observed differences was calculated using a two-tailed T-test using

a minimum of three biological replicates. Each biological replicate (independent telomerase expression and purification) was analyzed in technical triplicate.

CHAPTER 3: RIBONUCLEOPROTEIN MUTATIONAL PROFILING IN RIBONUCLEOPROTEIN ASSEMBLY

Basma M. Klump, Madison Turley, Chase Weidmann, Jens C. Schmidt

3.1: Introduction

Since the development of high-throughput RNA sequencing technology in 2008, increasingly numerous and diverse methodologies emerged (Marioni et al., 2008). One of the techniques that followed high-throughput RNA sequencing unraveled RNA structures through mutational profiling and sequencing. Regions of high mutational rate indicate secondary and tertiary folding because unpaired RNA regions are more susceptible to mutations (Wu et al., 1998).

One of the first approaches developed in RNA structural mapping was the dimethyl sulfate mutational profiling with sequencing which involves the highly-toxic DMS reagent to modify unpaired adenosine and cytosine nucleotides in dissecting folding patterns of RNAs (Zubradt et al., 2017). The least modified regions report on the folding capacity of the RNA. Likewise, selective 2'hydroxyl acylation analyzed by primer extension (SHAPE) also reports on RNA structure. To sequence RNA, it must be first reverse transcribed to DNA which requires a reverse transcriptase. In SHAPE, reverse transcription terminates when it encounters a modified RNA base, thereby limiting the number of modified RNA positions that can be identified in a single sequencing read (Wilkinson et al., 2006). Later, RNA technologies evolved to unravel RNA compositions in living cells via UV crosslinking and immunoprecipitation (CLIP-Seq) (Lee and Ule, 2018). However, CLIP-seq carries a similar limitation to SHAPE in that the reverse transcriptase is terminated at regions with bound protein. Additionally, proteins associated with the RNA must be known and the method also requires the purification of the proteins via an antibody or a tag. Importantly, these methods do not define binding sites of proteins (Lee and Ule, 2018).

To overcome the limitations in existing RNP methodologies, in 2021, Weidemann et al. developed an approach for the identification of RNA-protein assembly that paved the way to better

understand RNP assembly in a variety of knock-out models as discussed in this chapter, with potentially inhibitors and disease-associated mutants in future studies. The approach named, ribonucleoprotein mutational profiling (RNP-MaP) technique will especially be critical in aging, cancer and telomere syndromes by contributing to the understanding of the biogenesis of the telomerase RNP.

The telomerase RNP consists of the central RNA, TR on which the telomerase proteins assemble: TERT, TCAB1, dyskerin-NOP10-NHP2-GAR1 complex, and the most recently discovered telomerase-associated factor, H2A-H2B dimer (Ghanim et al., 2021). H2A and H2B are histone dimers that together with H3 and H4 package the DNA into a nucleosome. A condensed DNA covered with histones makes the DNA unavailable for replication and transcription (Luger et al., 1997). When nucleosomes unwind, the DNA becomes accessible to transcription, replication and telomere synthesis.

Telomere synthesis requires an assembled telomerase RNP. Previously, we showed that TCAB1 promotes telomerase RNP assembly using a variety of approaches in lysates, fixed and living cells (Klump et al., 2023). In this chapter, I will discuss how we demonstrated RNA-protein crosslinking using the RNP-MaP approach in defining telomerase RNP assembly and uncovering novel crosslinking patterns of histone proteins H2A and H2B in the telomerase RNP.

3.2: Method

RNP-MaP is a sequencing-based method to map protein-RNA contact sites in living cells. RNP-MaP involves site-specific crosslinking of proteins to RNA of interest and reverse transcribing the RNA using an error-prone buffer, which leads to mutations at sites on the RNA where a protein is bound. By Illumina RNA sequencing, the frequency of the mutations on the RNA library are aligned creating fingerprints on the RNA where proteins are cross-linked (Weidemann et al., 2021).

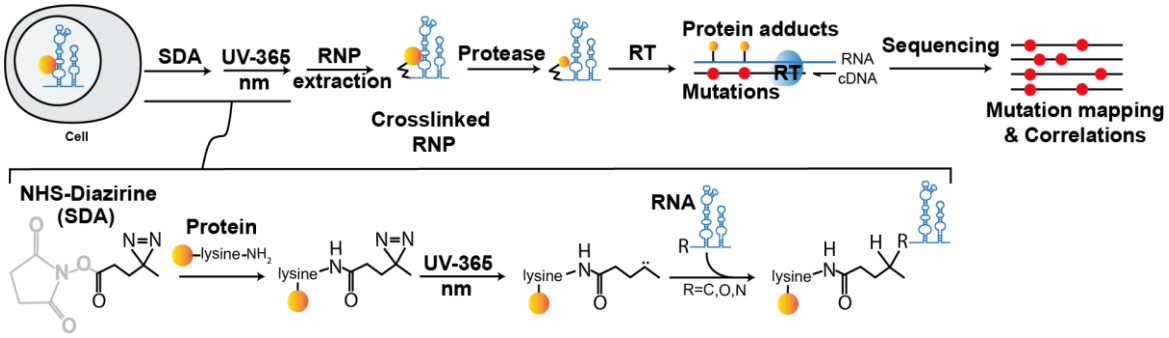

Figure 3.1. Method and workflow of the ribonucleoprotein mutational profiling (RNP-MaP) adapted from Weidmann et al 2021. Nature Biotechnology. (A) The crosslinking reagent NHS-Diazirine contains two parts that react with the RNP. NHS reacts with the amine side chain of lysine amino acids while diazirine, upon activation with ultraviolet light reacts with the RNA nucleotides. (B) Step-wise sequence of the method from the time of cross-linking to sequencing and library alignment (Weidmann et al 2021). RT: reverse transcription.

To crosslink the RNA to proteins in living cells, a non-methylating reagent, NHS-diazirine (SDA) is applied to cells in culture (Fig. 3.1). SDA has two reactive chemical groups: NHS (known as succinimidyl ester) and a diazirine. NHS reacts with the primary amine group in lysines, a common RNA-interacting amino acid. Therefore, a limitation of the RNP-MaP approach is that the RNA-binding protein must have lysines in close proximity to a nucleotide. When activated by UV, the diazirine group of the SDA reacts with nucleotides on RNA within 15 angstroms from the cross-linked lysine (Weidmann et al., 2021). Cells are then lysed and cross-linked RNPs are purified (Queiroz el al., 2019). Next, proteases are added to the purified RNP to digest the proteins into smaller adducts to enable reverse transcriptase with complementary reverse primers to read through a single RNA molecule without dissociating from the RNA due to encountering large protein adducts. A limitation here is that reverse transcriptase cannot synthesize DNA in primer-binding sites. The error-prone reverse transcriptase that reads through the RNA molecule incorporates random nucleotides where adducts are present. The sites of these mutations are representative of protein-RNA interactions or protein binding sites on the RNA. Paired nucleotides that are mutated in the same RNA molecule (i.e. sequencing reads) within a statistical significance are correlated to create a higher order network of protein interactions. The RNP-MaP results below are analyzed using a p-value of 0.01 and the shade of the green color marking the sites of

crosslinking on Figures 3.1-6 indicate the confidence in the crosslinking (the darker the green colored marks, the higher the confidence in a statistically significant crosslinking).

We adopted the RNP-MaP approach to further demonstrate a reduction in telomerase RNP assembly in the absence of TCAB1 and dissect other factors in the RNP. We cross-linked RNA-protein interactions in two parental cell lines and two TCAB1 knockout cell lines (cell line generation discussed in chapter 2).

3.3: Results

RNP-MaP uncovers two major aspects of an RNP; it identifies cross-linked sites where proteins are present on the RNA and correlations between crosslinking of different factors on the same RNA molecule. In other words, crosslinking of one protein on the RNA can be correlated to the cross-linking pattern of a different factor.

To confirm the proof of principle, we applied the RNP-MaP method to an ACA57 scaRNA that contains two CAB boxes where TCAB1 binds (Fig. 3.2). ACA57 is a 137-nucleotide RNA that guides pseudouridylation of U5 snRNA to promote stability, accumulation and folding necessary for spliceosome function (Kiss et al., 2004). ACA57 scaRNA contains two CAB boxes, starting at nucleotides U33 (UCAG) and U98 (UAAG) where TCAB1 binds (Tycowski et al., 2009).

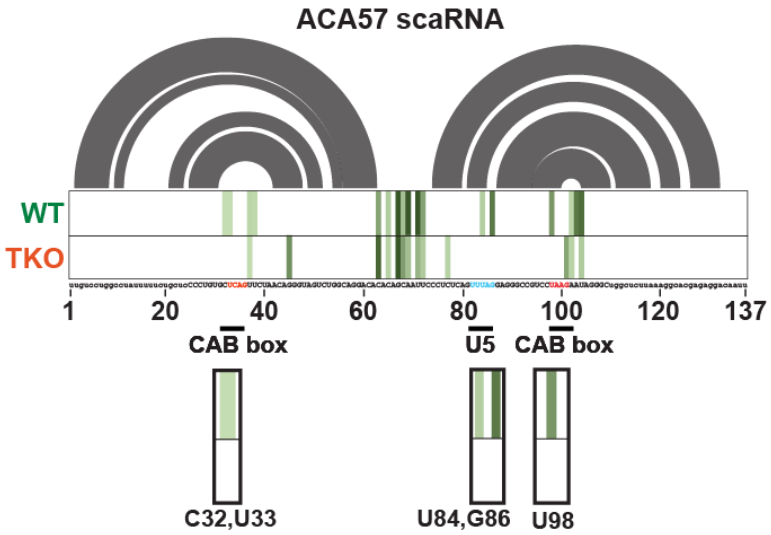

Figure 3.2. RNP MaP of the ACA57 scaRNA. The semicircles correspond to base pairing within

Figure 3.2 (cont'd)

the scaRNA creating secondary structures in wild type (WT) and TCAB1 knock-out (TKO) cells. The green columns correspond to the sites of crosslinking. The nucleotides colored in red indicate the CAB boxes while the nucleotides in teal indicate U5 base-pairing. The significant changes in the crosslinking between WT and TKO are zoomed in under the corresponding regions. P-value of 0.01 was used to determine significance. Figure design and data analysis was carried out by Chase Weidmann, Ph.D..

We sought to use RNP MaP to define the network association on ACA57 scaRNA TCAB1-depleted cells. Through RNP MaP, we demonstrated that the CAB boxes on ACA47 are unoccupied when TCAB1 is not present. In addition to the loss of crosslinking at the CAB boxes, we also observed a reduced crosslinking at the site where U5 snRNA base-pairs (U84, G86). This suggests that TCAB1 may promote pseudouridylation or impact assembly with U5 snRNA. Therefore, the role of TCAB1 in scaRNA-mediated modification of snRNAs must be further dissected.

As a negative control for TCAB1 crosslinking on RNA, we applied RNP-MaP on ncRNAs that do not contain CAB boxes: U1 snRNA and U3 snoRNAs (Fig. 3.3-4). Spliceosomal RNA, or U1 snRNA, is another non-coding RNA that is essential in cells. Base-pairing between U1 snRNA and U85 scaRNA directs dyskerin to pseudouridylate U1 (Kiss et al., 2006). Mature U1 RNA binds to the Sm complex which guides the RNP to coilin, a CB structural protein (Bellini and Gall, 1998; Kondo et al., 2015). We hypothesize that TCAB1, being a CB protein, may promote U1 RNP assembly and RNA modification. RNP-MaP revealed that depletion of TCAB1 is not associated with any loss in cross-linking with Sm complex necessary for U1 RNP assembly (Fig. 3.3). However, because the forward primer that was used to amplify the cDNA library overlaps with the pseudouridylated sites (nucleotides 3-12), we cannot exclude the possibility that TCAB1 impacts base-pairing with U85 in the same way that it potentially impacts ACA57 binding to U5.

Future studies on the impact of TCAB1 in the modification of U1 scaRNA is necessary to address downstream effects of TCAB1 on RNA splicing. Importantly, it is probable that the pseudouridylation of U1 takes place in CBs since U85 scaRNA is enriched there. However, the

role of CBs in the spliceosomal RNP maturity and assembly also has not been determined yet (Bellini and Gall, 1998). The next step is to develop coilin knock-out cell lines and dissect the cross-linking changes in the pseudouridylation and Sm binding sites to define the role CBs play in pseudouridylation and RNP assembly via RNP MaP. Another method is via U1 snRNA pull-down methods and analysis of the levels of co-purified Sm to determine assembly.

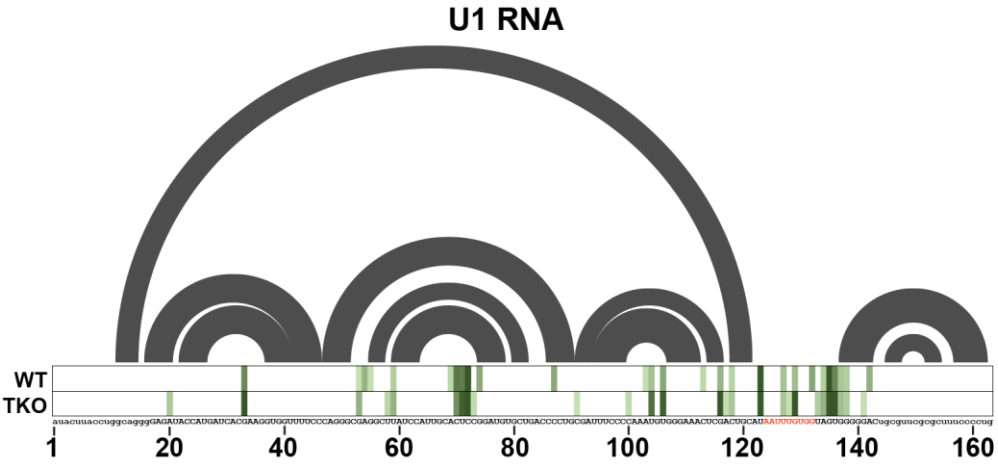

Figure 3.3. RNP MaP of the U1 snRNA. The semicircles correspond to base pairing within the snRNA creating secondary structures in wild type (WT) and TCAB1 knock-out (TKO) cells. The green columns correspond to the sites of crosslinking. The significant changes in the crosslinking between WT and TKO are zoomed in under the corresponding regions. The nucleotide colored in red indicate the binding site for the Sm complex. P-value of 0.01 was used to determine significance. Figure design and data analysis was carried out by Chase Weidmann, Ph.D..

Other RNPs that we applied RNP-MaP to are snoRNAs. Like scaRNAs, snoRNAs are non-coding RNAs transcribed by RNA polymerase II from intron regions of protein-encoding (Lestrade et al., 2006; Kiss-Laszlo et al., 1996). SnoRNAs are responsible for guiding dyskerin-mediated pseudouridylation on ribosomal RNAs. Unlike scaRNAs, U3 snoRNA does not contain a CAB box and does not interact with TCAB1, therefore U3 is unlikely to be impacted by a loss of TCAB1, and hence serves as a negative control for our experiment. A previous study showed that U3 snoRNA does not co-purify with TCAB1 (Venteicher et al., 2009). Given the lack of CAB box and binding with U3 snoRNA, we hypothesize that TCAB1 does not mediate U3 snoRNA crosslinking with other factors. RNP-MaP demonstrated that cross-linked sites at U3 are maintained in TCAB1 knock-out cells (Fig. 3.4). RNP-MaP can be used in dissecting the assembly

of snoRNAs with modifying factors such as fibrillarin and dyskerin and how phase-separated organelles (i.e. nucleoli where snoRNAs are enriched) impact their function. Future work may entail the development of knock-down strategies to target dyskerin and fibrillarin and dissect snoRNP assembly and the impact on pseudouridylation of rRNAs.

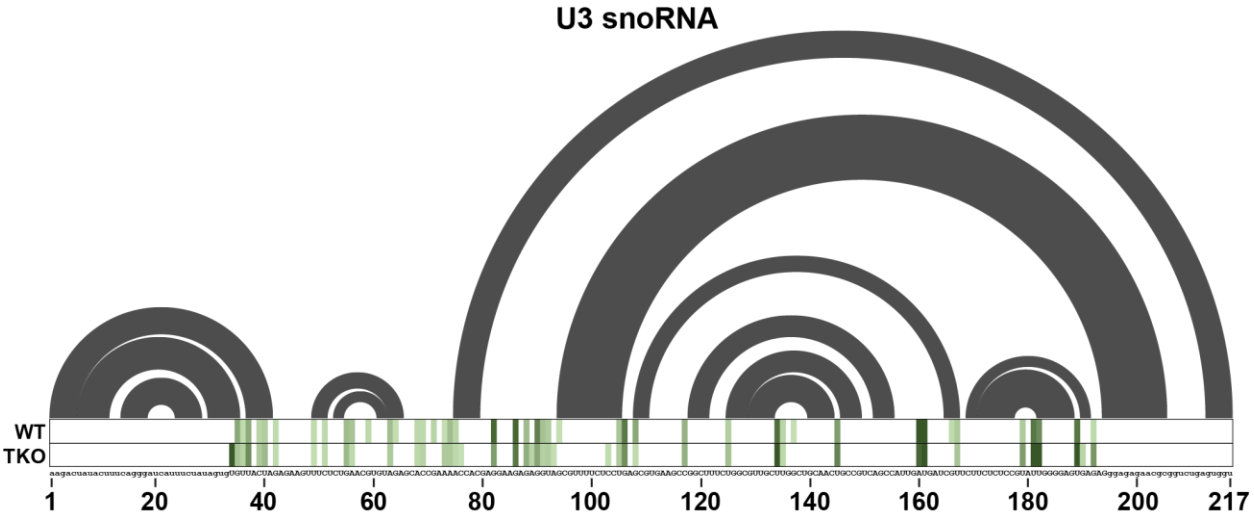

Figure 3.4. RNP MaP of the U3 snoRNA. The semicircles correspond to base pairing within the snoRNA creating secondary structures in wild type (WT) and TCAB1 knock-out (TKO) cells. The green columns correspond to the sites of crosslinking. The significant changes in the crosslinking between WT and TKO are zoomed in under the corresponding regions. P-value of 0.01 was used to determine significance. Figure design and data analysis was carried out by Chase Weidmann, Ph.D..

In parental HeLa cells, we found cross-linked sites on TR that indicate protein binding (Fig. 3.5-3.6). The identified cross-linked sites in control cell lines reveal an assembled telomerase RNP at the CAB box where TCAB1 binds (U411), at the H/ACA domain where dyskerin binds (A360-380), at H2A-H2B dimer binding sites (A163, G315, C317) and TERT binding sites: the template (U53), pseudoknot (A129) and CR4/5 region (G306-C307) (Fig. 3.5A-C).

In the absence of TCAB1, we observed changes in crosslinking patterns in TCAB1 binding sites at the CAB box in region U411 (Fig. 3.5A, 3.6). Consistent with our previous finding that TERT is less likely to bind TR in the absence of TCAB1 (Klump et al 2023), TR reveals a lack of cross-linking at sites where TERT binds: the CR4/5 region (G306, C307) (Fig. 3.5C, 3.6), pseudoknot (A129) (Fig. 3.5C, 3.6), and the template (U53) (Fig. 3.5C,6).

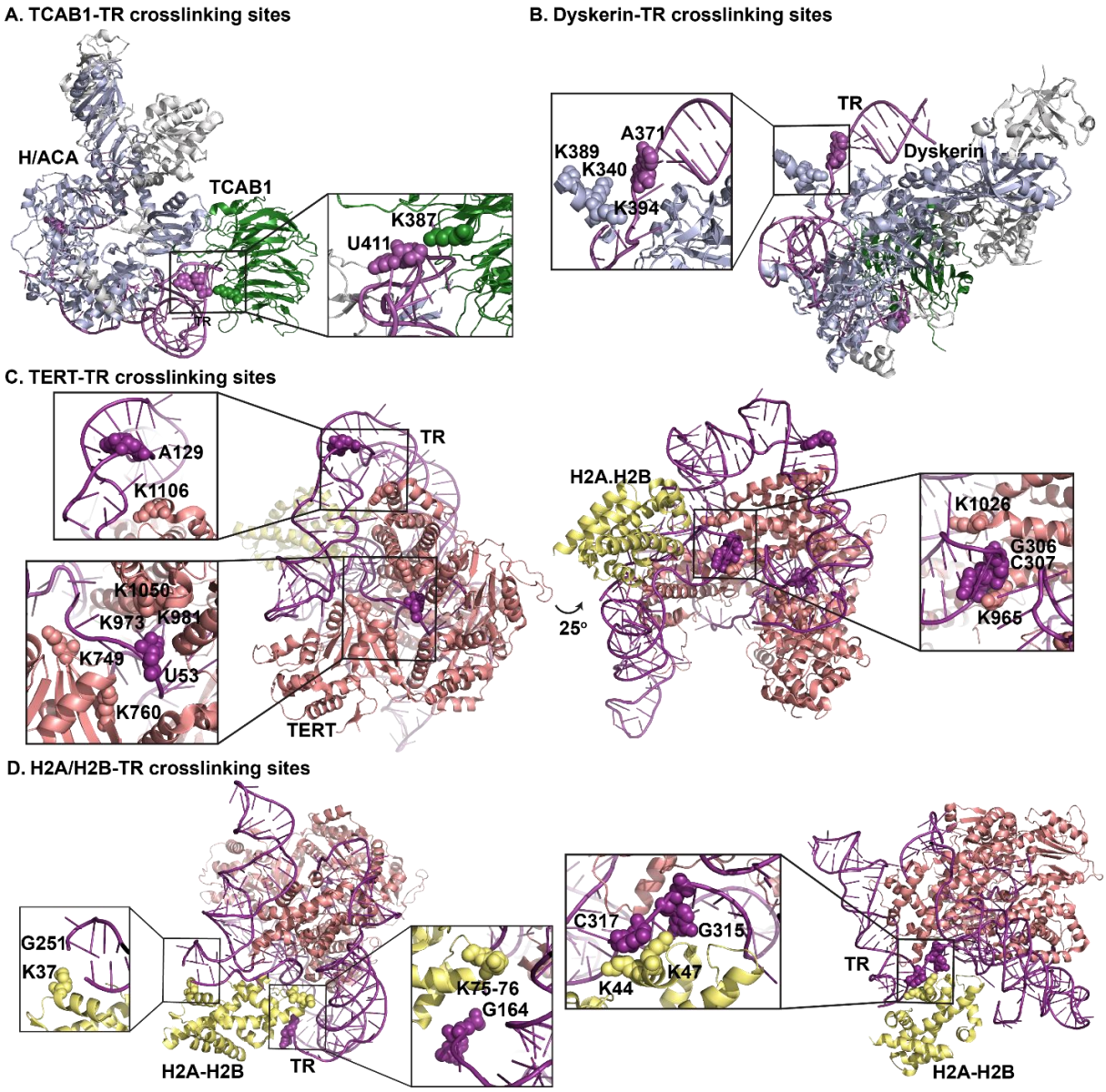

Figure 3.5. Structures and sites of crosslinking between TR and the telomerase RNP factors as revealed by RNP-MaP. All crosslinking sites annotated occur with lysine groups of amino acids. **(A)** TCAB1 and TR crosslinking site. **(B)** Dyskerin and TR crosslinking site. **(C)** TERT and TR crosslinking sites. (D) H2A-H2B and TR crosslinking sites. Structures were obtained via Pymol 7TRC (A-B) and 7TRF (C-D).

Though TCAB1 interacts with dyskerin, dyskerin-TR binding is not impacted by TCAB1 (Klump et al 2023). RNP-MaP directly reveals that cross-linked sites with dyskerin are maintained in the absence of TCAB1 (Fig. 3.5B, 3.6). Therefore dyskerin-TR binding is independent of

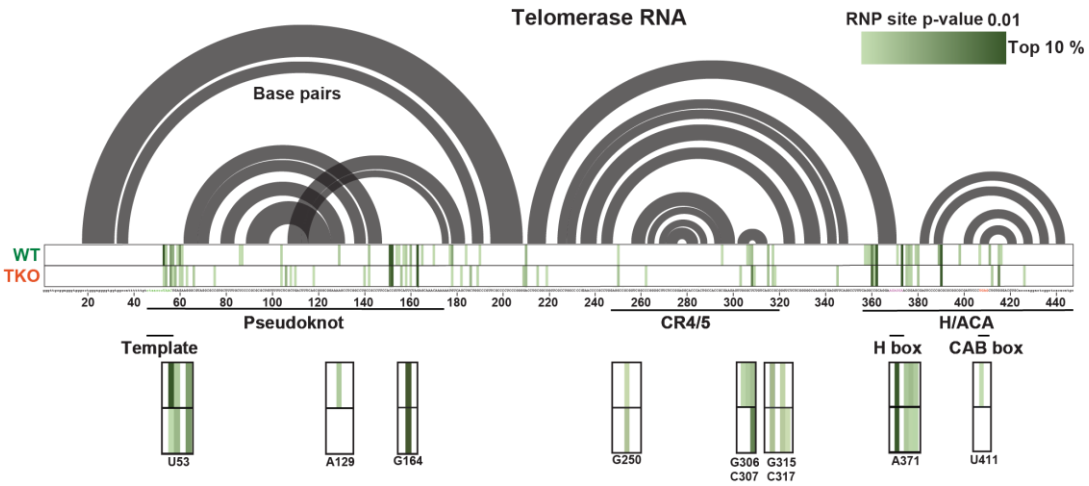

Figure 3.6. RNP MaP of the telomerase RNA (TR). The semicircles correspond to base pairing within TR creating secondary structures in wild type (WT) and TCAB1 knock-out (TKO) cells. The green columns correspond to the sites of crosslinking. The nucleotides in red indicate the CAB box. The nucleotides in green indicate the template region. The significant changes in the crosslinking between WT and TKO are zoomed in under the corresponding regions. P-value of 0.01 was used to determine significance. Figure design and data analysis was carried out by Chase Weidmann, Ph.D..

TCAB1. Conversely, the impact of dyskerin on TCAB1-TR interaction is unknown. Given that dyskerin binds TR co-transcriptionally (Darzacq et al 2006), dyskerin may bind first and if it impacts TCAB1-TR association, it may suggest that TCAB1 must recognize not only the CAB box on TR but also dyskerin. Further work must be done to dissect the impact of dyskerin on TCAB1-TR interaction and sequence of assembly.

Interestingly, we also found mutational patterns that are consistent with H2A-H2B binding (G164, G250, G315, C317); these are unaffected by the absence of TCAB1, therefore H2A-H2B binding to TR is unlikely to be affected by changes in assembly (Fig. 3.5D, 3.6). Therefore, TCAB1 impacts TERT crosslinking to TR but not dyskerin nor H2A-H2B binding.

3.4: Discussion

Since TCAB1 does not promote H2A-H2B association with TR, H2A/H2B may associate with TR early in telomerase RNP biogenesis. However, the role of H2A-H2B in telomere synthesis remains unclear. Altogether, RNP-MaP supports the claim we made previously in that TCAB1 promotes TERT-TR assembly and we further demonstrate for the first time H2A-H2B may

associate with TR independently of TCAB1. Importantly, since TERT is not present on TR in the absence of TCAB1, H2A-H2B may also be independent of TERT. Further studies are essential in dissecting the impact of TERT on H2A-H2B in the telomerase RNP. Taken together, RNP-MaP is an approach valuable in defining assembly molecular mechanisms related to RNP assembly and biogenesis when combined with other tools such as knock-outs, knock-downs or potentially small molecule inhibitors. These techniques can be applied to the essential spliceosomal RNP, ribosomal RNP, snoRNP, scaRNP or further dissect the telomerase RNP to uncover molecular mechanism of biogenesis essential to its function.

CHAPTER 4: THE ROLE OF GAR1 IN THE TELOMERASE RIBONUCLEOPROTEIN

4.1: Introduction

GAR1 is a small 22-kDa nucleolar and Cajal body protein that contains six evolutionary conserved beta sheets medial to two glycine-arginine-rich (GAR) domains (Girard et al., 1992). Its association with RNPs is highly conserved among eukaryotes. GAR1 is associated with mature states of RNPs, the telomerase RNP, spliceosomal snRNPs, scaRNPs and snoRNPs (Dundr et al., 2004; Nguyen et al., 2018; Ghanim et al., 2021; Fujikane et al., 2018; Whitehead et al., 2002; Pellizzoni et al., 2001). GAR1 does not specifically bind to RNAs; rather, it associates with RNPs through protein-protein binding.

GAR1 was first identified in yeast for its essential role in ribosomal RNA maturation and pseudouridylation through snoRNPs (Girard et al., 1992; Watkins et al., 1998; Bousquet-Antonelli et al., 1997). A common complex that GAR1 associates with is the H/ACA complex found on a subset of scaRNAs, snoRNAs, and TR (Dundr et al., 2004; Pellizzoni et al., 2001; Kiss et al., 2006). In the telomerase RNP, two GAR1 molecules associate with a single telomerase (Dragon et al., 2000; Nguyen et al., 2018; Ghanim et al., 2021). However, the role of GAR1 in the H/ACA complex and RNP remains unknown.

In the telomerase RNP and snoRNPs, GAR1 associates with the complexes via dyskerin which has binding specificity to TR and snoRNA, respectively (Darzacq et al., 2006). Likewise, in the spliceosomal snRNPs, GAR1 binds to the SMN complex which in turn binds spliceosomal snRNAs (Whitehead et al., 2002). Interestingly SMN mutations in spinal muscular dystrophy patients block its association with GAR1 (Whitehead et al., 2002). Additionally, GAR1 also promotes nucleolar localization of snoRNPs (Whitehead et al., 2002; Pellizzoni et al., 2001). The following year, it was revealed that GAR1 is also a factor in the telomerase RNP (Dragon et al., 2000). However, to date, no associated disease-causing mutations have been found in GAR1

that lead to spinal muscular atrophy nor telomerase dysfunctions. The role of GAR1 in spliceosomal RNP, assembly and trafficking of the spliceosomal snRNPs and its role in the telomerase RNP remain unclear. Therefore, this chapter lays out the foundation and methods in dissecting the role of GAR1 in the telomerase RNP.

4.2: Results

Our first aim was to determine the molecular behavior of GAR1. First, we determined the cellular accumulation and distribution of GAR1. We were unable to utilize immunofluorescence approach in detecting GAR1 likely due to failure of the specific antibody to detect fixed epitopes and fixation may obliterate signal in certain compartments of the cells as occurs with cytoplasmic TCAB1 using immunofluorescence (Chapter 2).

We adopted a cellular fractionation approach using sucrose gradient to isolate nucleoli based on differences in density of cellular compartments (Fig. 4.1A). Consistent with observations by others (Dundr et al., 2004), we demonstrated that GAR1 is enriched in the nucleus specifically in the nucleoli of HeLa cells (Fig. 4.1B). Since TCAB1 and GAR1 are present in the

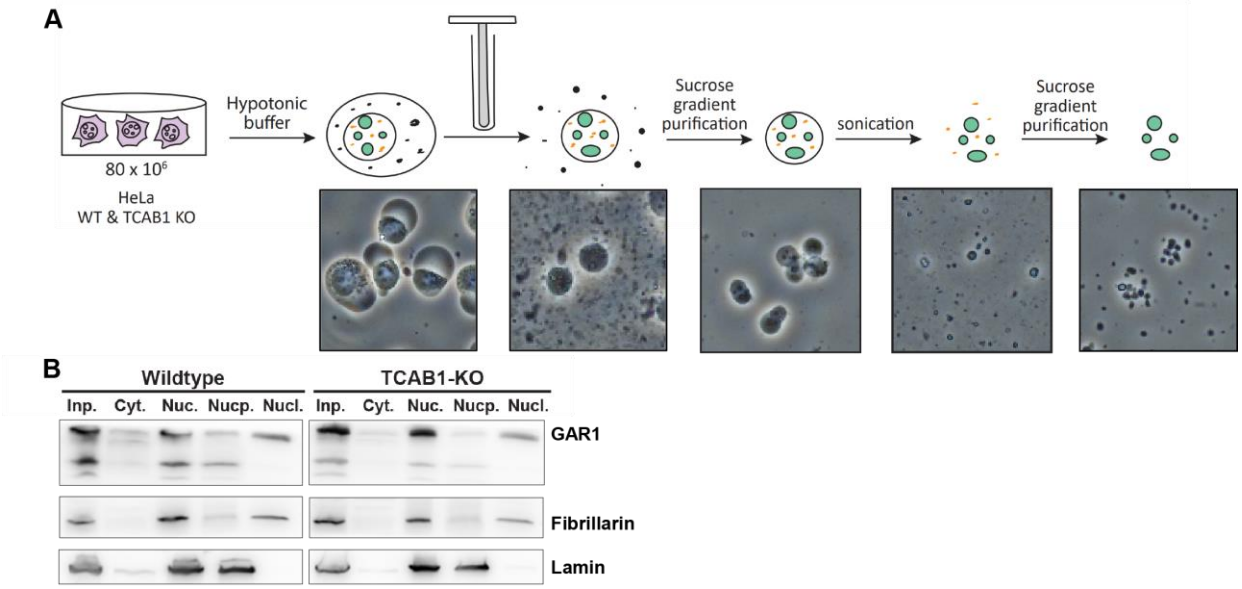

Figure 4.1. GAR1 is enriched in nucleoli. (A) Outline of cell fractionation by sucrose gradient to isolate nucleoli based on density. **(B).** Western blot of GAR1 in input (Inp.), cytoplasm (Cyt.), nucleus (Nuc.), Nucleoplasm (Nucp.), and nucleoli (Nucl.) with nucleolar and nucleoplasmic markers, fibrillarin and lamin B1, respectively.

telomerase RNP and that absence of TCAB1 promotes TR localization, we expect that GAR1 nucleoli localization would not differ in the absence of GAR1. We applied the approach in TCAB1 knock-out cell lines and, as expected, we detected nucleolar GAR1 in TCAB1 knock-out cells, which suggests that absence of TCAB1 does not impact GAR1 nucleolar localization (Fig. 4.1B). GAR1 does not contain a nucleolar localization signal (Nucleolar Localization Sequence Detecter, University of Dundee) thereby it is likely targeted to nucleoli via RNPs. We have previously determined that the majority of nucleolar TR is retained in nucleoli and its retention mechanism likely results from its bound state with the H/ACA complex (Klump et al., 2023). Since GAR1 associates with the H/ACA factors, GAR1 may be shuttled to nucleoli by the same retention mechanism as nucleolar TR (Klump et al., 2023). Therefore, we determined the dynamics of GAR1 in nucleoli using fluorescence recovery after photobleaching (FRAP) in living cells. We transiently expressed a HaloTagged GAR1 in HeLa and TCAB1 knock-out cells. We identified nucleoli using the marker nucleolin and bleached nucleolar GAR1 signal then quantified the fraction of signal recovered. GAR1 signal recovers to ~40% in HeLa cells and ~30% in TCAB1 knock-out cells over a time span of 5 minutes (Fig. 4.2). Interestingly, the fraction of GAR1 signal recovered is consistent with that of TR (~40%) suggesting that GAR1 and nucleolar TR share retention mechanism that sequesters them in nucleoli (Klump et al., 2023). The common binding factor in both GAR1 and TR is the H/ACA complex, therefore, it is likely that H/ACA complex shuttles GAR1 to nucleoli where it is retained.

Conversely, the fraction of dyskerin signal we previously reported is higher (~65%) suggesting that the majority of dyskerin may be freely diffusing (Klump et al., 2023). To reveal the states of their retention mechanism, in the future, we will employ live cell single molecule imaging to determine the fraction of bound and freely diffusing states of GAR1 and dyskerin. We expect to observe a higher bound fraction of GAR1 than dyskerin in nucleoli. Given that the majority of GAR1 in nucleoli is in bound states and is tightly associated with nucleoli, factors associating with GAR1 alters its kinetics and dictate its nucleolar retention.

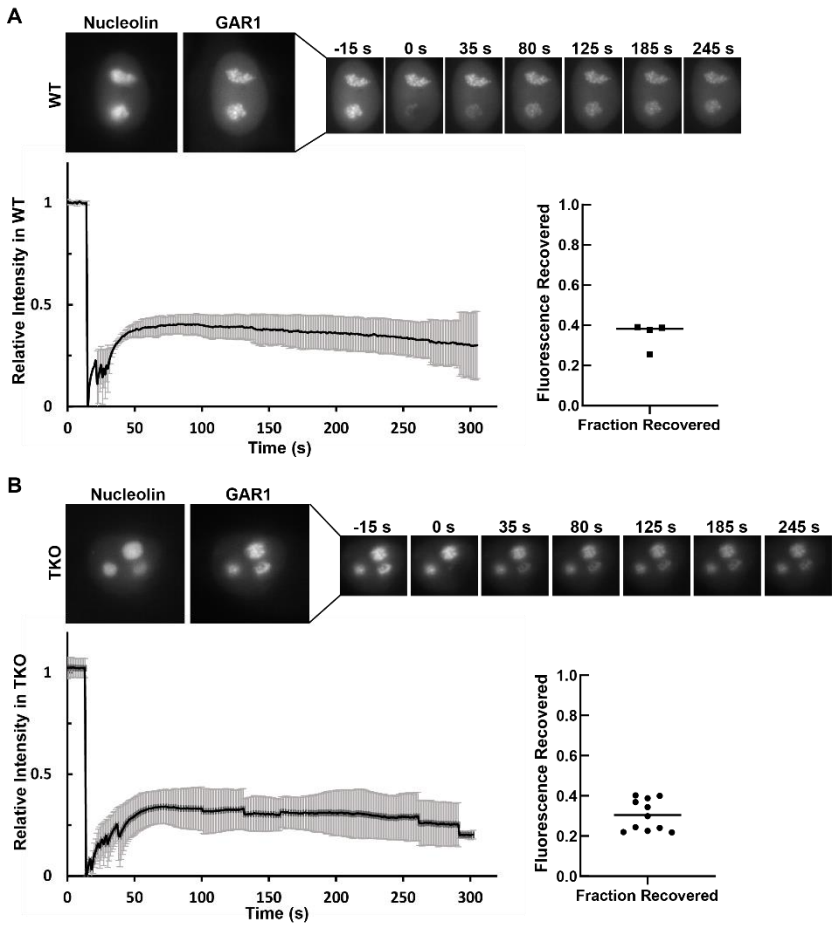

Figure 4.2. Fluorescence Recovery After Photobeaching (FRAP) of nucleolar HaloTag-GAR1 signal. **(A)** FRAP of GAR1 in wild type (WT) HeLa cells in relative intensity graph and fluorescent recovery plot **(B).** FRAP of GAR1 in wild type TCAB1 knock-out cells in relative intensity graph and fluorescent recovery plot.

In order to determine the diffusion properties of GAR1 and dyskerin, we are genetically editing HaloTagged dyskerin and HaloTagged GAR1 independently in HeLa cells using CRISPR-Cas9 approach. Preliminary results show HaloTag-dyskerin cell lines were validated by western blot (Fig. 4.3A) and live cell imaging (Fig. 4.3B). The next steps include confirming the cell lines via PCR, constructing HaloTag-GAR1 cell lines, then live cell single molecule imaging to determine diffusion coefficients of dyskerin and GAR1.

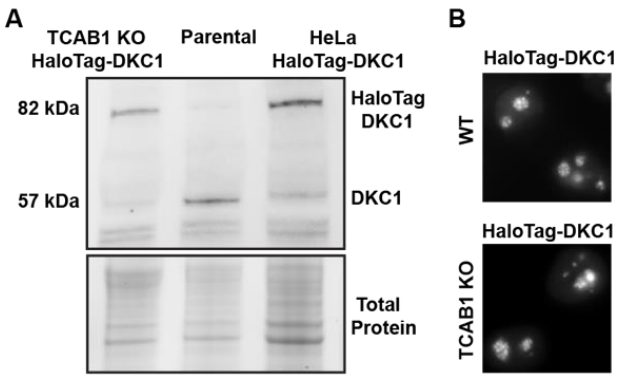

Figure 4.3. Validation of HaloTag-dyskerin cell lines in wild type HeLa and TCAB1 knock-out cell lines. (A) Western blot showing HaloTagged dyskerin (82 kDa) in TCAB1 knock-out cells (left lane), endogenous dyskerin (57 kDa) in parental cells (middle lane) and HaloTagged dyskerin in WT HeLa cells (right lane). **(B).** Live cells labeled with HaloTag ligand 100uM JF650 showing HaloTag-dyskerin in WT and TCAB1 KO cells in nucleoli and Cajal bodies.

Lastly, since GAR1 associates with dyskerin in the H/ACA complex, it is likely that dyskerin mediates GAR1 nucleolar retention. Future work includes determining the impact of dyskerin on GAR1 diffusion and exchange dynamics using dyskerin knock-down in single molecule imaging and FRAP.

Our second aim is to determine the role of GAR1 in the telomerase RNP. In TCAB1 knock-out cells, TR localization to nucleoli is dependent upon the H/ACA protein complex, which includes is GAR1 (Zhang et al., 2010; Vogan et al., 2016; Klump et al., 2023). I hypothesize that GAR1 promotes nucleolar retention of TR. To elucidate the role of GAR1 in mediating nucleolar TR localization in the absence of TCAB1, we knocked down GAR1 using a combination of silencing RNAs (siRNA) specific to the GAR1 mRNA (siGenome Reagents). Specifically, I nucleofected 2 uM of GAR1 siRNA and control siRNA in HeLa and TCAB1 knockout cells. We have determined that the GAR1 siRNA induces a 97% knockdown in GAR1 levels (Fig. 4.4). Next, we identified the impact of GAR1 on TR localization using Fluorescence *in situ* hybridization to probe for TR. We found that depletion of GAR1 does not impact nucleolar retention of TR in the absence of TCAB1 suggesting that GAR1 may not be necessary in promoting TR localization to nucleoli in the absence of TCAB1.

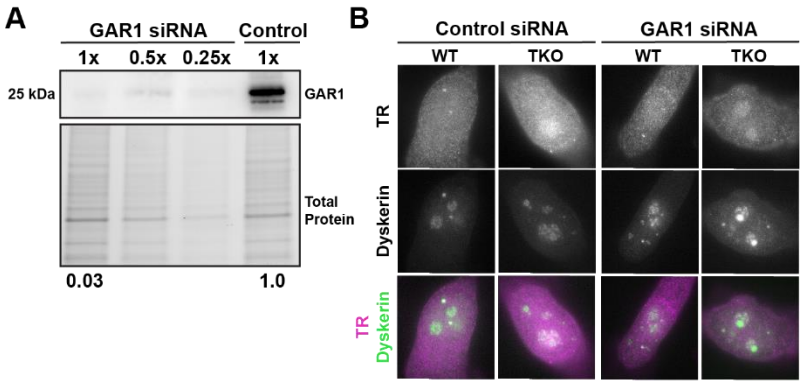

Figure 4.4. GAR1 does not impact TR localization. (A) Western blot to validate GAR1 siRNA knock-down compared to control siRNAs. **(B).** Immunofluorescence stainig for dyskerin and fluorescence in situ hybridization probing for TR in control vs. GAR1 siRNAs in WT and TCAB1 knock-out cells.

4.3: Discussion

One of the main roles of dyskerin, a component in the H/ACA complex, is to mediate TR stability (Shukla et al., 2016). Given that GAR1 along with dyskerin is a factor in the H/ACA complex, I hypothesize that GAR1 may promote RNA stability. I will dissect the role of GAR1 in the stability of TR and U1 spliceosomal snRNA. I will dissect TR accumulation using northern blot by quantifying the amount of TR intensity in GAR1 depleted cells. If GAR1 has a role in the H/ACA complex in mediating TR stability, I would expect TR levels to decrease in the GAR1 knock-down due to increased degradation.

In the absence of TCAB1, telomerase assembly is significantly decreased but not completely abolished; about 40% of assembly still occurs in the absence of TCAB1 (Klump et al., 2023). To date, the roles that other factors in the telomerase RNP play in its function such as GAR1 is unknown. Since GAR1 localizes to CBs, it may have a role in shuttling TR to CBs where TCAB1 then associates with TR to mediate assembly with TERT (Dundr et al., 2004). I hypothesize that GAR1 and TCAB1 play an additive role in promoting telomerase RNP assembly. In this aim, I will uncover the role of GAR1 in telomerase RNP assembly in GAR1 knock-out versus GAR1/TCAB1 double knock-out using an established telomerase assembly assay (Klump et al., 2023). I expect to observe TR localization to nucleoplasm and a further decrease in

telomerase RNP assembly if cells are deficient in both TCAB1 and GAR1 due to the lack of sequestration in the nucleoli thereby exposing TR to exonucleases in the nucleoplasm. Alternatively, since GAR1 localizes to the nucleoli and plays a role in promoting nucleolar snoRNP localization for the modification of RNAs (Pellizzoni et al., 2001), GAR1, as a nucleolar protein, may be present on the telomerase RNP to oppose the role of TCAB1 in promoting telomerase assembly by sequestering TR in the nucleoli when TCAB1 is deficient.

One weakness to using siRNAs in studying roles of factors is that siRNAs may not be sufficient to deplete all of GAR1. We demonstrate that the GAR1 siRNAs knocked down GAR1, nevertheless, a small fraction of GAR1 may be sufficient to maintain telomerase RNP stability. To clearly define the role of GAR1 in TR localization and telomerase assembly, our future work involves knocking out GAR1 using CRISPR-Cas9 and 2 sgRNAs targeting exon 2. Then, we will define the role of GAR1 in TR stability, localization, telomerase assembly, and activity, in addition to U1 snRNA stability and localization. Altogether, GAR1 may be retained in the nucleolus by similar mechanisms to TR nucleolar retention and dyskerin may be necessary in promoting nucleolar sequestration, thereby future work will dissect the role of dyskerin in the nucleolar localization of GAR1. Importantly, the proposed aims will reveal the role of GAR1 in the telomerase RNP to uncover new potential therapeutic targets for telomere diseases and spinal muscular dystrophies.

CHAPTER 5: CONCLUSIONS AND FUTURE DIRECTIONS

5.1: Conclusions

Chromosomes undergo the end replication problem which lead to the production of a 3' overhang. The ends are recognized and resected by exonucleases leading to telomere shortening. With subsequent cellular divisions, telomeres shorten until reaching their Hayflick limit. During the crisis, short telomeres become depleted of the shelterin complex which covers and protects telomeres from being identified as sites of DNA damage. Loss of telomere protection triggers ATM and ATR signaling, resulting in cell senescence and apoptosis.

To counteract telomere shortening, cells may use either of the two mechanisms to maintain their proliferative capacity: alternative lengthening of telomeres or expression of the telomerase RNP. Most proliferating cells such as stem cells, germline cells and cancer cells express TERT, a highly-conserved reverse transcriptase, which elongates telomeres by reverse transcribing the RNA repeat template, located on TR, into DNA comprised of telomeric repeats.

Loss-of-function mutations in the telomerase RNP are hallmarks of premature aging diseases such as dyskeratosis congenita. Conversely, aberrant upregulation of the telomerase RNP occurs in over 90% of cancers. Previous therapies targeting TERT and TR failed in clinical trials due to their toxic side effects in premature aging patients and there are no telomerase therapies that have been developed to combat cancer. Therefore, it is crucial to dissect the mechanism of the telomerase RNP in telomere elongation in cancer cells in order to understand and identify potential therapeutic targets.

Critical steps in the telomerase RNP ensure telomere synthesis. The telomerase RNP must be assembled, recruited to chromosome ends and catalytically active to synthesize telomeres. Telomere synthesis requires an assembled TERT-TR complex. In our previous work, we demonstrated using a combination of methods that for telomerase assembly to occur, TCAB1 must prevent nucleolar sequestration of TR (Klump et al 2023). Otherwise, for cells lacking

TCAB1, the majority of TR is tightly sequestered in the phase separated sub-nuclear organelle, the nucleolus, and does not exchange with the nucleoplasm (Klump et al 2023).

Additionally, we employed a recently developed method, RNP-MaP, in dissecting telomerase RNP assembly. Consistent with our previous findings, RNP-MaP revealed that that crosslinking of TERT to TR is disrupted in the absence of TCAB1. Importantly, we uncovered the mechanism by which disruption of assembly occurs in the absence of TCAB1. We have shown that TCAB1 does not enter nucleoli therefore it is likely that TCAB1 prevents nucleolar retention of TR rather than extracting TR from the nucleoli into the nucleoplasm. The mechanism by which TCAB1 prevents sequestration of TR and other scaRNA in the nucleolus remains unanswered.

Next, we aimed to define the role of GAR1 in RNPs. First, we uncovered by FRAP that GAR1 shares similar nucleolar retention kinetics with that of TR. It is plausible that they share similar mechanisms for their retention. Future work on dissecting the mechanism of nucleolar retention of GAR1 may uncover a mechanism of TCAB1-mediated nucleolar exclusion.

5.2: Future Directions

5.2.1: Mechanism of TCAB1-mediated exclusion of scaRNAs from nucleoli

Our work demonstrated that phase-separated organelles play a role in the sequestration of TR which is prevented by the telomerase RNP component, TCAB1, to promote telomerase RNP. It has been shown that arginine-glycine motifs are sufficient to mediate phase separation (Feric et al., 2016). Importantly, GAR1 is an arginine-glycine rich factor in the telomerase RNP. As a result, GAR1 may mediate sequestration of TR by phase separation with nucleolar proteins while TCAB1 may repel this mechanism to prevent RNP nucleolar sequestration.

The telomerase RNP spends most of the cell cycle in another phase-separated compartment, Cajal bodies. Based on preliminary data, the negatively charged disordered terminus of TCAB1 can phase separate with a positively charged peptide (Fig. 5.1) which suggests that, in vivo, TCAB1 may bind positively-charged Cajal-body factors such as coilin to direct RNPs to Cajal

bodies away from nucleoli. It is plausible that TCAB1 recruits the telomerase RNP to Cajal bodies by phase separating with Cajal body factors. TCAB1 phase separation properties may be the mechanism behind telomerase RNP recruitment to Cajal bodies and exclusion from nucleoli.

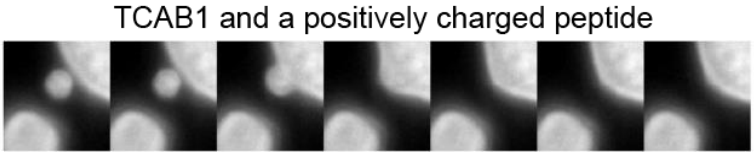

Figure 5.1. Phase separation of TCAB1. Frames from a movie showing the fusion of the disordered termini of TCAB1 with a positively charged peptide.

5.2.2: The contribution of other telomerase RNP factors in telomerase RNP

5.2.2.1: The role of H2A-H2B in the telomerase RNP

Though absence of TCAB1 reduces telomerase RNP assembly, a small fraction of telomerase RNP still assembles. This suggests that other factors in the RNP may promote a fraction of telomerase RNP assembly. Interestingly, through RNP-MaP, we found crosslinking sites of H2A-H2B histone dimers on TR which were maintained in the absence of TCAB1. It is imperative to dissect the role of H2A-H2B in potentially promoting a slight amount of assembled telomerase RNP in TCAB1-depleted cells. Importantly, the role of H2A-H2B in the telomerase RNP is unknown therefore, future work potentially involves uncovering the role of histones in mediating telomerase RNP assembly, activity and recruitment to chromosome where histones reside.

Future work with telomerase RNP and RNP-MaP will further uncover the association of histone 2A and 2B (H2A/H2B) with an assembled telomerase RNP. To dissect whether H2A/H2B association with TR requires an assembled telomerase, we will knock-out TERT from HeLa cell and TCAB1 knock-out cell lines as previously done via the CRISPR-Cas9 approach (Laprade et al., 2020). Using the approaches described in this dissertation, we will pull down TR to measure co-purified H2A/H2B in the TERT knock-out cell lines. To confirm, we will also apply RNP-MaP as an additional approach in measuring the impact of TERT on H2A/H2B assembly with TR. If

TERT does not impact H2A/H2B-TR, it may suggest that H2A/H2B may bind to TR before TR assembly with TERT which contributes to understanding biogenesis of the telomerase RNP.

To assess the impact of TERT on the association of H2A and H2B with TR in living cells, I will apply the RNP-MaP approach of TR on TERT knock-out cells. According to our preliminary findings in the TCAB1 knock-out cells, H2A and H2B crosslinking to TR is unaffected by the reduction in assembly in the absence of TCAB1; therefore, I predict that in TERT knock-out cells, H2A/H2B will remain intact on TR suggesting that H2A/H2B may interact with TR before TCAB1mediates TR-TERT assembly. Similar to its role in the structural regulation of chromatin, H2A/H2B may also serve a role in stabilizing TR and regulating the telomerase RNP on telomere lengthening (Recht et al., 1996).

Mutations in H2A/H2B cause aberrant gene expression promoting cancer progression. The H2A/H2B mutations cause the dimers to dissociate from the DNA making it available for transcription (Wan and Chan, 2021). These types of mutations may also support telomerase RNP-mediated telomere synthesis if H2A/H2B has a negative the telomerase RNP. Alternatively, mutations that disrupt H2A/H2B association with the DNA may not impact its association with TR and thereby does not impact telomere elongation. Dissecting the impact of H2A-H2B cancer-promoting mutations on promoting telomerase RNP activity may be imperative in uncovering a role of H2A-H2B in regulating telomere synthesis and cellular proliferation.

5.2.2.2: The role of the H/ACA complex in the telomerase RNP

The H/ACA complex is known to stabilize TR, snoRNAs and scaRNAs however the roles of H/ACA factors in other steps of the RNP biogenesis and function has not been elucidated. We have shown that GAR1, an H/ACA factor, has exchange kinetics similar to that of TR. Neither GAR1 nor TR have nucleolar localization signal. However, their intermediate factor, dyskerin does. It is likely that dyskerin shuttles TR and GAR1 to nucleoli therefore, further approaches in understanding whether dyskerin is necessary and sufficient in mediated nucleolar retention is

important to define the mechanism of retention. Approaches to use in answering this question involves measuring diffusion kinetics of GAR1 and TR in dyskerin depleted cells.

Alternatively, GAR1 may have potential nucleolar retaining capabilities that support its localization. A possible mechanism by which GAR1 is sequestered in nucleoli is by phase separation with nucleolar factors such as dyskerin. Further work includes dissecting phase separation of TCAB1 and GAR1 in the presence of TR and other factors in the telomerase RNP to uncover the mechanism of phase separation in the biogenesis of mature RNPs such as TR, snoRNPs, snRNPs, and scaRNPs in nucleoli and Cajal bodies.

Since a small fraction of telomerase RNP still occurs in the absence of TCAB1 and that a subset of H/ACA complex containing RNAs that do not bind TCAB1 can still localize to Cajal bodies, it is plausible that factors of the H/ACA complex may mediate shuttling outside the nucleoli. To dissect the role of the H/ACA complex, a knock-out or knock-down of each factor, NHP2, NOP10 and GAR1, must be established. Then methods such as those described in previous chapters can be applied such as RNP-MaP, telomerase assembly assays, genomic editing and live cell single-molecule imaging.

Additionally, the efficiency of assembly of the H/ACA complex onto TR has been shown to also be dependent on biogenesis-promoting (BIO) box, a region downstream of the TCAB1-binding region. Mutations in BIO region are associated with a reduction of H/ACA complex binding with TR (Egan et al., 2012). However, the impact of BIO on TERT-TR assembly was not established in this study. Therefore, future work is essential in defining the role of BIO region in assembly with TCAB1 and TERT by mutating BIO region and determining localization, assembly and function of the telomerase RNP.

5.2.2.3: Chronological sequence in the biogenesis of the telomerase RNP

The sequence of telomerase RNP biogenesis has not been dissected. Applications of RNP-MaP in the future involves dissecting the sequence of telomerase RNP biogenesis by correlating cross-linking of one factor to another. To dissect biogenesis of the telomerase RNP,

first the dependence of TCAB1 on the H/ACA complex must be determined. Whereas the other components of the H/ACA complex are bound to dyskerin, dyskerin interacts directly with TR. The necessity of the dyskerin for TCAB1-TR association can be established by first knocking down dyskerin using a previously established shRNA (with inhibition of the nuclease PAPD5 to prevent TR degradation) (Agarwal et al., 2010; Shukla et al., 2016). Next, TR can be pulled down (using an established method (Ivanyi-Magy et al., 2018) then the amount of co-purified TCAB1 can be measured. If TCAB1 were dependent on the presence of the H/ACA factors to bind with TR, then I would expect less TCAB1 to co-purify with TR in the absence of dyskerin. In addition to TR purification, RNP-MaP can be applied to determine crosslinking of TCAB1 to a single TR molecule in the absence of dyskerin.

5.2.3: Dissecting the biogenesis of other non-coding RNPs

Though coilin, a structural Cajal body protein, does not impact telomere synthesis, coilin interacts with snRNPs and snoRNPs (Machyna et al., 2014; Bellini and Gall, 2007; Morris, 2008; Darzacq et al., 2002). Importantly, coilin also co-localizes with histone pre-mRNAs and is associated with regulating recruitment of DNA damage repair factors (Henricksson et al., 2015). The role of CBs and its structural protein, coilin, in snoRNPs, snRNPs, and scaRNPs is yet to be defined. We aim to uncover the role of coilin in the RNPs by generating coilin knock-out cell lines via CRISPR-Cas9 approach. To dissect the impact of coilin on the biogenesis of the spliceosomal RNP, snoRNPs and scaRNPs, a variety of approaches we used previously in telomerase RNP can be applied in this aim such as RNP-MaP, immunopurification assays and molecular imaging such as immunofluorescence with fluorescence in situ hybridization, live cell single molecule imaging.

In addition to its association with the telomerase RNP, GAR1 interacts with mediators in the spliceosome formation, however the role it plays in the assembly and trafficking of the spliceosomal snRNPs remains elusive. Therefore, assembly assays such as those used in our work to demonstrate the role of TCAB1 in the telomerase RNP such as immuno-purification and

RNP MaP combined with CRSPR-Cas9 mediated knock-out, can be used to dissect the role of GAR1 in spliceosome RNP biogenesis specifically the U1, U2, U4 and U5 snRNP.

Altogether, determining the mechanism of the telomerase RNP and non-coding RNAs may define pathologies of diseases and uncover novel therapeutic targets for the treatments of premature aging diseases and cancers.

BIBLIOGRAPHY

Agarwal S, Loh YH, McLoughlin EM, et al. Telomere elongation in induced pluripotent stem cells from dyskeratosis congenita patients. *Nature*. 2010;464(7286):292-296. doi:10.1038/nature08792

Angrisani A, Vicidomini R, Turano M, Furia M. 2014. Human dyskerin: beyond telomeres. *Biol Chem. 2014;*395:593–610. doi:10.1515/hsz-2013-0287

Armanios M. Telomerase and Idiopathic Pulmonary Fibrosis. *Mutat Res*. 2012;730(1-2):52-58. doi:10.1016/j.mrfmmm.2011.10.013

Armanios M. The Role of Telomeres in Human Disease. *Annual Review of Genomics and Human Genetics*. 2022;23(1):363-381. doi:10.1146/annurev-genom-010422-091101

Armanios M, Blackburn EH. The telomere syndromes. *Nat Rev Genet*. 2012;13(10):693-704. doi:10.1038/nrg3246

Armanios M, Chen JL, Chang YPC, et al. Haploinsufficiency of telomerase reverse transcriptase leads to anticipation in autosomal dominant dyskeratosis congenita. *Proc Natl Acad Sci U S A*. 2005;102(44):15960-15964. doi:10.1073/pnas.0508124102

Autexier C, Lue NF. The structure and function of telomerase reverse transcriptase. *Annu Rev Biochem*. 2006;75:493-517. doi:10.1146/annurev.biochem.75.103004.142412

Aplastic anemia - Symptoms and causes. Mayo Clinic. Accessed November 2, 2022. https://www.mayoclinic.org/diseases-conditions/aplastic-anemia/symptoms-causes/syc-20355015

Beattie TL, Zhou W, Robinson MO, Harrington L. Reconstitution of human telomerase activity in vitro. *Curr Biol*. 1998;8(3):177-180. doi:10.1016/s0960-9822(98)70067-3

Bellini M, Gall JG. Coilin Can Form a Complex with the U7 Small Nuclear Ribonucleoprotein. *MBoC*. 1998;9(10):2987-3001. doi:10.1091/mbc.9.10.2987

Bergstrand S, Böhm S, Malmgren H, et al. Biallelic mutations in WRAP53 result in dysfunctional telomeres, Cajal bodies and DNA repair, thereby causing Hoyeraal–Hreidarsson syndrome. *Cell Death Dis*. 2020;11(4):1-14. doi:10.1038/s41419-020-2421-4

Blackburn EH, Greider CW, Szostak JW. Telomeres and telomerase: the path from maize, Tetrahymena and yeast to human cancer and aging. *Nat Med*. 2006;12(10):1133-1138. doi:10.1038/nm1006-1133

Bottius E, Bakhsis N, Scherf A. Plasmodium falciparum Telomerase: De Novo Telomere Addition to Telomeric and Nontelomeric Sequences and Role in Chromosome Healing. *Mol Cell Biol*. 1998;18(2):919-925.

Bousquet-Antonelli C, Henry Y, G'elugne JP, Caizergues-Ferrer M, Kiss T. A small nucleolar RNP protein is required for pseudouridylation of eukaryotic ribosomal RNAs. *EMBO J*. 1997;16(15):4770-4776. doi:10.1093/emboj/16.15.4770

Chen JL, Greider CW. Telomerase RNA structure and function: implications for dyskeratosis congenita. *Trends in Biochemical Sciences*. 2004;29(4):183-192. doi:10.1016/j.tibs.2004.02.003

Cesare AJ, Reddel RR. Alternative lengthening of telomeres: models, mechanisms and implications. *Nat Rev Genet*. 2010;11(5):319-330. doi:10.1038/nrg2763

Chen L, Roake CM, Freund A, et al. An Activity Switch in Human Telomerase Based on RNA Conformation and Shaped by TCAB1. *Cell*. 2018;174(1):218-230.e13. doi:10.1016/j.cell.2018.04.039

Chen Y, Deng Z, Jiang S, et al. Human cells lacking coilin and Cajal bodies are proficient in telomerase assembly, trafficking and telomere maintenance. *Nucleic Acids Research*. 2015;43(1):385-395. doi:10.1093/nar/gku1277

Chiappori AA, Kolevska T, Spigel DR, et al. A randomized phase II study of the telomerase inhibitor imetelstat as maintenance therapy for advanced non-small-cell lung cancer. *Annals of Oncology*. 2015;26(2):354-362. doi:10.1093/annonc/mdu550

Clerici M, Mantiero D, Lucchini G, Longhese MP. The Saccharomyces cerevisiae Sae2 protein promotes resection and bridging of double strand break ends. *J Biol Chem*. 2005;280(46):38631-38638. doi:10.1074/jbc.M508339200

Cohen SB, Graham ME, Lovrecz GO, Bache N, Robinson PJ, Reddel RR. Protein Composition of Catalytically Active Human Telomerase from Immortal Cells. *Science*. 2007;315:1850–1853. doi:10.1126/science.1138596

Collins K. Physiological Assembly and Activity of Human Telomerase Complexes. *Mech Ageing Dev*. 2008;129(1-2):91-98. doi:10.1016/j.mad.2007.10.008

Cong L, Ran FA, Cox D, Lin S, Barretto R, Habib N, Hsu PD, Wu X, Jiang W, Marraffini LA, Zhang F. Multiplex Genome Engineering Using CRISPR/Cas Systems. *Science*. 2013;339:819–823. doi:10.1126/science.1231143

Cristofari G, Lingner J. Telomere length homeostasis requires that telomerase levels are limiting. *Embo J. 2006;*25:565 574. doi:10.1038/sj.emboj.7600952

Darzacq X, Jády BE, Verheggen C, Kiss AM, Bertrand E, Kiss T. Cajal body-specific small nuclear RNAs: a novel class of 2′-O-methylation and pseudouridylation guide RNAs. *EMBO J*. 2002;21(11):2746-2756. doi:10.1093/emboj/21.11.2746

Darzacq X, Kittur N, Roy S, Shav-Tal Y, Singer RH, Meier UT. Stepwise RNP assembly at the site of H/ACA RNA transcription in human cells. *J Cell Biol*. 2006;173(2):207-218. doi:10.1083/jcb.200601105

De Lange T. T-loops and the origin of telomeres. *Nat Rev Mol Cell Biol*. 2004;5(4):323-329. doi:10.1038/nrm1359

Denchi EL, de Lange T. Protection of telomeres through independent control of ATM and ATR by TRF2 and POT1. *Nature*. 2007;448(7157):1068-1071. doi:10.1038/nature06065

Ding Z, Wu CJ, Jaskelioff M, et al. Telomerase reactivation following telomere dysfunction yields murine prostate tumors with bone metastases. *Cell*. 2012;148(5):896-907. doi:10.1016/j.cell.2012.01.039

Doksani Y, Wu JY, de Lange T, Zhuang X. Super-resolution fluorescence imaging of telomeres reveals TRF2-dependent T-loop formation. *Cell*. 2013;155(2):345-356. doi:10.1016/j.cell.2013.09.048

Dragon F, Pogačić V, Filipowicz W. In Vitro Assembly of Human H/ACA Small Nucleolar RNPs Reveals Unique Features of U17 and Telomerase RNAs. *Mol Cell Biol*. 2000;20(9):3037-3048.

Dundr M, Hebert MD, Karpova TS, et al. In vivo kinetics of Cajal body components. *Journal of Cell Biology*. 2004;164(6):831-842. doi:10.1083/jcb.200311121

Egan ED, Collins K. Specificity and stoichiometry of subunit interactions in the human telomerase holoenzyme assembled in vivo. *Mol Cell Biol. 2010* 30:2775 2786. doi:10.1128/mcb.00151-10

Egan ED, Collins K. An Enhanced H/ACA RNP Assembly Mechanism for Human Telomerase RNA. *Molecular and Cellular Biology*. 2012;32(13):2428-2439. doi:10.1128/MCB.00286-12

Egan ED, Collins K. Biogenesis of telomerase ribonucleoproteins. *RNA*. 2012;18(10):1747-1759. doi:10.1261/rna.034629.112

Fagagna F d'Adda di, Reaper PM, Clay-Farrace L, et al. A DNA damage checkpoint response in telomere-initiated senescence. *Nature*. 2003;426(6963):194-198. doi:10.1038/nature02118

Feric M, Vaidya N, Harmon TS, et al. Coexisting liquid phases underlie nucleolar sub-compartments. *Cell*. 2016;165(7):1686-1697. doi:10.1016/j.cell.2016.04.047

Freund A, Zhong FL, Venteicher AS, et al. Proteostatic control of telomerase function through TRiC-mediated folding of TCAB1. *Cell*. 2014;159(6):1389-1403. doi:10.1016/j.cell.2014.10.059

Fu D, Collins K. Distinct biogenesis pathways for human telomerase RNA and H/ACA small nucleolar RNAs. *Mol Cell*. 2003;11(5):1361-1372. doi:10.1016/s1097-2765(03)00196-5

Fujikane R, Behm-Ansmant I, Tillault AS, et al. Contribution of protein Gar1 to the RNA-guided and RNA-independent rRNA:Ψ-synthase activities of the archaeal Cbf5 protein. *Sci Rep*. 2018;8:13815. doi:10.1038/s41598-018-32164-0

Gadelha RB, Machado CB, Pessoa FMC de P, et al. The Role of WRAP53 in Cell Homeostasis and Carcinogenesis Onset. *Current Issues in Molecular Biology*. 2022;44(11):5498-5515. doi:10.3390/cimb44110372

Garus A, Autexier C. Dyskerin: an essential pseudouridine synthase with multifaceted roles in ribosome biogenesis, splicing, and telomere maintenance. *RNA*. 2021;27(12):1441-1458. doi:10.1261/rna.078953.121

George SL, Parmar V, Lorenzi F, et al. Novel therapeutic strategies targeting telomere maintenance mechanisms in high-risk neuroblastoma. *J. Exp. Clin. Cancer Res.* 2020;39(1):78. doi:10.1186/s13046-020-01582-2.

Genest O, Wickner S, Doyle SM. Hsp90 and Hsp70 chaperones: Collaborators in protein remodeling. *J Biol Chem*. 2019;294(6):2109-2120. doi:10.1074/jbc.REV118.002806

Ghanim GE, Fountain AJ, van Roon AMM, et al. Structure of human telomerase holoenzyme with bound telomeric DNA. *Nature*. 2021;593(7859):449-453. doi:10.1038/s41586-021-03415-4

Girard JP, Lehtonen H, Caizergues-Ferrer M, Amalric F, Tollervey D, Lapeyre B. GAR1 is an essential small nucleolar RNP protein required for pre-rRNA processing in yeast. *EMBO J*. 1992;11(2):673-682. doi:10.1002/j.1460-2075.1992.tb05099.x

Glousker G, Touzot F, Revy P, Tzfati Y, Savage SA. Unraveling the pathogenesis of Hoyeraal–Hreidarsson syndrome, a complex telomere biology disorder. *British Journal of Haematology*. 2015;170(4):457-471. doi:10.1111/bjh.13442

Greider CW, Blackburn EH. The telomere terminal transferase of Tetrahymena is a ribonucleoprotein enzyme with two kinds of primer specificity. *Cell*. 1987;51(6):887-898. doi:10.1016/0092-8674(87)90576-9

Greider CW. Telomeres, telomerase and senescence. *BioEssays*. 1990;12(8):363-369. doi:10.1002/bies.950120803

Greider CW, Blackburn EH. Identification of a specific telomere terminal transferase activity in tetrahymena extracts. *Cell*. 1985;43(2):405-413. doi:10.1016/0092-8674(85)90170-9

Greider CW, Blackburn EH. The telomere terminal transferase of tetrahymena is a ribonucleoprotein enzyme with two kinds of primer specificity. *Cell*. 1987;51(6):887-898. doi:10.1016/0092-8674(87)90576-9

Greider CW, Blackburn EH. A telomeric sequence in the RNA of Tetrahymena telomerase required for telomere repeat synthesis. *Nature*. 1989;337(6205):331-337. doi:10.1038/337331a0

Grimm JB, Xie L, Casler JC, et al. *Deuteration Improves Small-Molecule Fluorophores*. Cell Biology; 2020. doi:10.1101/2020.08.17.250027

Grimm JB, English BP, Chen J, Slaughter JP, Zhang Z, Revyakin A, Patel R, Macklin JJ, Normanno D, Singer RH, Lionnet T, Lavis LD. A general method to improve fluorophores for live-cell and single-molecule microscopy. *Nat Methods.* 2015;12:244 50–3 p following 250. doi:10.1038/nmeth.3256

Hansen AS, Woringer M, Grimm JB, Lavis LD, Tjian R, Darzacq X. Robust model-based analysis of single-particle tracking experiments with Spot-On. *Elife.* 2018;7. doi:10.7554/elife.33125

Harley CB, Futcher AB, Greider CW. Telomeres shorten during ageing of human fibroblasts. *Nature*. 1990;345(6274):458-460. doi:10.1038/345458a0

Harrington L, Zhou W, McPhail T, et al. Human telomerase contains evolutionarily conserved catalytic and structural subunits. *Genes Dev*. 1997;11(23):3109-3115.

Hastie ND, Dempster M, Dunlop MG, Thompson AM, Green DK, Allshire RC. Telomere reduction in human colorectal carcinoma and with ageing. *Nature*. 1990;346(6287):866-868. doi:10.1038/346866a0

Hayflick L. The limited in vitro lifetime of human diploid cell strains. *Experimental Cell Research*. 1965;37(3):614-636. doi:10.1016/0014-4827(65)90211-9

Hebert MD, Szymczyk PW, Shpargel KB, Matera AG. Coilin forms the bridge between Cajal bodies and SMN, the Spinal Muscular Atrophy protein. *Genes Dev*. 2001;15(20):2720-2729. doi:10.1101/gad.908401

Heidenreich B, Rachakonda PS, Hemminki K, Kumar R. TERT promoter mutations in cancer development. *Curr Opin Genet Dev*. 2014;24:30-37. doi:10.1016/j.gde.2013.11.005

Heiss NS, Girod A, Salowsky R, Wiemann S, Pepperkok R, Poustka A. Dyskerin localizes to the nucleolus and its mislocalization is unlikely to play a role in the pathogenesis of dyskeratosis congenita. *Hum Mol Genet*. 1999;8(13):2515-2524. doi:10.1093/hmg/8.13.2515

Henriksson S, Farnebo M. On the road with WRAP53β: guardian of Cajal bodies and genome integrity. *Front Genet*. 2015;6:91. doi:10.3389/fgene.2015.00091

Henriksson S, Rassoolzadeh H, Hedström E, et al. The scaffold protein WRAP53β orchestrates the ubiquitin response critical for DNA double-strand break repair. *Genes Dev*. 2014;28(24):2726-2738. doi:10.1101/gad.246546.114

Hiyama E, Hiyama K. Telomere and telomerase in stem cells. *Br J Cancer*. 2007;96(7):1020-1024. doi:10.1038/sj.bjc.6603671

Holt SE, Wright WE, Shay JW. Regulation of telomerase activity in immortal cell lines. *Mol Cell Biol*. 1996;16(6):2932-2939.

Holt SE, Aisner DL, Baur J, et al. Functional requirement of p23 and Hsp90 in telomerase complexes. *Genes Dev*. 1999;13(7):817-826.

Holt SE, Aisner DL, Shay JW, Wright WE. Lack of cell cycle regulation of telomerase activity in human cells. *Proc Natl Acad Sci USA*. 1997;94(20):10687-10692. doi:10.1073/pnas.94.20.10687

Huang FW, Hodis E, Xu MJ, Kryukov GV, Chin L, Garraway LA. Highly Recurrent TERT Promoter Mutations in Human Melanoma. *Science*. 2013;339(6122):957-959. doi:10.1126/science.1229259

Hyman AA, Weber CA, Jülicher F. Liquid-Liquid Phase Separation in Biology. *Annual Review of Cell and Developmental Biology*. 2014;30(1):39-58. doi:10.1146/annurev-cellbio-100913-013325

Ivanyi-Nagy R, Ahmed SM, Peter S, et al. The RNA interactome of human telomerase RNA reveals a coding-independent role for a histone mRNA in telomere homeostasis. *eLife*. 7:e40037. doi:10.7554/eLife.40037

Jády BE, Bertrand E, Kiss T. Human telomerase RNA and box H/ACA scaRNAs share a common Cajal body–specific localization signal. *J Cell Biol*. 2004;164(5):647-652. doi:10.1083/jcb.200310138

Jády BE, Richard P, Bertrand E, Kiss T. Cell Cycle-dependent Recruitment of Telomerase RNA and Cajal Bodies to Human Telomeres. *MBoC*. 2006;17(2):944-954. doi:10.1091/mbc.e05-09-0904

Jiang J, Chan H, Cash DD, et al. Structure of Tetrahymena telomerase reveals previously unknown subunits, functions, and interactions. *Science*. 2015;350(6260):aab4070. doi:10.1126/science.aab4070

Kelleher C, Kurth I, Lingner J. Human Protection of Telomeres 1 (POT1) Is a Negative Regulator of Telomerase Activity In Vitro. *Mol Cell Biol*. 2005;25(2):808-818. doi:10.1128/MCB.25.2.808-818.2005

Kim NW, Piatyszek MA, Prowse KR, et al. Specific Association of Human Telomerase Activity with Immortal Cells and Cancer. *Science*. 1994;266(5193):2011-2015.

Kiss AM, Jády BE, Bertrand E, Kiss T. Human Box H/ACA Pseudouridylation Guide RNA Machinery. *Mol Cell Biol*. 2004;24(13):5797-5807. doi:10.1128/MCB.24.13.5797-5807.2004

Kiss T, Fayet E, Jády BE, Richard P, Weber M. Biogenesis and intranuclear trafficking of human box C/D and H/ACA RNPs. *Cold Spring Harb Symp Quant Biol*. 2006;71:407-417. doi:10.1101/sqb.2006.71.025

Kiss-László Z, Henry Y, Bachellerie JP, Caizergues-Ferrer M, Kiss T. Site-Specific Ribose Methylation of Preribosomal RNA: A Novel Function for Small Nucleolar RNAs. *Cell*. 1996;85(7):1077-1088. doi:10.1016/S0092-8674(00)81308-2

Klump BM, Perez GI, Adams-Boone K, et al. TCAB1 prevents nucleolar accumulation of the telomerase RNA to promote telomerase assembly. *Cell Reports*

Laine RF, Tosheva KL, Gustafsson N, Gray RDM, Almada P, Albrecht D, Risa GT, Hurtig F, Linds A-C, Baum B, Mercer J, Leterrier C, Pereira PM, Culley S, Henriques R. NanoJ: a high-performance open-source super-resolution microscopy toolbox. *J Phys D Appl Phys.* 2019;52:163001. doi:10.1088/1361-6463/ab0261

Lam YW, Lamond AI. Cell Biology (Third Edition). *Part Organelles Cell Struct Sect 1isolation Plasma Membr Organelles Cell Struct Sect 1 Isol Plasma Membr Organelles Cell Struct.* 2006;103–107. doi:10.1016/b978-012164730-8/50087-3

Laprade H, Querido E, Smith MJ, et al. Single-Molecule Imaging of Telomerase RNA Reveals a Recruitment-Retention Model for Telomere Elongation. *Molecular Cell*. 2020;79(1):115-126.e6. doi:10.1016/j.molcel.2020.05.005

Lee FCY, Ule J. Advances in CLIP Technologies for Studies of Protein-RNA Interactions. *Molecular Cell*. 2018;69(3):354-369. doi:10.1016/j.molcel.2018.01.005

Lee JS, Mandell EK, Tucey TM, Morris DK, Victoria L. The Est3 protein associates with yeast telomerase through an OB-fold domain. *Nat Struct Mol Biol*. 2008;15(9):990-997.

Lee JH, Lee YS, Jeong SA, Khadka P, Roth J, Chung IK. Catalytically active telomerase holoenzyme is assembled in the dense fibrillar component of the nucleolus during S phase. *Histochem Cell Biol*. 2013;141(2):137-152. doi:10.1007/s00418-013-1166-x

Lemm I, Girard C, Kuhn AN, et al. Ongoing U snRNP Biogenesis Is Required for the Integrity of Cajal Bodies. *MBoC*. 2006;17(7):3221-3231. doi:10.1091/mbc.e06-03-0247

Lestrade L, Weber MJ. snoRNA-LBME-db, a comprehensive database of human H/ACA and C/D box snoRNAs. *Nucleic Acids Res*. 2006;34(Database issue):D158-D162. doi:10.1093/nar/gkj002

Lingner J, Hughes TR, Shevchenko A, Mann M, Lundblad V, Cech TR. Reverse transcriptase motifs in the catalytic subunit of telomerase. *Science*. 1997;276(5312):561-567. doi:10.1126/science.276.5312.561

Loayza D, De Lange T. POT1 as a terminal transducer of TRF1 telomere length control. *Nature*. 2003;423(6943):1013-1018. doi:10.1038/nature01688

Longhese MP, Bonetti D, Manfrini N, Clerici M. Mechanisms and regulation of DNA end resection. *EMBO J*. 2010;29(17):2864-2874. doi:10.1038/emboj.2010.165

Luger K, Mäder AW, Richmond RK, Sargent DF, Richmond TJ. Crystal structure of the nucleosome core particle at 2.8 Å resolution. *Nature*. 1997;389(6648):251-260. doi:10.1038/38444

Machyna M, Kehr S, Straube K, et al. The Coilin Interactome Identifies Hundreds of Small Noncoding RNAs that Traffic through Cajal Bodies. *Molecular Cell*. 2014;56(3):389-399. doi:10.1016/j.molcel.2014.10.004

Mahmoudi S, Henriksson S, Farnebo L, Roberg K, Farnebo M. WRAP53 promotes cancer cell survival and is a potential target for cancer therapy. *Cell Death Dis*. 2011;2(1):e114-e114. doi:10.1038/cddis.2010.90

Mahmoudi S, Henriksson S, Corcoran M, Méndez-Vidal C, Wiman KG, Farnebo M. Wrap53, a natural p53 antisense transcript required for p53 induction upon DNA damage. *Mol Cell*. 2009;33(4):462-471. doi:10.1016/j.molcel.2009.01.028

Mahmoudi S, Henriksson S, Weibrecht I, et al. WRAP53 Is Essential for Cajal Body Formation and for Targeting the Survival of Motor Neuron Complex to Cajal Bodies. *PLOS Biology*. 2010;8(11):e1000521. doi:10.1371/journal.pbio.1000521

Marioni JC, Mason CE, Mane SM, Stephens M, Gilad Y. RNA-seq: An assessment of technical reproducibility and comparison with gene expression arrays. *Genome Res*. 2008;18(9):1509-1517. doi:10.1101/gr.079558.108

Markowitz JA, Singh P, Darras BT. Spinal Muscular Atrophy: A Clinical and Research Update. *Pediatric Neurology*. 2012;46(1):1-12. doi:10.1016/j.pediatrneurol.2011.09.001

Mercadante AA, Kasi A. Genetics, Cancer Cell Cycle Phases. In: *StatPearls*. StatPearls Publishing; 2022. Accessed November 4, 2022. http://www.ncbi.nlm.nih.gov/books/NBK563158/

Middleton G, Silcocks P, Cox T, et al. Gemcitabine and capecitabine with or without telomerase peptide vaccine GV1001 in patients with locally advanced or metastatic pancreatic cancer (TeloVac): an open-label, randomised, phase 3 trial. *The Lancet Oncology*. 2014;15(8):829-840. doi:10.1016/S1470-2045(14)70236-0

Mizukoshi E, Kaneko S. Telomerase-Targeted Cancer Immunotherapy. *Int J Mol Sci*. 2019;20(8):1823. doi:10.3390/ijms20081823

Mir T, Huang SH, Kobryn K. The telomere resolvase of the Lyme disease spirochete, Borrelia burgdorferi, promotes DNA single-strand annealing and strand exchange. *Nucleic Acids Research*. 2013;41(22):10438-10448. doi:10.1093/nar/gkt832

Mitchell JR, Cheng J, Collins K. A Box H/ACA Small Nucleolar RNA-Like Domain at the Human Telomerase RNA 3′ End. *Mol Cell Biol*. 1999;19(1):567-576.

Mitchell JR, Wood E. A telomerase component is defective in the human disease dyskeratosis congenita. *Nature*. 1999;402(6761):551. doi:10.1038/990141

Mitrea DM, Kriwacki RW. 2016. Phase separation in biology; functional organization of a higher order. *Cell Commun Signal Ccs.* 2016;14:1. doi:10.1186/s12964-015-0125-7

Moon DH, Segal M, Boyraz B, et al. Poly(A)-specific ribonuclease (PARN) mediates 3'-end maturation of the telomerase RNA component. *Nat Genet*. 2015;47(12):1482-1488. doi:10.1038/ng.3423

Moon DH, Segal M, Boyraz B, et al. Mutations in the Poly(A)-Specific Ribonuclease (PARN) Impair Telomerase RNA 3' End Maturation in Dyskeratosis Congenita Patients. *Blood*. 2015;126(23):669. doi:10.1182/blood.V126.23.669.669

Morris GE. The Cajal body. *Biochimica et Biophysica Acta (BBA) - Molecular Cell Research*. 2008;1783(11):2108-2115. doi:10.1016/j.bbamcr.2008.07.016

Mullassery D, Horton C, Wood C, White M. Single Live Cell Imaging for Systems Biology. *Essays Biochem*. 2008;45:121-133. doi:10.1042/BSE0450121

Nagpal N, Wang J, Zeng J, et al. Small molecule PAPD5 inhibitors restore telomerase activity in patient stem cells. *Cell Stem Cell*. 2020;26(6):896-909.e8. doi:10.1016/j.stem.2020.03.016

Nakamura TM, Morin GB, Chapman KB, et al. Telomerase catalytic subunit homologs from fission yeast and human. *Science*. 1997;277(5328):955-959. doi:10.1126/science.277.5328.955

Nandakumar J, Bell CF, Weidenfeld I, Zaug AJ, Leinwand LA, Cech TR. The TEL patch of telomere protein TPP1 mediates telomerase recruitment and processivity. *Nature*. 2012;492:285 289. doi:10.1038/nature11648

Nandakumar J, Cech TR. Finding the end: recruitment of telomerase to telomeres. *Nat Rev Mol Cell Bio.* 2013;14. doi:10.1038/nrm3505

Nault JC, Ningarhari M, Rebouissou S, Zucman-Rossi J. The role of telomeres and telomerase in cirrhosis and liver cancer. *Nat Rev Gastroenterol Hepatol*. 2019;16(9):544-558. doi:10.1038/s41575-019-0165-3

Nguyen THD, Tam J, Wu RA, et al. Cryo-EM structure of substrate-bound human telomerase holoenzyme. *Nature*. 2018;557(7704):190-195. doi:10.1038/s41586-018-0062-x

NOD: NucleOlar localization sequence Detector. Accessed April 12, 2023. http://www.compbio.dundee.ac.uk/www-nod/downloads.jsp

Noble PW, Barkauskas CE, Jiang D. Pulmonary fibrosis: patterns and perpetrators. *J Clin Invest*. 2012;122(8):2756-2762. doi:10.1172/JCI60323

Ogg SC, Lamond AI. Cajal bodies and coilin—moving towards function. *Journal of Cell Biology*. 2002;159(1):17-21. doi:10.1083/jcb.200206111

Olovnikov AM. A theory of marginotomy: The incomplete copying of template margin in enzymic synthesis of polynucleotides and biological significance of the phenomenon. *Journal of Theoretical Biology*. 1973;41(1):181-190. doi:10.1016/0022-5193(73)90198-7

Palm W, de Lange T. How Shelterin Protects Mammalian Telomeres. *Annu Rev Genet*. 2008;42(1):301-334. doi:10.1146/annurev.genet.41.110306.130350

Pellizzoni L, Baccon J, Charroux B, Dreyfuss G. The survival of motor neurons (SMN) protein interacts with the snoRNP proteins fibrillarin and GAR1. *Current Biology*. 2001;11(14):1079-1088. doi:10.1016/S0960-9822(01)00316-5

Pellizzoni L, Yong J, Dreyfuss G. Essential Role for the SMN Complex in the Specificity of snRNP Assembly. *Science*. 2002;298(5599):1775-1779. doi:10.1126/science.1074962

Penev A, Bazley A, Shen M, Boeke JD, Savage SA, Sfeir A. Alternative splicing is a developmental switch for hTERT expression. *Mol Cell*. 2021;81(11):2349-2360.e6. doi:10.1016/j.molcel.2021.03.033

Peng Y, Mian IS, Lue NF. Analysis of Telomerase Processivity: Mechanistic Similarity to HIV-1 Reverse Transcriptase and Role in Telomere Maintenance. *Molecular Cell*. 2001;7(6):1201-1211. doi:10.1016/S1097-2765(01)00268-4

Queiroz RML, Smith T, Villanueva E, et al. Comprehensive identification of RNA–protein interactions in any organism using orthogonal organic phase separation (OOPS). *Nat Biotechnol*. 2019;37(2):169-178. doi:10.1038/s41587-018-0001-2

Querido E, Sfeir A, Chartrand P. 2020. Imaging of Telomerase RNA by Single-Molecule Inexpensive FISH Combined with Immunofluorescence. *Star Protoc.* 2020;1:100104. doi:10.1016/j.xpro.2020.100104

Rao X, Huang D, Sui X, et al. Overexpression of WRAP53 Is Associated with Development and Progression of Esophageal Squamous Cell Carcinoma. *PLOS ONE*. 2014;9(3):e91670. doi:10.1371/journal.pone.0091670

Recht J, Dunn B, Raff A, Osley MA. Functional analysis of histones H2A and H2B in transcriptional repression in Saccharomyces cerevisiae. *Mol Cell Biol*. 1996;16(6):2545-2553. doi:10.1128/MCB.16.6.2545

Riback JA, Zhu L, Ferrolino MC, Tolbert M, Mitrea DM, Sanders DW, Wei M-T, Kriwacki RW, Brangwynne CP. Composition-dependent thermodynamics of intracellular phase separation. *Nature.* 2020;581:209–214. doi:10.1038/s41586-020-2256-2

Richard P, Darzacq X, Bertrand E, Jády BE, Verheggen C, Kiss T. A common sequence motif determines the Cajal body-specific localization of box H/ACA scaRNAs. *EMBO J*. 2003;22(16):4283-4293. doi:10.1093/emboj/cdg394

Sarkar G, Bolander ME. Telomeres, telomerase, and cancer. *Science*. 1995;268(5214):1115-1117. doi:10.1126/science.7761821

Savage SA, Zhong F, Giri N, et al. Mutations In TCAB1 Cause Dyskeratosis Congenita. *Blood*. 2010;116(21):197. doi:10.1182/blood.V116.21.197.197

Schmidt JC, Dalby AB, Cech TR. Identification of human TERT elements necessary for telomerase recruitment to telomeres. Greider C, ed. *eLife*. 2014;3:e03563. doi:10.7554/eLife.03563

Schmidt JC, Cech TR. Human telomerase: biogenesis, trafficking, recruitment, and activation. *Genes Dev*. 2015;29(11):1095-1105. doi:10.1101/gad.263863.115

Schmidt JC, Zaug AJ, Cech TR. Live Cell Imaging Reveals the Dynamics of Telomerase Recruitment to Telomeres. *Cell*. 2016;166(5):1188-1197.e9. doi:10.1016/j.cell.2016.07.033

Schmidt JC, Zaug AJ, Kufer R, Cech TR. Dynamics of human telomerase recruitment depend on template-telomere base pairing. *MBoC*. 2018;29(7):869-880. doi:10.1091/mbc.E17-11-0637

Sergé A, Bertaux N, Rigneault H, Marguet D. Dynamic multiple-target tracing to probe spatiotemporal cartography of cell membranes. *Nature Methods*. 2008;5(8):687-694. doi:10.1038/nmeth.1233

Shao Y, Feng S, Huang J, Huo J, You Y, Zheng Y. A unique homozygous WRAP53 Arg298Trp mutation underlies dyskeratosis congenita in a Chinese Han family. *BMC Medical Genetics*. 2018;19(1):40. doi:10.1186/s12881-018-0549-1

Shay JW. Are short telomeres predictive of advanced cancer? *Cancer Discov*. 2013;3(10):1096-1098. doi:10.1158/2159-8290.CD-13-0506

Shay JW, Wright WE. Hayflick, his limit, and cellular ageing. *Nat Rev Mol Cell Biol*. 2000;1(1):72-76. doi:10.1038/35036093

Shukla S, Jeong HC, Sturgeon CM, Parker R, Batista LFZ. Chemical inhibition of PAPD5/7 rescues telomerase function and hematopoiesis in dyskeratosis congenita. *Blood Advances*. 2020;4(12):2717-2722. doi:10.1182/bloodadvances.2020001848

Shukla S, Schmidt JC, Goldfarb KC, Cech TR, Parker R. Inhibition of telomerase RNA decay rescues telomerase deficiency caused by dyskerin or PARN defects. *Nature Structural & Molecular Biology*. 2016;23(4):286-292. doi:10.1038/nsmb.3184

Silwal-Pandit L, Russnes H, Borgen E, et al. The Sub-Cellular Localization of WRAP53 Has Prognostic Impact in Breast Cancer. *PLOS ONE*. 2015;10(10):e0139965. doi:10.1371/journal.pone.0139965

Sleeman JE, Ajuh P, Lamond AI. snRNP protein expression enhances the formation of Cajal bodies containing p80-coilin and SMN. *J Cell Sci*. 2001;114(Pt 24):4407-4419. doi:10.1242/jcs.114.24.4407

Sloan KE, Warda AS, Sharma S, Entian KD, Lafontaine DLJ, Bohnsack MT. Tuning the ribosome: The influence of rRNA modification on eukaryotic ribosome biogenesis and function. *RNA Biology*. 2017;14(9):1138-1152. doi:10.1080/15476286.2016.1259781

Southern E. Southern blotting. *Nat Protoc.* 2006;1:518–525. doi:10.1038/nprot.2006.73

Steczkiewicz K, Zimmermann MT, Kurcinski M, et al. Human telomerase model shows the role of the TEN domain in advancing the double helix for the next polymerization step. *Proc Natl Acad Sci U S A*. 2011;108(23):9443-9448. doi:10.1073/pnas.1015399108

Stern JL, Zyner KG, Pickett HA, Cohen SB, Bryan TM. Telomerase Recruitment Requires both TCAB1 and Cajal Bodies Independently. *Molecular and Cellular Biology*. 2012;32(13):2384-2395. doi:10.1128/MCB.00379-12

Stuart BD, Choi J, Zaidi S, Xing C, Holohan B, Chen R, Choi M, Dharwadkar P, Torres F, Girod CE, Weissler J, Fitzgerald J, Kershaw C, Klesney-Tait J, Mageto Y, Shay JW, Ji W, Bilguvar K, Mane S, Lifton RP, Garcia CK. Exome sequencing links mutations in PARN and RTEL1 with familial pulmonary fibrosis and telomere shortening. *Nat Genet.* 2015;47:512 517. doi:10.1038/ng.3278

Takai H, Smogorzewska A, de Lange T. DNA damage foci at dysfunctional telomeres. *Curr Biol*. 2003;13(17):1549-1556. doi:10.1016/s0960-9822(03)00542-6

Takagi M, Absalon MJ, McLure KG, Kastan MB. Regulation of p53 translation and induction after DNA damage by ribosomal protein L26 and nucleolin. *Cell.* 2005;123:49 63. doi:10.1016/j.cell.2005.07.034

TCAB1: a potential target for diagnosis and therapy of head and neck carcinomas | Molecular Cancer | Full Text. Accessed September 22, 2022. https://molecular-cancer.biomedcentral.com/articles/10.1186/1476-4598-13-180

The Nobel Prize in Physiology or Medicine 2009. NobelPrize.org. Accessed October 14, 2022. https://www.nobelprize.org/prizes/medicine/2009/press-release/

Tokunaga M, Imamoto N, Sakata-Sogawa K. Highly inclined thin illumination enables clear single-molecule imaging in cells. *Nat Methods.* 2008;5:159 161. doi:10.1038/nmeth1171

Tomlinson RL, Ziegler TD, Supakorndej T, Terns RM, Terns MP. Cell Cycle-regulated Trafficking of Human Telomerase to Telomeres. *Mol Biol Cell*. 2006;17(2):955-965. doi:10.1091/mbc.E05-09-0903

Tseng C-K, Wang H-F, Burns AM, Schroeder MR, Gaspari M, Baumann P. 2015. Human Telomerase RNA Processing and Quality Control. *Cell Reports.* 2015;13:2232–2243. doi:10.1016/j.celrep.2015.10.075

Tummala H, Walne A, Collopy L, Cardoso S, Fuente J de la, Lawson S, Powell J, Cooper N, Foster A, Mohammed S, Plagnol V, Vulliamy T, Dokal I. 2015. Poly(A)-specific ribonuclease deficiency impacts telomere biology and causes dyskeratosis congenita. *J Clin Invest.* 2015;125:2151–2160. doi:10.1172/jci78963

Tycowski KT, Shu MD, Kukoyi A, Steitz JA. A Conserved WD40 Protein Binds the Cajal Body Localization Signal of scaRNP Particles. *Molecular Cell*. 2009;34(1):47-57. doi:10.1016/j.molcel.2009.02.020

Venteicher AS, Abreu EB, Meng Z, et al. A human telomerase holoenzyme protein required for Cajal body localization and telomere synthesis. *Science*. 2009;323(5914):644-648. doi:10.1126/science.1165357

Venteicher AS, Artandi SE. TCAB1: driving telomerase to Cajal bodies. *Cell Cycle*. 2009;8(9):1329-1331. doi:10.4161/cc.8.9.8288

Vogan JM, Zhang X, Youmans DT, et al. Minimized human telomerase maintains telomeres and resolves endogenous roles of H/ACA proteins, TCAB1, and Cajal bodies. *eLife*. 5:e18221. doi:10.7554/eLife.18221

Vulliamy T, Beswick R, Kirwan M, et al. Mutations in the telomerase component NHP2 cause the premature ageing syndrome dyskeratosis congenita. *Proceedings of the National Academy of Sciences*. 2008;105(23):8073-8078. doi:10.1073/pnas.0800042105

Vulliamy T, Marrone A, Szydlo R, Walne A, Mason PJ, Dokal I. Disease anticipation is associated with progressive telomere shortening in families with dyskeratosis congenita due to mutations in TERC. *Nat Genet*. 2004;36(5):447-449. doi:10.1038/ng1346

Walne AJ, Vulliamy T, Marrone A, et al. Genetic heterogeneity in autosomal recessive dyskeratosis congenita with one subtype due to mutations in the telomerase-associated protein NOP10. *Human Molecular Genetics*. 2007;16(13):1619-1629. doi:10.1093/hmg/ddm111

Wang F, Podell ER, Zaug AJ, et al. The POT1-TPP1 telomere complex is a telomerase processivity factor. *Nature*. 2007;445(7127):506-510. doi:10.1038/nature05454

Wang W, Budhu A, Forgues M, Wang XW. Temporal and spatial control of nucleophosmin by the Ran–Crm1 complex in centrosome duplication. *Nat Cell Biol.* 2005;7:823–830. doi:10.1038/ncb1282

Watkins NJ, Gottschalk A, Neubauer G, et al. Cbf5p, a potential pseudouridine synthase, and Nhp2p, a putative RNA-binding protein, are present together with Gar1p in all H BOX/ACA-motif snoRNPs and constitute a common bipartite structure. *RNA*. 1998;4(12):1549-1568.

Watson JD. Origin of Concatemeric T7DNA. *Nature New Biology*. 1972;239(94):197-201. doi:10.1038/newbio239197a0

Weidenfeld I, Gossen M, Löw R, Kentner D, Berger S, Görlich D, Bartsch D, Bujard H, Schönig K. Inducible expression of coding and inhibitory RNAs from retargetable genomic loci. *Nucleic Acids Res.* 2009;37:e50. doi:10.1093/nar/gkp10

Weidmann CA, Mustoe AM, Jariwala PB, Calabrese JM, Weeks KM. Analysis of RNA–protein networks with RNP-MaP defines functional hubs on RNA. *Nat Biotechnol*. 2021;39(3):347-356. doi:10.1038/s41587-020-0709-7

Weinrich SL, Pruzan R, Ma L, et al. Reconstitution of human telomerase with the template RNA component hTR and the catalytic protein subunit hTRT. *Nat Genet*. 1997;17(4):498-502. doi:10.1038/ng1297-498

Whitehead SE, Jones KW, Zhang X, Cheng X, Terns RM, Terns MP. Determinants of the Interaction of the Spinal Muscular Atrophy Disease Protein SMN with the Dimethylarginine-modified Box H/ACA Small Nucleolar Ribonucleoprotein GAR1*. *Journal of Biological Chemistry*. 2002;277(50):48087-48093. doi:10.1074/jbc.M204551200

Wilkinson KA, Merino EJ, Weeks KM. Selective 2′-hydroxyl acylation analyzed by primer extension (SHAPE): quantitative RNA structure analysis at single nucleotide resolution. *Nat Protoc*. 2006;1(3):1610-1616. doi:10.1038/nprot.2006.249

Wright WE, Shay JW. Telomere dynamics in cancer progression and prevention: fundamental differences in human and mouse telomere biology. *Nat Med*. 2000;6(8):849-851. doi:10.1038/78592

Wu M, Tinoco I. RNA folding causes secondary structure rearrangement. *Proceedings of the National Academy of Sciences*. 1998;95(20):11555-11560. doi:10.1073/pnas.95.20.11555

Wu RA, Upton HE, Vogan JM, Collins K. Telomerase Mechanism of Telomere Synthesis. *Annu Rev Biochem.* 2017;86:439 460. doi:10.1146/annurev-biochem-061516-045019

Xi L, Cech TR. Inventory of telomerase components in human cells reveals multiple subpopulations of hTR and hTERT. *Nucleic Acids Research*. 2014;42(13):8565-8577. doi:10.1093/nar/gku560

Yamaguchi H, Calado RT, Ly H, et al. Mutations in TERT, the gene for telomerase reverse transcriptase, in aplastic anemia. *N Engl J Med*. 2005;352(14):1413-1424. doi:10.1056/NEJMoa042980

Yao R-W, Xu G, Wang Ying, Shan L, Luan P-F, Wang Yang, Wu M, Yang L-Z, Xing Y-H, Yang L, Chen L-L. Nascent Pre-rRNA Sorting via Phase Separation Drives the Assembly of Dense Fibrillar Components in the Human Nucleolus. *Mol Cell.* 2019;76:767-783.e11. doi:10.1016/j.molcel.2019.08.014

Zaug AJ, Linger J, Cech TR. Method for determining RNA 3’ ends and application to human telomerase RNA. *Nucleic Acids Res*. 1996;24(3):532-533.

Zhang H, Wang DW, Adell G, Sun XF. WRAP53 is an independent prognostic factor in rectal cancer- a study of Swedish clinical trial of preoperative radiotherapy in rectal cancer patients. *BMC Cancer*. 2012;12:294. doi:10.1186/1471-2407-12-294

Zhong F, Savage SA, Shkreli M, et al. Disruption of telomerase trafficking by TCAB1 mutation causes dyskeratosis congenita. *Genes Dev*. 2011;25(1):11-16. doi:10.1101/gad.2006411

Zhu X, Kumar R, Mandal M, et al. Cell cycle-dependent modulation of telomerase activity in tumor cells. *Proc Natl Acad Sci U S A*. 1996;93(12):6091-6095.

Zhu Y, Ding L, Chen BF, Song JG, Yao YS. Oncogenic Activity of Wrap53 in Human Colorectal Cancer In Vitro and in Nude Mouse Xenografts. *Med Sci Monit*. 2018;24:6129-6136. doi:10.12659/MSM.910214

Zubradt M, Gupta P, Persad S, Lambowitz AM, Weissman JS, Rouskin S. DMS-MaPseq for genome-wide or targeted RNA structure probing in vivo. *Nat Methods*. 2017;14(1):75-82. doi:10.1038/nmeth.4057

APPENDIX A: SUPPLEMENTAL FIGURES

Supplemental figures for chapter 2:

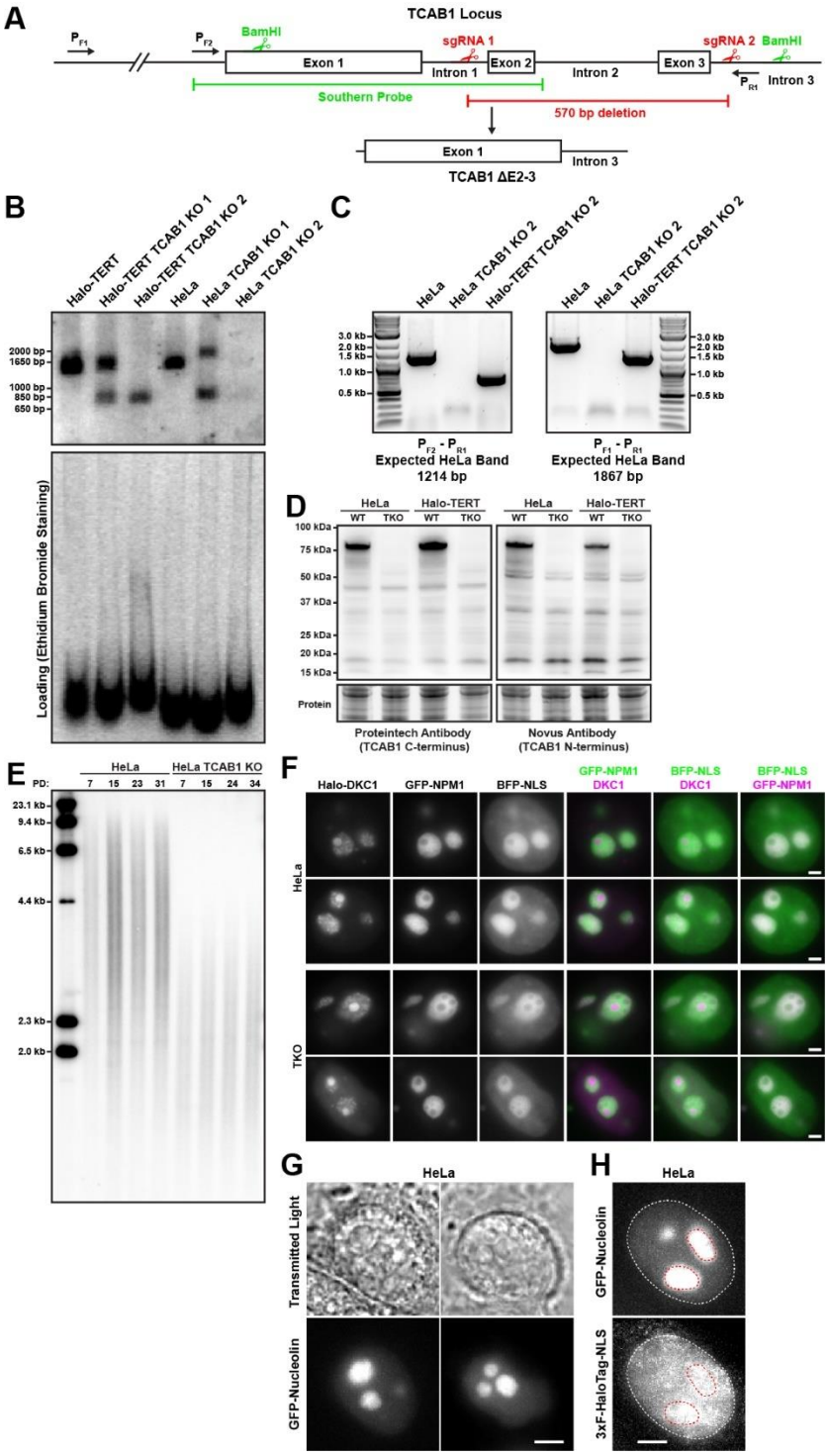

Figure A1. TCAB1 knock-out strategy, telomere length, and HaloTag localization. (A) Strategy to knock-out TCAB1 using Cas9 and two sgRNAs targeting introns 1 and 3. **(B)** Southern blot of genomic DNA digested with BamHI from parental cells and TCAB1 knock-out

Figure A1 (cont'd)

clones using probes generated from a PCR product of the TCAB1 gene indicated in **(A)** demonstrating the expected truncation of the *TCAB1* gene in Halo-TERT TCAB1 KO 2. HeLa TCAB1 KO 2 carries larger deletions completely removing exons 1 and 2 from the *TCAB1* gene. **(C)** PCR using primers indicated in **(A)** of genomic DNA from parental cells and TCAB1 knock-out clones confirming the deletion of critical regions of the *TCAB1* gene show in **(B)**. **(D)** Western blots demonstrating the absence of TCAB1 protein in TCAB1 knock-out cell lines generated in HeLa and Halo-TERT cells lines using two antibodies targeting the N-terminus and C-terminus of TCAB1. **(E)** Telomere length analysis by Southern blot of telomeric restriction fragments, indicating that telomeres in TCAB1 knock-out cells are short but stable in length. **(G)** Images of HeLa cells transiently expressing GFP-nucleolin to mark nucleoli. The GFP-nucleolin signal overlaps with circular shapes visible under transmitted light illumination (scale bar = 2 µm). **(H)** Images of HeLa cells transiently expressing GFP-nucleolin and 3xFLAG-HaloTag-NLS labeled with JF646. The 3xFLAG-HaloTag-NLS signal (maximum intensity projection of 1000 frames of a single-molecule imaging movie) clearly overlaps with the GFP-nucleolin signal (red dashed outline), demonstrating that 3xFLAG-HaloTag-NLS can enter the nucleolus (scale bar = 2 µm).

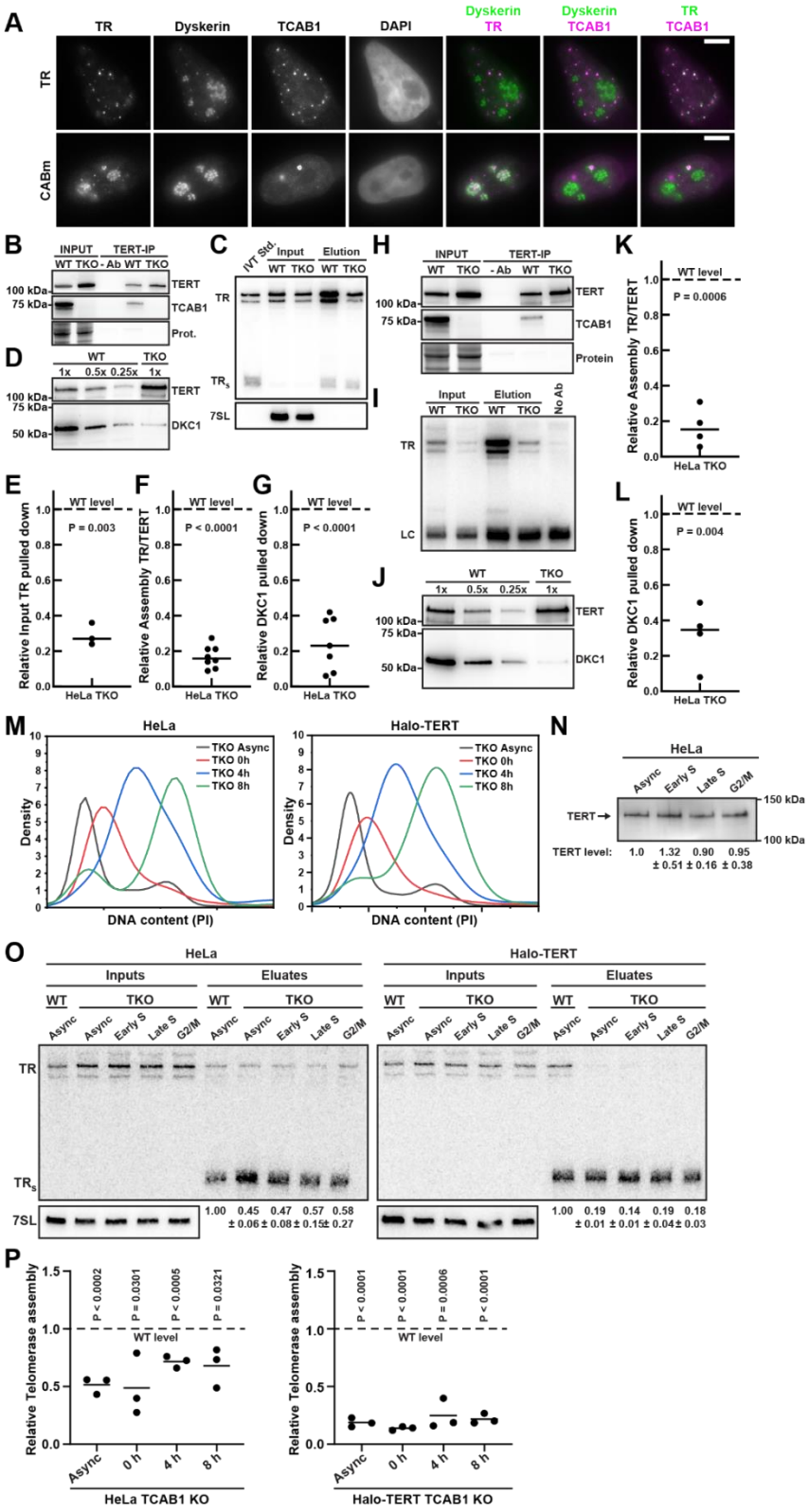

Figure A2. TR CABmut localization and cell cycle distribution. (A) Immuno-fluorescence with anti-dyskerin and anti-TCAB1 antibodies coupled to fluorescence in-situ hybridization with probes against TR, demonstrating TR localization to nucleoli in cells expressing TERT and TR G414C

Figure A2 (cont'd)

(CABm) (scale bar = 5 µm). **(B-L)** TERT immuno-purification (using a sheep anti-TERT antibody) from **(B-G)** Hela cells and the corresponding TCAB1 knock-out cells and **(H-L)** Halo-TERT cells and the corresponding TCAB1 knock-out cells, overexpressing TERT and TR. **(B, H)** Western blots analyzing TERT immuno-purification (using a sheep anti-TERT antibody) probed with a rabbit anti-TERT antibody (Abcam) and a TCAB1 antibody. **(C, I)** Northern blot of RNA extracted from input and purified TERT samples from probed with radiolabeled DNA oligonucleotides complementary to TR. Standards are *in vitro* transcribed full-length TR and truncated TR_S. TR_S was added to samples prior to RNA extraction as loading and recovery control. **(D, J)** Western blots to analyze immuno-purified telomerase RNP composition. A single membrane was cut into two pieces that were probed with TERT and dyskerin antibodies, respectively. (**E**) Quantification of the amount of TR purified relative to input TR in TERT purifications from TCAB1 knock-out cells overexpressing TERT and TR compared to parental controls (mean, T-Test). **(F, K)** Quantification of the ratio of TR to TERT (n = 4) in TERT purifications from TCAB1 knock-out cells overexpressing TERT and TR compared to parental controls (mean, T-Test). **(G, L)** Quantification of the amount of dyskerin (n = 4) in TERT purifications from TCAB1 knock-out cells overexpressing TERT and TR compared to parental controls (mean, T-Test). The dashed lines indicate the level in telomerase purified from wild-type TCAB1 control cells which was normalized to 1.0. **(M)** DNA content analysis (PI staining) by flow cytometry of synchronized cell populations used for telomerase purifications. **(N)** Western blots analyzing endogenous TERT immuno-purifications (using a sheep anti-TERT antibody) from synchronized control HeLa and TCAB1 knock-out cells probed with a rabbit anti-TERT antibody (Abcam). **(O)** Northern blot of RNA extracted from input and purified TERT samples from asynchronous control HeLa cells and asynchronous and synchronized TCAB1 knock-out cells probed with radiolabeled DNA oligonucleotides complementary to TR. Standards are *in vitro* transcribed full-length TR and truncated TR_S. TR_S was added to samples prior to RNA extraction as loading and recovery control. Input samples were also probed for 7SL RNA as loading control. **(P)** Quantification of fraction of input TR (normalized to 7SL) co-purified with TERT or HaloTag-TERT (normalized to TR_s) from TCAB1 knock-out cells relative to control cells (dashed line).

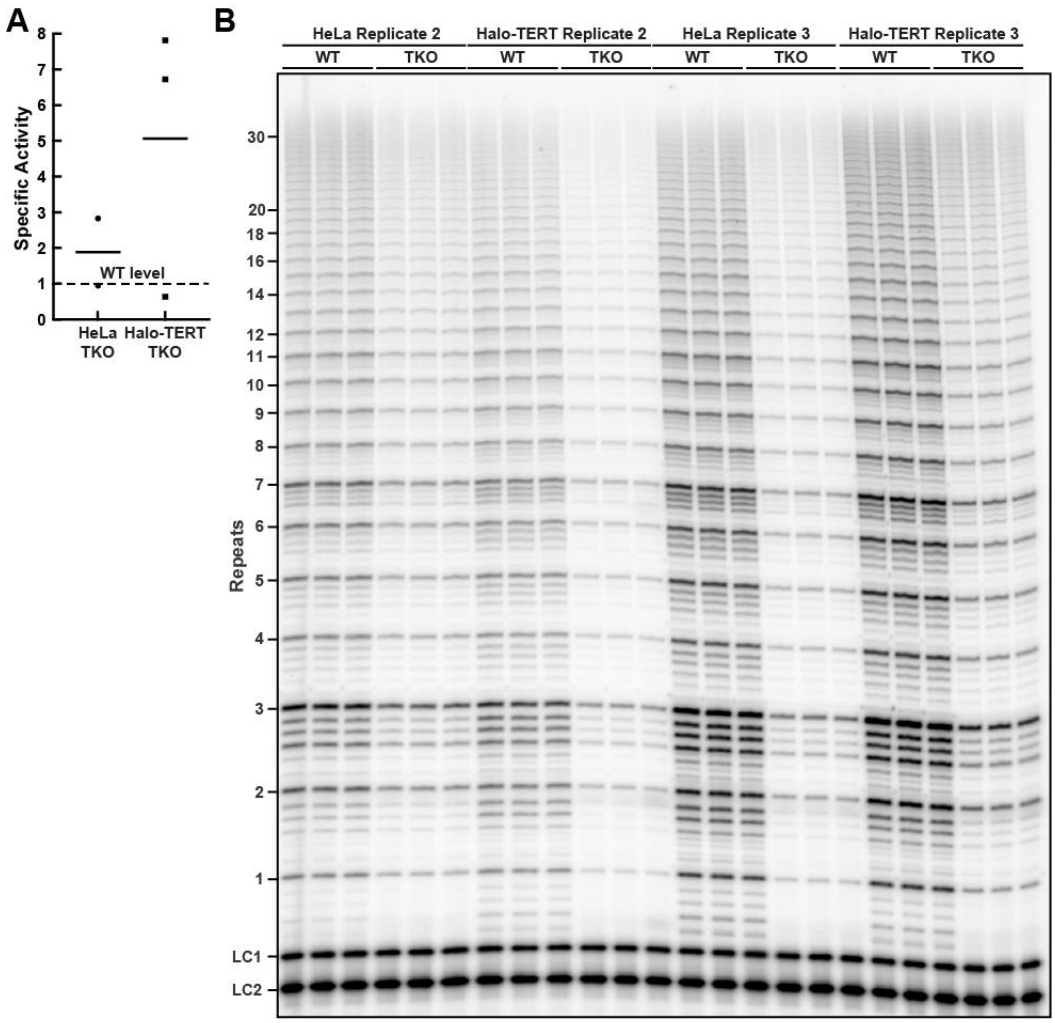

Figure A3. Telomerase activity assay in absence of TCAB1 (A) Specific activity of endogenous telomerase purified from TCAB1 knock-out cells relative to parental controls. Specific activity was calculated by dividing the relative activity (see Fig. 2.3A,B) by the relative amount of TR present in immuno-purified TERT samples (Fig. 2B). The dashed lines indicate the activity level in telomerase purified from wild-type TCAB1 control cells which was normalized to 1.0. **(B)** Direct telomerase extension assay of overexpressed telomerase immuno-purified from parental (WT) and TCAB1 knock-out (TKO) HeLa and Halo-TERT cell lines. LC1 and LC2, radiolabeled DNA oligonucleotide loading controls.

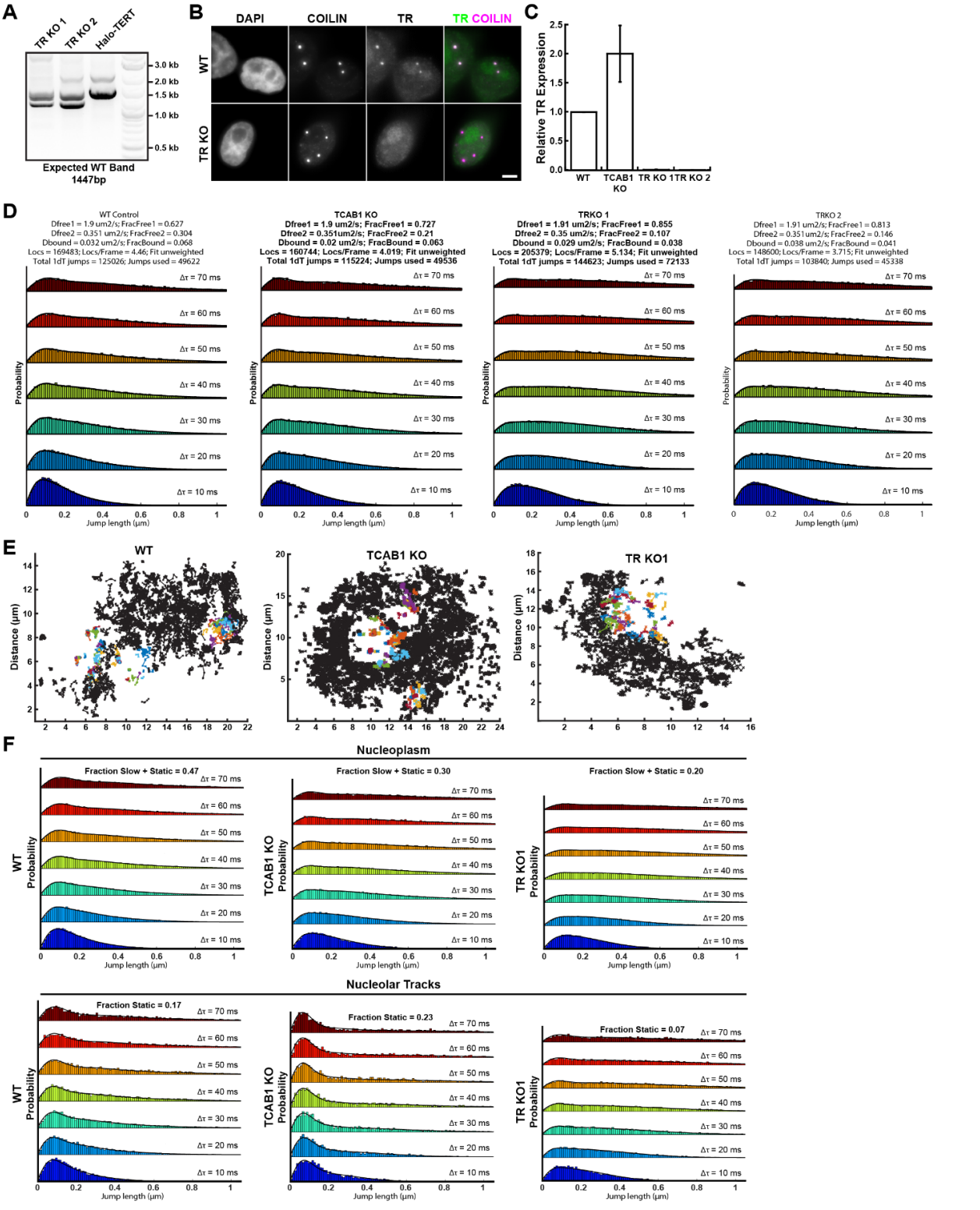

Figure A4. TR knock-out clone verification and probability density functions. (A) PCR analysis of the TR locus in parental and TR knock-out clones. Both TR knock-out clones show PCR products with reduced length that were confirmed to be knock-outs

Figure A4 (cont'd)

by Sanger sequencing. **(B)** Images of control and TR knock-out cells probed with an antibody against coilin and FISH probes specific for TR, demonstrating the lack of TR signal in TR knock-out cells (scale bar = 5 μm). **(C)** Determination of TR levels in control, TCAB1 knock-out, and TR knock-out cells, using RT-qPCR with primers specific to TR normalized to GAPDH (3 independent biological replicates, 3 technical replicates for each biological replicate, mean ± standard deviation). **(D)** Probability density function of step sizes of HaloTag-TERT molecules from control, TCAB1 knock-out, and TR knock-out cells and the corresponding 3-state model fit using the spot on tool (Data from one of three biological replicates, >15 cells per cell line) (Fig. 2.4A-B) **(E)** Graphs of HaloTag-TERT tracks that are nucleoplasmic (black) or overlap with the nucleolus for at least one frame (color) in control (WT), TCAB1 knock-out, and TR knock-out cells. **(F)** Probability density functions of the step-sizes derived from HaloTag-TERT molecules that overlap with the nucleoplasm or the nucleolus for at least one frame and the corresponding 3-state model fit using the SpotOn tool (pooled data from 3 independent experiments, >18 cells total per cell line).

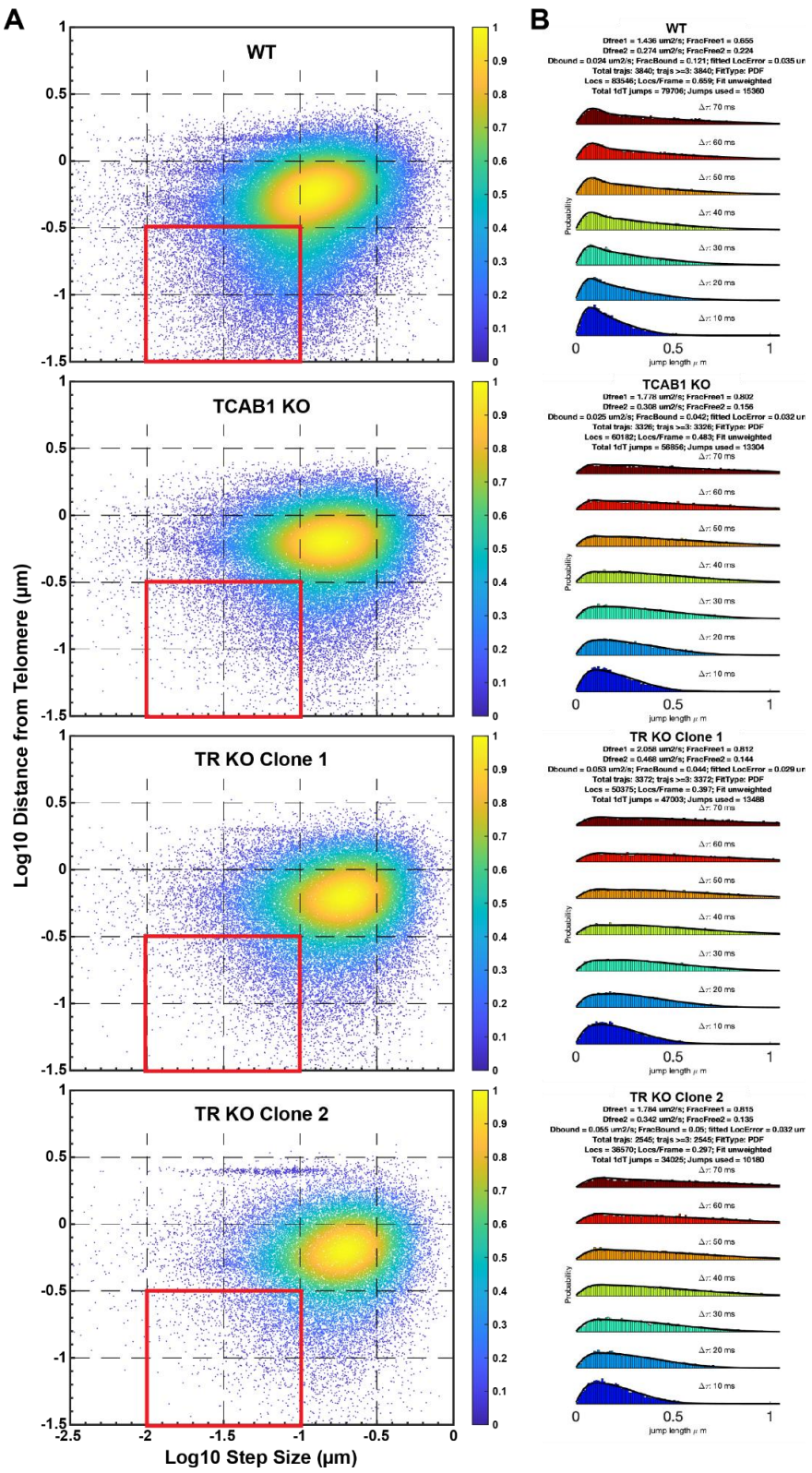

Figure A5. Step-size analysis of TERT molecules. (A) Analysis if the step size of telomeric TERT particles relative to the distance of the particle to the closest telomere (pooled results from 3 independent biological replicates with 19-30 cells analyzed per replicate). TERT molecules

Figure A5 (cont'd)

bound to the telomere are expected to have small step sizes and a short distance to the closest telomere, which is apparent in the enrichment of events in the lower left quadrants in the WT control (red box). This enrichment is not observed in TCAB1 and TR knock-out cells (red box). **(B)** Spot-On analysis of telomeric TERT particles (pooled results from 3 independent biological replicates with 19-30 cells analyzed per replicate). The fraction of bound TERT particles in TCAB1 and TR knock-out cells is 4-5%, compared to 12% in the WT control cells.

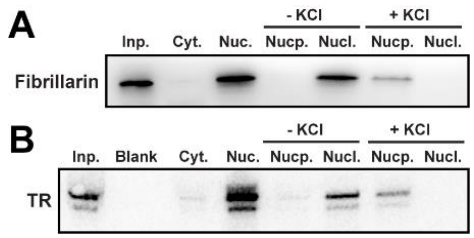

Figure A6. Nucleolar isolation in a high salt concentration. (A) Western blot and **(B)** Northern blot of cellular fractions from TCAB1 knock-out cells probed with an antibody against fibrillarin and probes for TR, respectively. Ruptured nuclei were either maintained at a low salt concentration or exposed to 357.5 mM KCl. The results demonstrate that nucleoli are dissolved in the presence of a high salt concentration, releasing fibrillarin and TR into the nucleoplasmic fraction.

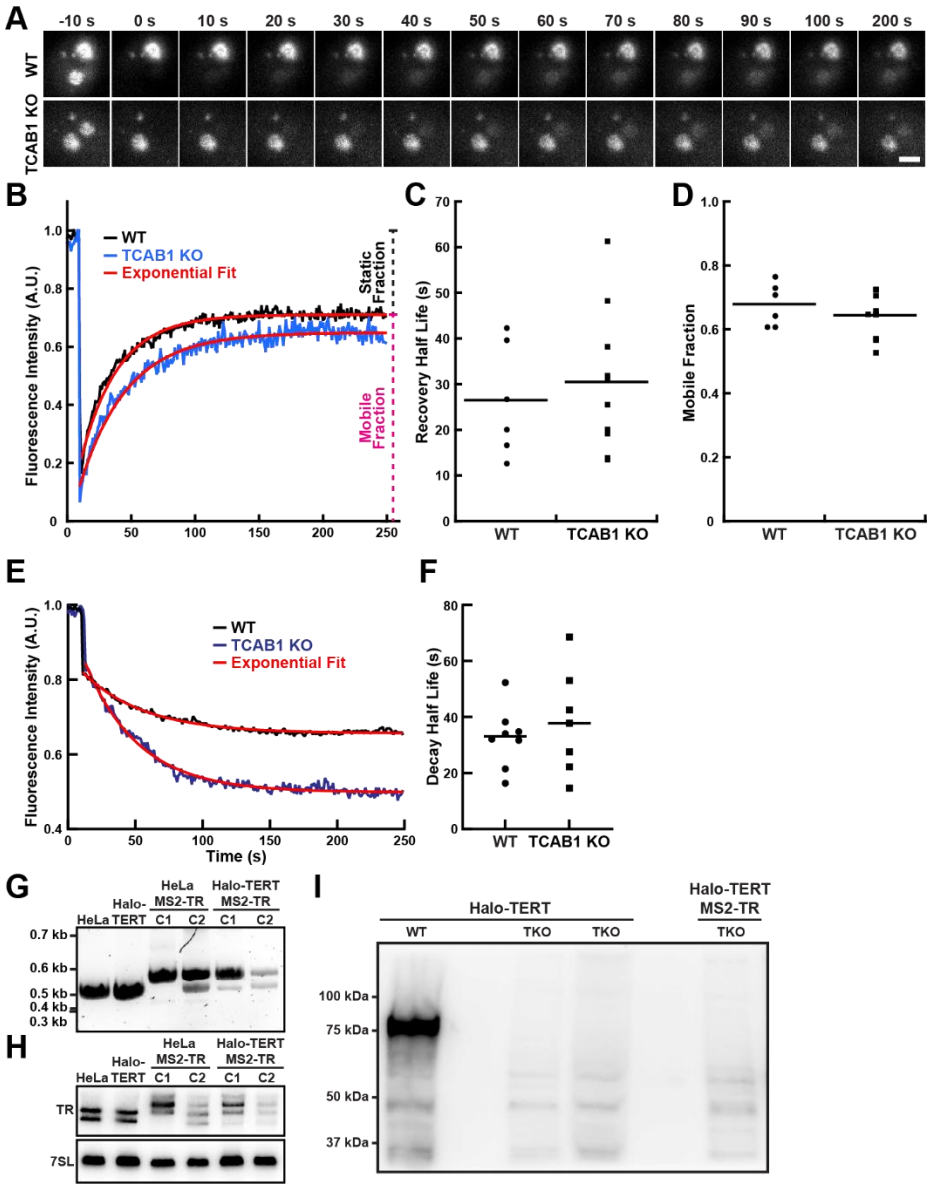

Figure A7. FRAP of dyskerin and verifications of MS2-TR clones. (A) Images of control and TCAB1 knock-out cells expressing 3xFLAG-HaloTag-dyskerin before and after photobleaching of nucleolar dyskerin (JFX650, scale bar = 5 µm). **(B)** Fluorescence recovery curves of nucleolar dyskerin in control and TCAB1 knock-out cells. Data was fit with a single exponential function. **(C)** Quantification of half-life of fluorescence recovery, calculated from the rate constant of the single exponential fit of the data shown in (B) (n = 6 and 9, mean). **(D)** Quantification of the mobile fraction of nucleolar dyskerin based on the single exponential fit of the data shown in (B) (n = 6 and 9, mean). **(E)** Fluorescence decay curves of unbleached nucleolar dyskerin in control and TCAB1 knock-out cells. Data was fit with a single exponential function. **(F)** Quantification of half-life of fluorescence decay, calculated from the rate constant of the single exponential fit of the data shown in **(E)** (n = 8 and 7, mean). **(G)** Western blot probed with an antibody against TCAB1, demonstrating the knock-out of TCAB1 in Halo-TERT MS2-TR HeLa cells. **(H)** PCR analysis of

Figure A7 (cont'd)

the endogenous TR locus after insertion of the 3xMS2 sequence. **(I)** Northern blot probed with radioactively labeled anti-TR oligonucleotides of control cells and genome edited clones expressing 3xMS2-TR.

Movie Legends:

Movie S1. Single-molecule imaging of 3xFLAG-HaloTag-TERT labeled with JFX650 and GFP-NPM1 to mark nucleoli in a control cell acquired at 100 frames per second using an Andor iXon 897 Ultra camera. 200x200 pixels with a pixel size of 0.16 µm.

Movie S2. Single-molecule imaging of 3xFLAG-HaloTag-TERT labeled with JFX650 and GFP-NPM1 to mark nucleoli in a TCAB1 knock-out cell acquired at 100 frames per second second using an Andor iXon 897 Ultra camera. 200x200 pixels with a pixel size of 0.16 µm.

Movie S3. Movie of cell expressing GFP-nucleolin (red) and 3xFLAG-HaloTag-NLS (green) labeled with JF646 acquired at 100 frames per second using an Andor iXon 897 Ultra camera, showing overlap of 3xFLAG-HaloTag-NLS with nucleoli. 140x140 pixels with a pixel size of 0.16 µm.

Movie S4. Movie of 3xFLAG-HaloTag-TERT labeled with JF646 in a control (left), TCAB1 knock-out (middle), and TR knock-out (right) cell acquired at 100 frames per second using an Andor iXon 897 Ultra camera. Each panel is 150x150 pixels in size with a pixel size of 0.16 µm.

Movie S5. Single-particle tracking of 3xFLAG-HaloTag-TERT labeled with JF646 in a TR knock-out cells acquired at 100 frames per second using an Andor iXon 897 Ultra camera. Trajectories with a minimum of 5 localizations are displayed. 150x150 pixels with a pixel size of 0.16 µm.

Movie S6. Single-molecule imaging of 3xFLAG-HaloTag-TERT labeled with JFX650 and GFP-NPM1 to mark nucleoli in a control (left), TCAB1 knock-out (middle), and TR knock-out cells 6-hours after release from a double-thymidine block acquired at 100 frames per second using a Hamamatsu ORCA BT fusion camera. 220x220 pixels with a pixel size of 0.108 µm.

Movie S7. Single-molecule imaging of 3xFLAG-HaloTag-TCAB1 labeled with JFX650, GFP-NPM1 to mark nucleoli, and BFP-coilin to mark Cajal bodies acquired at 100 frames per second using an Andor iXon 897 Ultra camera. GFP-NPM1 and BFP-coilin signals were acquired before and after single-molecule imaging of 3xFLAG-HaloTag-TCAB1. 190x190 pixels with a pixel size of 0.16 µm.

Movie S8. Single-molecule imaging of 3xFLAG-HaloTag-TCAB1 labeled with JFX650 and GFP-NPM1 to mark nucleoli acquired at 100 frames per second using an Andor iXon 897 Ultra camera. GFP-NPM1 signal was acquired before and after single-molecule imaging of 3xFLAG-HaloTag-TCAB1. 190x190 pixels with a pixel size of 0.16 µm.

Movie S9. Fluorescence recovery after photobleaching of HaloTag-dyskerin labeled with JFX650 HaloTag-ligand expressed in control cells acquired at 1 frame per second.

Movie S10. Fluorescence recovery after photobleaching of HaloTag-dyskerin labeled with JFX650 HaloTag-ligand expressed in TCAB1 knock-out cells, acquired at 1 frame per second.

Movie S11. Fluorescence recovery after photobleaching of nucleolar 3xMS2-TR bound by MCP-mNeonGreen in TCAB1 knock-out cells, acquired at 1 frame per 2 seconds. Nucleoli were identified by transient expression of mTagBFP-Nucleus-7.

Movie S12. Fluorescence recovery after photobleaching of nucleolar 3xMS2-TR bound by MCP-mNeonGreen in TCAB1 knock-out cells, acquired at 1 frame per 2 seconds. Nucleoli were identified by transient expression of mTagBFP-Nucleus-7.

Movie S13. Fluorescence recovery after photobleaching of nucleolar 3xMS2-TR bound by MCP-mNeonGreen in control cells, acquired at 1 frame per 2 seconds. Nucleoli were identified by transient expression of mTagBFP-Nucleus-7.

APPENDIX B: KEY RESOURCE TABLE

Table B1. Key resource table. Table contains reagents and chemicals used in the projects.

Reagents and Resources	Source	Identifier
Antibodies		
anti-TCAB1 rabbit polyclonal antibody	Proteintech	14761-1-AP
anti-TCAB1 rabbit polyclonal antibody	Abcam	ab224444
anti-TCAB1 rabbit polyclonal antibody	Novus Biologicals	NB100-68252
anti-GAR1 rabbit polyclonal antibody	Proteintech	11711-1-AP
anti-Coilin mouse monoclonal antibody	Abcam	ab87913
anti-Dyskerin mouse monoclonal antibody	Santa Cruz Biotech.	sc-373956
anti-TERT recombinant rabbit monoclonal antibody	Abcam	ab30202
anti-TERT sheep polyclonal antibody	Scott Cohen	Abx120550
anti-Fibrillarin mouse monoclonal antibody	Novus Biologicals	NB300-269
anti-Lamin B1 rabbit polyclonal antibody	Proteintech	12987-1-AP
anti-Rabbit Cy3 secondary antibody	Invitrogen	A-10520
anti-Mouse Alexa 647 secondary antibody	Invitrogen	A-21235
anti-Mouse Alexa 405 secondary antibody	Invitrogen	A-31553
anti-Mouse HRP	Invitrogen	A-31430
anti-Rabbit HRP	Invitrogen	A-31460
Chemicals, Peptides, and Recombinant Proteins		
JF646 HaloTag Ligand	Grimm et al., 2015	N/A
GAR1 siRNA	siGENOME Reagents	54433
Prolong Diamond Antifade Mountant	Life Technologies	P36970
Thymidine	Sigma	T1895
Puromycin 10 mg/ml	Gibco	A1113803
Lipofectamine 2000	Invitrogen	11668019
dGTP [α-32P] 3000 Ci/mmol 10 mCi/ml	Perkin Elmer	BLU514H250UC
TERT peptide ARPAEEATSLEGALSGTRH	Cohen et al. 2008	N/A
Dextrane sulfate	Sigma	D8906-10G
E. coli tRNA	Sigma	10109541001
Salmon Sperm DNA	Invitrogen	15632011
Vanadyl Ribonucleoside Complexes	Sigma	R3380-5ML
CHAPS	Fisher BioReagents	211911
SuperSignal West Femto Maximum Sensitivity Substrate	Thermo Scientific	34096
Clarity Western ECL substrate	Bio-Rad	1705061
Experimental Models: Cell Lines		
HeLa EM2-11ht, TCAB1 KO	Klump et al. 2023	N/A
HeLa EM2-11ht, FLAG-HaloTag-TERT WT, HA-mEOS3.2-TRF2	Schmidt et al. 2016	N/A
HeLa EM2-11ht, FLAG-HaloTag-TERT WT, HA-mEOS3.2-TRF2, TCAB1 KO	Klump et al. 2023	N/A
HeLa EM2-11ht, FLAG-HaloTag-TERT WT, HA-mEOS3.2-TRF2, TR KO	Klump et al. 2023	N/A
HeLa EM2-11ht, FLAG-HaloTag-TERT WT, HA-mEOS3.2-TRF2, 3xMS2-TR	Klump et al. 2023	N/A

Table B1 (cont'd)

HeLa EM2-11ht, FLAG-HaloTag-TERT WT, HA-mEOS3.2-TRF2, 3xMS2-TR, TCAB1 KO	Klump et al. 2023	N/A
Oligonucleotides		
TCAB1 KO sgRNA1 aaacctgggtcgccaagcaa	Klump et al. 2023	N/A
TCAB1 KO sgRNA2 ctgcacatttaagtccttcg	Klump et al. 2023	N/A
TCAB1 HaloTag KI sgRNA ctgcagTATGAAGACTTTGG	Klump et al. 2023	N/A
TR KO sgRNA1 ACCCTAACTGAGAAGGGCGT	Klump et al. 2023	N/A
TR KO sgRNA2 TCAGGCCGCAGGAAGAGGAA	Klump et al. 2023	N/A
3xMS2-TR KI sgRNA1 cgactcgcccggcagcgcac	Klump et al. 2023	N/A
3xMS2-TR KI sgRNA2 acccccaaacctgactgact	Klump et al. 2023	N/A
TR^{G414C} Forward CTGTGGGACGTGCACCCAGGACT	Klump et al. 2023	N/A
TR^{G414C} Reverse GTCAGGGAATCGCGCCGCGC	Klump et al. 2023	N/A
mCherry-dyskerin Backbone forward TGAGAATTCTGCAGTCGACGG	Klump et al. 2023	N/A
mCherry-dyskerin Backbone reverse GTCGAGACTAGTACCTCCACC	Klump et al. 2023	N/A
mCherry-dyskerin insert forward GGAGGTACTAGTCTCGACATGGCGGATGCGGAAG	Klump et al. 2023	N/A
mCherry-dyskerin insert reverse GTCGACTGCAGAATTCTCACTCAGAAACCAATTCTACCTCTTTTG	Klump et al. 2023	N/A
TR HRD Puro cassette forward GGATCCGGTGTGGAAAGTC	Klump et al. 2023	N/A
TR HRD Puro cassette reverse AAGCTTCACACAAAAAACCAACAC	Klump et al. 2023	N/A
3xFLAG-HaloTag-dysekrin Backbone forward TGAGCGGCCGCTTGCTG	Klump et al. 2023	N/A
3xFLAG-HaloTag-dysekrin Backbone reverse GGTACCGGAAGCGATCGC	Klump et al. 2023	N/A
3xFLAG-HaloTag-dysekrin insert forward ATCGCTTCCGGTACCATGGCGGATGCGGAAGTAATT	Klump et al. 2023	N/A
3xFLAG-HaloTag-dysekrin insert reverse GCAAGCGGCCGCTCACTCAGAAACCAATTCTACCTCTTTTGC	Klump et al. 2023	N/A
3xFLAG-HaloTag-NLS iPCR forward GATGACGATGACAAGATAACTTCGTATAATGTATGCTATACGAAGTTATCCGGTACCATGGCAGAAATCGGTACTGG	Klump et al. 2023	N/A
3xFLAG-HaloTag-NLS iPCR reverse CTTGTAATCGATATCATGATCTTTATAATCACCGTCATGGTCTTTGTAGTCCATGGTGGCTTTGCTAGCCC	Klump et al. 2023	N/A
pHAGE-UBC-MCP iPCR forward tctagaatccgcgtagatgcc	Klump et al. 2023	N/A

Table B1 (cont'd)

pHAGE-UBC-MCP iPCR reverse atcgatagatcctaatcaacctctgg	Klump et al. 2023	N/A
mNeonGreen forward with Gibson overlap gcatctacgcggattctagaGTGAGCAAGGGCGAGGAG	Klump et al. 2023	N/A
mNeonGreen reverse with Gibson overlap ggttgattaggatctatcgatTTACTTGTACAGCTCGTCCATGC	Klump et al. 2023	N/A
TR northern probe 1 CTTTTCCGCCCGCTGAAAGTCAGCGAG	Schmidt et al. 2018	N/A
TR northern probe 2 CTCCAGGCGGGGTTCGGGGGCTGGGCAG	Schmidt et al. 2018	N/A
TR northern probe 3 CGTGCACCCAGGACTCGGCTCACACATG	Schmidt et al. 2018	N/A
7SL northern probe GCGGACACCCGATCGGCATAGC	Shukla et al. 2014	N/A
U3 GCCGGCTTCACGCTCAGGAGAAAACGCTACCTCTC TTCCTCGTGG	Ripmeester et al. 2020	N/A
7SK GTGTCTGGAGTCTTGGAAGC	Prasanth et al. 2010	N/A
TCAB1 southern probe forward gagaacttcgaagccatcctg	Klump et al. 2023	N/A
TCAB1 southern probe reverse cagtgaaaatctcgggggtgg	Klump et al. 2023	N/A
TR qPCR forward cgctgtttttctcgctgact	Xi et al. 2014	N/A
TR qPCR reverse gctctagaatgaacggtggaa	Xi et al. 2014	N/A
GAPDH qPCR forward acagcaacagggtggtggac	Xi et al. 2014	N/A
GAPDH qPCR reverse gaccattgctggggctggtg	Xi et al. 2014	N/A
Recombinant DNA		
pHTN HaloTag® CMV-neo	Promega	G7721
pFastBac1	Life Technologies	10360014
pX330	Cong et al., 2013	Addgene: 42230
pmaxGFP	Lonza	Control from Kits
mCherry-TERT	Schmidt et al. 2014	N/A to be deposited
TERT (pVAN107)	Cristofari et al. 2006	N/A
mCherry-Dyskerin	Klump et al. 2023	N/A to be deposited
3xFLAG-HaloTag-dyskerin	Klump et al. 2023	N/A to be deposited
GFP-Nucleolin	Takagi et al. 2005	Addgene: 28176
GFP-NPM1	Wang et al. 2005	Addgene: 17578
mTagBFP-Nucleus-7 (BFP-NLS)	Addgene	Addgene: 55265

Table B1 (cont'd)

BFP-coilin	Schmidt et al. 2016	N/A to be deposited
pSUPER TR	Cristofari et al. 2006	N/A
LhTRmin	Vogan et al. 2016	N/A
pBS U3-hTR-500	Fu et al. 2003	Addgene: 28170
TR knockout HRD	Klump et al. 2023	N/A to be deposited
pHAGE-UBC-MCP-mNeonGreen	Klump et al. 2023	N/A to be deposited
3xMS-TR-100-PURO HRD	Klump et al. 2023	N/A to be deposited
Software and Algorithms		
MATLAB 2019a	Mathworks Inc., USA	http://mathworks.com
ParallelProcess_fastSPT_JF646.m		
ImageQuant TL 8.2	Hansen et al. 2018	https://github.com/elifesciences-publications/SPT_LocAndTrack
Spot-On	Hansen et al. 2018	https://github.com/elifesciences-publications/spot-on-matlab
Other		
Maxima SYBR Green qPCR Master Mix	Invitrogen	18080044
RiboLock RNase Inhibitor	Invitrogen	N8080127
HOECHST 33342	Thermo Scientific	EO0382
Protein G Agarose	Invitrogen	62249
4-15% Mini-PROTEAN TGX precast protein gels	Millipore Sigma	11243233001
Trans-Blot Turbo RTA Mini 0.2 µm Nitrocellulose Kit	Bio-Rad	4561083
FxCycle Propidium iodide/RNase staining solution	Bio-Rad	1704270
RNeasy Mini Kit	Thermo Scientific	F10797